

The Preserve: Lehigh Library Digital Collections

Developing A Cold Thermal Energy Storage System (ctess) By Using Phase Change Material (pcm) Encapsulated In Pervious Concrete (pc)

Citation

Yaghmour, Emad. *Developing A Cold Thermal Energy Storage System (ctess) By Using Phase Change Material (pcm) Encapsulated In Pervious Concrete (pc)*. 2024, https://preserve.lehigh.edu/lehigh-scholarship/graduate-publications-theses-dissertations/theses-dissertations/developing-cold.

Find more at https://preserve.lehigh.edu/

This document is brought to you for free and open access by Lehigh Preserve. It has been accepted for inclusion by an authorized administrator of Lehigh Preserve. For more information, please contact preserve@lehigh.edu.

DEVELOPING A COLD THERMAL ENERGY STORAGE SYSTEM (CTESS) BY USING PHASE CHANGE MATERIAL (PCM) ENCAPSULATED IN PERVIOUS CONCRETE (PC)

By

Emad Yaghmour

A Dissertation

Presented to the Graduate and Research Committee

of Lehigh University

In Candidacy for the Degree of

Doctor of Philosophy

In

Structural Engineering

Lehigh University

May, 2024

©2024 Copyright

Emad Yaghmour

Emad Yaghmour

Developing a Cold Thermal Energy Storage System (CTESS) by Using Phase Change Material (PCM) Encapsulated in Pervious Concrete (PC)

Approved and recommended for acceptance as a dissertation in partial fulfillment of the requirements for the degree of Doctor of Philosophy in Civil Engineering on this date of _____.

_____	_____
Spencer E. Quiel, Ph.D., P.E.	Clay J. Naito, Ph.D., P.E
Dissertation Committee Chair	Dissertation Supervisor
Department of Civil and Environmental Engineering	*Department of Civil and Environmental Engineering*
Lehigh University	Lehigh University
_____	_____
Muhannad T. Suleiman, Ph.D.	John Fox, Ph.D., P.E
Dissertation Co-advisor	Internal Committee Member
Department of Civil and Environmental Engineering	*Department of Mechanical Engineering and Mechanics*
Lehigh University	Lehigh University

_____

Carlos Romero, Ph.D.

External Committee Member

Department of Mechanical Engineering and Mechanics

Lehigh University

Date Accepted: _____

DEDICATION

To my beloved ones

My dad, Khalid

My mom, Nadia

My brothers and sister

ACKNOWLEDGMENT

I want to express my deepest gratitude to Professor Clay Naito, my dedicated dissertation supervisor, for his unwavering support, scholarly guidance, and insightful mentorship. Professor Naito's commitment to academic excellence has been a guiding force throughout this research journey. His feedback and encouragement have not only shaped the quality of this dissertation but have also fostered my intellectual growth. I extend my heartfelt appreciation to the esteemed members of my dissertation committee: Professor Muhannad Suleiman, Professor John Fox, and Professor Carlos Romero. Their expertise, scholarly contributions, and constructive feedback have played a pivotal role in enhancing the depth and breadth of this research.

My Dad’s soul, Khalid, I pay tribute to the enduring influence he had on my academic pursuits. His wisdom, encouragement, and values of diligence and perseverance have left an indelible mark on my journey. This dissertation is a reflection of the principles instilled by him and a testament to the impact he had on my scholarly endeavors.

To my family, my pillar of strength, I express my deepest love and gratitude. My mom, Nadia, has been a constant source of support and encouragement. My brothers, Odai and Ala'a and my sister, Abeer, have provided unwavering support and understanding. This dissertation is a shared achievement, a testament to the resilience and unity of our family.

Finally, I want to acknowledge the wider network of friends, colleagues, and mentors who have contributed to my academic journey. Your encouragement, wisdom, and camaraderie have been invaluable. This dissertation stands as a collective effort, reflecting the support and collaboration of a diverse community.

Thank you to each person who has been a part of this journey, contributing to its success and making it a truly enriching experience.

TABLE OF CONTENTS

1 INTRODUCTION 2
1.1 OVERVIEW 2
1.2 SCOPE AND ORGANIZATION 5
2 LITERATURE REVIEW 10
2.1 COOLING TOWER SYSTEMS 10
2.2 THERMAL ENERGY STORGE (TES) SYSTEM 13
2.3 PERVIOUS CONCRETE (PC) 15
2.4 PRESSURE DROP IN THE POROUS MEDIA 16
3 PERFORMANCE OF PERVIOUS CONCRETE WITH LIGHTWEIGHT AND NORMAL WEIGHT AGGREGATES 20
3.1 INTRODUCTION 20
3.2 MATERIALS 22
3.2.1 Normal and Lightweight Coarse Aggregates Characteristics 22
3.2.2 Aggregate Crushing Value 24
3.2.3 Pervious Concrete Design 26
3.2.4 Mix Design and PC Fabrication 28
3.3 METHODOLOGY 29
3.3.1 Cement Paste Flowability 29
3.3.2 Porosity of Hardened Samples 31
3.3.3 Water Permeability 32
3.3.4 Mechanical Properties Measurements 33
3.4 RESULTS AND DISSCUSION 33
3.4.1 Effect of aggregate type 34
3.4.2 Effect of LWA volumetric replacement 38
3.4.3 Effect of w/c ratio 40
3.4.4 Effect of PC Porosity and V_{PA} 42
3.4.5 Split and Compressive Strength Relationship 44
3.5 SUMMARY AND CONCLUSIONS 45
4 PRESSURE DROP AND HEAT TRANSFER PROPERTIES FOR NORMAL WEIGHT AND LIGHTWEIGHT PERVIOUS CONCRETE 48

4.1 INTRODUCTION 48
4.2 EXPERIMENTAL PROGRAM 51
4.2.1 Materials 51
4.2.2 Test Equipment and Methods 53
4.2.3 Pervious Concrete Design 57
4.3 EXPERIMENTAL RESULTS 59
4.3.1 Porosity Measurement 59
4.3.2 Validation of Air Permeability Setup 63
4.3.3 Air Permeability Results for Pervious Concrete 64
4.3.4 Thermal Properties Results for Pervious Concrete (PC) 73
4.3.5 Heat Transfer for Pervious Concrete (PC) 74
4.4 SUMMARY AND CONCLUSIONS 76
5 ENERGY STORAGE IN LIGHTWEIGHT AGGREGATE AND PERVIOUS CONCRETE INFUSED WITH PHASE CHANGE MATERIALS 79
5.1 INTRODUCTION 79
5.2 MATERIALS 81
5.2.1 Phase Change Material (PCM) 81
5.2.2 Lightweight Aggregate (LWA) 82
5.2.3 PCM-LWA 83
5.2.4 Macro-Encapsulated PCM 87
5.3 METHODOLOGY 88
5.3.1 Pervious Concrete Design 88
5.3.2 PC w/o PCM 90
5.3.3 Microencapsulated PCM PC 91
5.3.4 Macro-Encapsulated PCM PC 91
5.4 TESTING PROCEDURE 92
5.4.1 Mechanical Properties 92
5.4.2 Porosity and Permeability Measurements 93
5.4.3 Heat Capacity Measurements 95
5.5 RESULTS AND DISSCUSION 97
5.5.1 Mechanical and Hydraulic Properties 97
5.5.2 Water and Air Permeability 101

5.5.3 Heat Transfer of Pecked Bed and PC 102
5.6 DESIGN RECOMENDATIONS 106
5.7 SUMMARY AND CONCLUSION 109
6 SUMMARY AND CONCLUSIONS 112
6.1 RESEARCH CONTRBUTIONS 112
6.2 FUTURE RESEARCH 114
7 REFERENCES 116
8 VITA 135

LIST OF TABLES

Table 3-1: Properties of aggregates used in this study to prepare PC mixes. 23

Table 3-2 Normal weight and lightweight PC mix proportions (kg/m^3). 27

Table 3-3: HRWR dosage and paste spread for varying w/c ratios. 31

Table 3-4: Measured engineering properties of PC mixes. 34

Table 4-1: The physical properties of granular materials. 52

Table 4-2: HRWR dosage for varying w/c ratios. 58

Table 4-3**:** PC mix proportions 59

Table 4-4**:** The mean square error between measured pressure drop and predicted values based on the Ergun equation. 72

Table 4-5: Heat capacity for PC 75

Table 5-1: Physical and thermal properties of PCM 81

Table 5-2: Physical and thermal properties of the aggregates 83

Table 5-3: Physical and thermal properties of the encapsulated LWAs. 87

Table 5-4: Pervious concrete proportions 90

Table 5-5: Mechanical and hydraulic concrete properties 99

Table 5-6: Heat capacity for PC 104

LIST OF FIGURES

Figure 1-1: (a) dry cooling tower (DCT); (b) improved dry cooling tower. 4

Figure 2-1: (a) Wet cooling tower (WCT); (b) Dry cooling tower (DCT); (c) Wetted media pre-cooling DCT; (d) Water spray pre-cooling DCT. 12

Figure 3-1: Normal weight and lightweight aggregates used, scale: cm. 22

Figure 3-2**:** SEM images of different aggregate. 24

Figure 3-3: (a) Aggregate crushing value test setup, and (b) aggregate specimen during compression loading. 25

Figure 3-4: Flow measurement of recommended HRWR dosage. 30

Figure 3-5**:** Falling head permeameter used to measure the water permeability of PC specimens. 33

Figure 3-6: Cross sections of PC mix specimens made with different aggregate types. 35

Figure 3-7**:** (a) Mechanical performance of PC specimens with different aggregate type; (b) Relationship between aggregate crushing value and PC specimens' compressive strength; (c) hydraulic properties of PC specimens with different aggregate type. 37

Figure 3-8**:** Cross sections of PC specimens prepared at different replacement ratios. 38

Figure 3-9: (a) Effect of aggregate replacement on compressive, split tensile strength, and modulus of elasticity; (b) Effect of aggregate replacement on hydraulic properties. 39

Figure 3-10**:** (a) Compressive, split tensile strengths, and stiffness of PC specimens fabricated with LWA 2 at different w/c ratio; (b) Porosity and permeability of PC specimens fabricated with LWA 2 at different w/c ratio. 41

Figure 3-11**:** Failure surface of lightweight PC specimens prepared at different water to cement (w/c) ratios. 42

Figure 3-12: (a) Compressive, split tensile strengths, and stiffness of PC specimens fabricated with LWA 2 at different porosity; (b) permeability of PC specimens fabricated with LWA 2 at different porosity..... 44

Figure 3-13**:** Failure characteristics of LWA-PC specimens fabricated at different porosity. 44

Figure 3-14: The relationship between compressive strength and split tensile strength for all PC mixes. 45

Figure 4-1: Bed materials..... 53

Figure 4-2: Air permeability test setup. 54

Figure 4-3: Transient plane source (TPS) setup used to determine thermal properties of PC..... 55

Figure 4-4: Heat transfer setup. 56

Figure 4-5: (a) Effect of w/c ratio measured porosity, (b) Effect of normal weight aggregate replacement ratio on measured porosity and (c) Effect of V_P/V_{Agg} on the measured porosity. 62

Figure 4-6**:** Normalized pressure drop for steel beads. 64

Figure 4-7**:** Normalized pressure drop for different granular materials. 64

Figure 4-8**:** The normalized pressure drop for mixes with different w/c ratios. 66

Figure 4-9: The cross section of PC samples with different V_P/V_{Agg} ratios. 67

Figure 4-10 : The normalized pressure drop for mixes with different design void ratios. 67

Figure 4-11: The normalized pressure drop for mixes with different LWA replacement ratios..... 68

Figure 4-12: Ergun packed bed and equivalent pipe model. 69

Figure 4-13: Optimized equivalent diameter. 71

Figure 4-14: The comparison between the measured normalized pressure drop and predicted values. 72

Figure 4-15: The relationship between % of LWA replacement ratio with the measured thermal conductivity and specific heat of PC mixes prepared with different LWA replacement ratios. 73

Figure 4-16: The thermal properties of PC samples with different V_P/V_{Agg} ratios. 74

Figure 4-17: Temperature difference between inlet and outlet in charging phase for different replacement ratio. 76

Figure 5-1: (a) dry cooling tower (DCT); (b) improved dry cooling tower. 80

Figure 5-2: (a) Real image of LWAs (scale in cm); (b) SEM images of LWA. 83

Figure 5-3: Water absorption of LWA (a) by soaking, (b) by vacuum method. 84

Figure 5-4: Infusion vacuum setup. 86

Figure 5-5: Microencapsulation coating procedure: (a) LWA immersion in epoxy; (b) cement coating of epoxy; (c) air curing of coated LWA; (d) PCM-LWAs following water curing. 86

Figure 5-6: (a) Coated encapsulated LWAs (scale in cm); (b) SEM image of coated encapsulated shale. 87

Figure 5-7: Macro-Encapsulated PCM: (a) Solid PCM balls; (b) Coated PCM balls. 88

Figure 5-8: (a) Macro-encapsulated PCM prior to mixing; (b) Macro-encapsulated PCM PC sample. 92

Figure 5-9: (a) Schematic model of water permeability setup; (b) Top view of water permeability sample. 94

Figure 5-10: (a) Schematic model; (b) Pressure drop setup. 95

Figure 5-11**:** (a) Schematic model; (b) Thermal heat transfer setup. 96

Figure 5-12: failure mode of PCM-PC samples: (a) Shale PC w/o PCM; (b) Clay PC w/o PCM; (c) Glass PC w/o PCM; (d) Shale PC w/ PCM; (e) Clay PC w/ PCM; (f) Glass PC w/ PCM. 100

Figure 5-13: Failure mode in PCM macro-encapsulated PC: (a) liquid phase; (b) solid phase. 100

Figure 5-14: Pressure drop for all mixes. 102

Figure 5-15: Temperature difference between inlet and outlet in charging phase: (a) PCM infused packed bed; (b) PCM infused PC; (c) PC w/o PCM. 104

Figure 5-16: (a) Temperature difference between inlet and outlet in charging phase for glass PCM-PC at different velocities; (b) a time duration needs to maintain a temperature change of 2 °C. 106

Figure 5-17: The compressive strength and total heat capacity of PC w/ PCM for different types of aggregate at the same porosity (30%). 109

ABSTRACT

Condensers and cooling towers are commonly used in coal power plants to condense the steam from condenser in a power plant and to recycle the condensed-water into the boiler in a closed-loop system. Cooling tower facilitates are used to release the heat of the warm water flow in the condenser. There are two main types of cooling tower depending on the heat transfer mechanism: wet cooling towers (WCTs) and dry cooling towers (DCTs). This work investigates the development, design, and evaluates an effective pre-cooling system to enhance the performance of a mechanical draft dry cooling system (DCS) for coal power plant applications. The dry pre-cooling system is provided by designing a cold thermal energy storage system (CTESS) which consists of a PCM encapsulated in PC. The research presented in this dissertation focuses on: (1) Examination of the replacement of normal weight aggregates (NWAs) by lightweight aggregates (LWAs) in pervious concrete fabrication, and its impact on mechanical properties, with the aim of developing an optimal concrete mix that balances strength and permeability; (2) Quantification of the pressure drop and thermal properties of pervious concrete as well as the development of an empirical model that predicts the pressure drop in pervious concrete; (3) a feasibility study on the utilization of pervious concrete (PC) incorporating diverse lightweight aggregates (LWAs) and phase change materials (PCM) for dry cooling purposes.

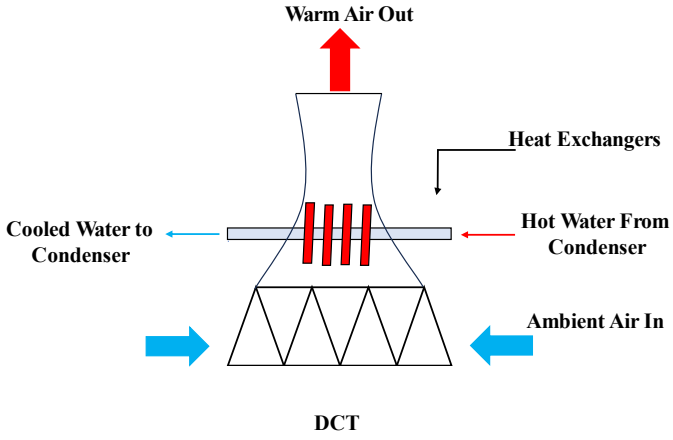
1 INTRODUCTION

1.1 OVERVIEW

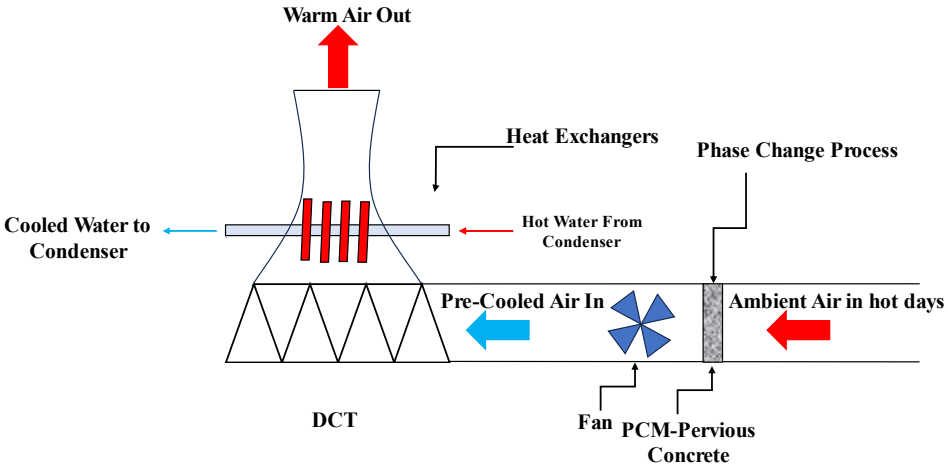
Nowadays, population growth and the energy demand are increasing significantly, which leads to a rise in the consumption of freshwater resources. For example, the power plants in the US consumed approximately 40% of freshwater, with 90% of it used in condenser cooling [1]. The most used cooling technology in coal-fired power plants needs high water withdrawal rates (75-150 m3/MWh) leads to thermal pollution of the water source [2]. According to the kind of heat transfer mechanism, there are two major categories of cooling tower technologies depending on the contact between the working fluid (e.g., hot water) and the air flow, wet cooling tower and dry cooling tower. The wet cooling towers (WCTs) are a recirculation water system that carries out cooling by providing direct mixing of hot water and air. The hot water flows from condenser in a power plant through the pipes to the cooling tower then spread over the tower's fill material. Fill material is used in cooling towers to provide as much contact surface as possible to enhance evaporation and heat transfer. The water, after cooling down by a combination of evaporation and convective heat transfer, is pumped through the condenser to condense the turbine steam in a continuous circuit [3]. The dry cooling towers (DCTs) depend on convection heat transfer to release heat from the working fluid by indirect contact between air and working fluid as shown in Figure 1-1 (a) [4]. All the cooling system efficiency depends on the air-in temperature. Hence, during the peak of a hot day, particularly around noon, the ambient temperature has a negative effect on the cooling process. Early studies found that pre-cooling may be a cost-effective solution, like evaporative pre-cooling process (e.g., fogging

cooling, wet-media cooling, and spray cooling). The main shortcomings of fogging and spray cooling are the corrosion risk and the need for expensive water demineralization both to minimize corrosion and fouling and to prevent nozzle clogging. On the other hand, in wetted-media cooling, the water quality and corrosion of heat exchanger should not be noticeable issues [5,6]. However, water lost by evaporation, especially in areas that suffer from scarcity of water resources, is a major obstacle to the use of these pre-cooling methods. This study proposed to minimize the consumption of fresh water in pre-cooling process by providing a dry pre-cooling process by developing a cold thermal energy storge system (CTESS) using phase change material encapsulated in pervious concrete. The pervious concrete (PC) is a porous concrete type that is made of a single-sized coarse aggregate with small amount or no fine aggregate (e.g., sand) [7–10]. On the other word, cold thermal energy can be stored at nighttime in thermal energy storge (TES) system for daily usage in pre-cooling the air entering a dry cooling tower. TES units are advantageous for redistribution of solar energy. Thermal energy can be readily stored as sensible and latent heat. The capacity of sensible heat storage is determined by the specific heat and mass of the storage media. Consequently, sensible heat storage requires a larger volume than other types of TES systems since most storage media have low volumetric energy density [11]. Latent heat is absorbed or released energy when the PCM changes phase from solid to liquid or liquid to solid at a melting temperature, respectively. PCM are classified into three categories: organic, inorganic, and eutectic. Organic PCMs (e.g., paraffins and fatty acids) [12], are chemically stable materials with negligible supercooling effect [13]. These materials have a relatively high cost and are flammable, limiting their use in building applications. Inorganic PCM are salt hydrates and metals having a rather high heat of

fusion. Salt hydrates have a high latent heat value, are non-flammable, low cost, and readily available. Eutectic PCM consists of at least two different PCMs, resulting in a lower phase change temperature than the parent PCMs. Therefore, inorganic phase-change material (PCM) has been used in this study since it has a high latent heat, high energy densities, and low cost.



(a)



(b)

Figure 1-1: (a) dry cooling tower (DCT); (b) improved dry cooling tower.

1.2 SCOPE AND ORGANIZATION

The goals of the presented study are to develop, design, and evaluate an effective pre-cooling system to enhance the performance of a mechanical draft (e.g., by fan) dry cooling system (DCS) for coal power plant applications. The dry pre-cooling system is provided by designing a cold thermal energy storage system (CTESS) which consists of a PCM encapsulated in PC as shown in Figure 1-1 (b). The outline of this dissertation research activities that focused on achieving the research goal is listed below:

- Chapter Two: This chapter provides a comprehensive overview of dry cooling systems, pervious concrete, and thermal storage materials and systems. Additionally, a literature review that specifically explores the pressure drop and heat transfer characteristics when air flows through porous mediums.
- Chapter Three: This chapter explores various types of lightweight aggregates and their ability to absorb water, crush resisting, and their use in designing pervious concrete. Pervious concrete mixes without PCM are fabricated using two types of aggregates: normal and lightweight aggregates, in different proportions, along with varying water-to-cement ratios and cement paste ratios. Moreover, investigating the effect of cement paste flowability on the porosity of pervious concrete and develops a design to achieve the same porosity with different water-to-cement ratios and aggregate types. Mechanical properties, water permeability, and porosity of porous concrete are studied in addition to its mechanical properties.
- Chapter Four: This chapter delves into the study of the pressure drop and thermal properties of pervious concrete without PCM. These properties form the foundation for studying the ability of use pervious concrete as cooling system. Air permeability

setup is developed to measure the pressure drop of air flowing through pervious concrete at various velocities. The investigation of the pressure drop involves a modification on the Ergun equation for enhanced prediction of pressure drop. This modification accounts for the influence of both water-to-cement ratio and cement paste content on the pressure drop characteristics.

- Chapter Five: This chapter entails a comprehensive study on the integration of salt hydrate Phase Change Material (PCM) within pervious concrete. Two encapsulation methods are employed to produce PCM pervious concrete samples, utilizing both macro- and micro-encapsulation techniques. The fabrication process involves the development of infusion and coating methods to encapsulate PCM within lightweight aggregates (LWA). Three types of LWAs—shale aggregate, clay aggregate, and glass aggregate—are examined for microencapsulation purposes. The PCM-pervious concrete samples undergo rigorous testing for mechanical properties, air and water permeability, and thermal characteristics. Additionally, a heat transfer setup is devised to assess the thermal capacity of various PCM lightweight pervious concrete compositions. Furthermore, the chapter presents a recommended mix design to produce panels suitable for dry cooling.
- Chapter Six: This chapter provides general conclusions and offers recommendations for future research studies.

NOMENCLATURE

ACV: aggregate crushing value, %.

M_1: total mass of aggregate specimen, kg.

M_2: mass of specimen portion passing 2.36 mm sieve after compression loading, kg.

R_{e1}: modified Reynold's number.

A, B: Ergun coefficients.

ε: porosity %.

S_v: specific surface, m^{-1}.

μ: dynamic viscosity, kg/m^3.

D_p: particle diameter, m.

ρ: density of flow, kg/m^3.

v: superficial velocity, m/s.

ΔP: predicted pressure drop, Pa.

ΔP_M: measured pressure drop, Pa.

L: length of sample, m.

ΔP_1: the predicted pressure drop through the pipe, Pa.

C_1 and C_2: fraction factors.

v : the interstitial velocity, m/s.

D_{eq}: the equivalent diameter, m.

W_1: the dry sample mass, kg.

W_2: the submerge sample mass, kg.

V_T: the volume of the sample, m^3.

V_v: the volume of voids, m^3.

V_m: the volume of bed material, m^3.

SG: the specific gravity of bed material.

ρ_W: the density of water, kg/m^3.

m_s: the total mass of sample, kg.

C_{pair}: air specific heat, kJ/kg. ^oC.

C_p: the pervious concrete specific heat kJ/kg. ^oC.

$\dot{m}$: air mass flow, kg/s.

$E_{theortical}$: theoretical energy stored in the PC, J.

E_{stored}: instantaneous amount of energy stored in the PC, J.

T_{in}: the temperature at inlet of PC, ^oC.

T_{out}: the temperature at the outlet of PC, ^oC.

A: internal cross-sectional area of the pipe, m^2.

T_f: final temperature of the PC, ^{o}C.

T_i: initial temperature of the PC at t = 0, ^{o}C.

ρ_{air}: air density, kg/m^3.

2 LITERATURE REVIEW

2.1 COOLING TOWER SYSTEMS

The cooling system in a power plant expels heat at roughly twice the rate of electric power generation [14]. Generally, even slight improvements to the cooling system can yield notable fuel savings and, as a result, enhance overall efficiency due to the typically substantial energy flows in power plants [15]. Based on the type of heat transfer mechanism, cooling tower technologies can be broadly categorized into two main types, depending on the interaction between the working fluid (e.g., hot water) and the airflow: wet cooling towers and dry cooling towers. In 1959, McKelvey and Brooke provided the fundamental design of the wet cooling towers (WCT's) [16]. WCTs are a recirculation water system designed to provide cooling by directly mixing hot water and air. The hot water flows from condenser in a power plant through the pipes to the cooling tower then spread over the tower's fill bed material as shown in Figure 2-1 (a). Optimizing the efficiency of WCTs is mainly depending on mass and heat transfer mechanisms occurring between water and air flows inside them [17]. In this heat transfer process, over two-thirds of the heat is transferred through evaporation, while the remaining portion is transferred through convection [15].On other hand, the dry cooling towers (DCTs) mainly depend on convection heat transfer to release heat from the working fluid by indirect contact between air and working fluid as shown in Figure 2-1 (b) [4]. The history of DCTs traces back to the 1930s, However, its substantial deployment and evolution commenced in 1962 with the introduction of an indirect, natural draft system at Rugeley in the UK [18]. Although WCTs exhibit higher heat transfer efficiency compared to the DCTs [19], their substantial water consumption poses a challenge, particularly in regions with limited and costly

freshwater resources. With the growing focus on renewable thermal power generation, such as geothermal and solar thermal power plants, which often operate in areas with water scarcity, dry cooling technology has gained increased attention in recent years [14,20–22]. While dry cooling systems outperform water conservation compared to wet cooling systems, there is a lack of performance at high ambient temperatures [23]. Hence, during the peak of a hot day, particularly around noon, the ambient temperature has a negative effect on the cooling process. Early studies found that pre-cooling may be a cost-effective solution, like evaporative pre-cooling process (e.g., fogging cooling, wet-media cooling, and spray cooling). For example, He et al., study on pre-cooling of inlet air using Munters media to enhance the performance of a Natural Draft Dry Cooling Tower (NDDCT) on hot and dry days as shown in Figure 2-1 (c). The ambient humidity was kept constant at 30% while the ambient temperature ranged from 10 to 50 °C during simulation. Three Munters media with three thicknesses, were employed to pre-cool the tower inlet air. It was found that there is a critical ambient temperature below which pre-cooling application does not benefit NDDCT performance. The value of this critical temperature is a function of the tower design and the selection of wetted media. Amongst the studied media, only the pre-cooling with 0.10 m and 0.15 m [6]. Sun et al., studied the use of water spray in pre-cooling systems as shown in Figure 2-1 (d). Integrate multiple LNN1.5 nozzles to enhance the cooling efficiency of the Natural Draft Dry Cooling Tower (NDDCT). Their study emphasizes the importance of strategically arranging the spray nozzles to optimize cooling while minimizing water usage. Their results show the installation of five nozzles resulted in a 6.3 °C reduction in inlet air temperature, corresponding to a 51.2% cooling efficiency. The pre-cooling system's notable advantage is its efficient water usage, with over 96% of

injected water effectively extracting heat from hot air and evaporating into vapor, thereby facilitating a pre-cooled airflow [24]. Efforts to enhance the performance of dry cooling systems are still ongoing, with a focus on providing pre-cooling through a wet cooling approach [5,25–31]. The main shortcomings of wet pre-cooling are the corrosion risk and the need for expensive water demineralization both to minimize corrosion and fouling and to prevent nozzle clogging [6]. For this reason, there is a growing need to develop a dry pre-cooling system using thermal energy storage (TES) system.

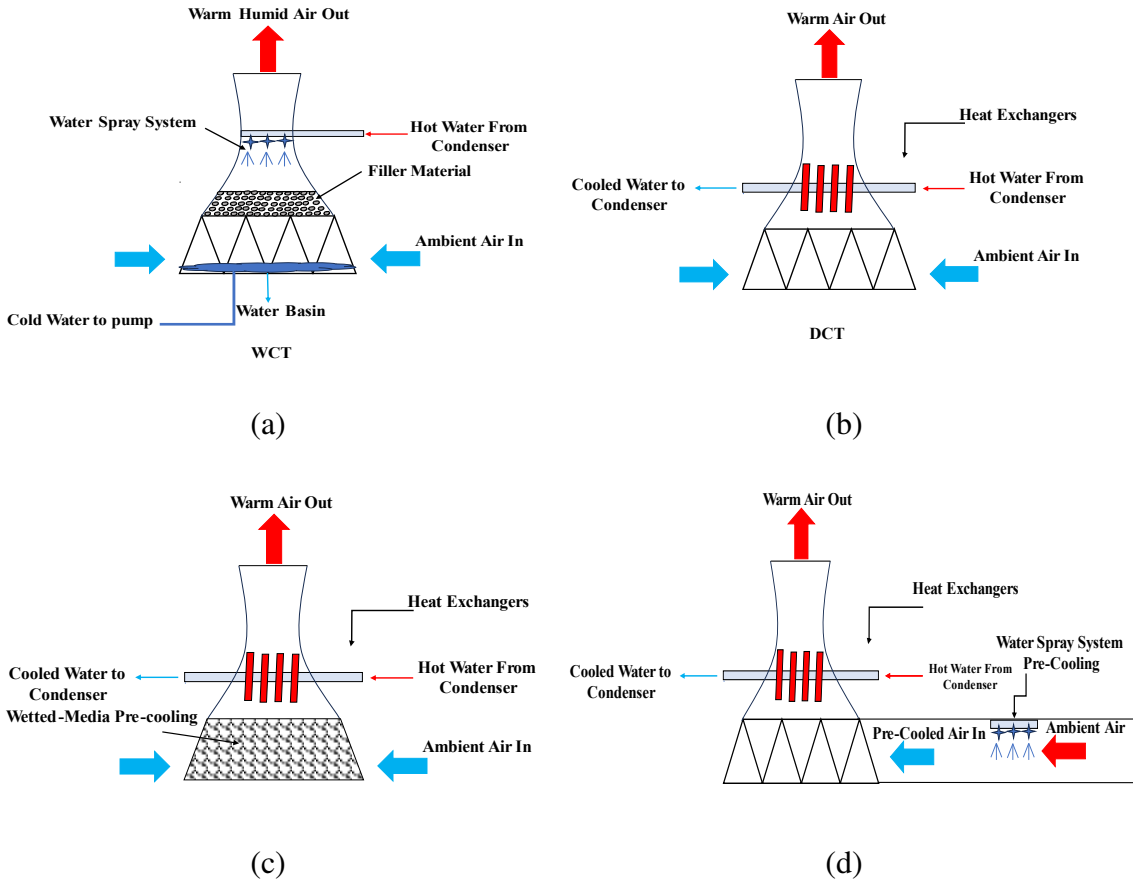


Figure 2-1: (a) Wet cooling tower (WCT); (b) Dry cooling tower (DCT); (c) Wetted media pre-cooling DCT; (d) Water spray pre-cooling DCT.

2.2 THERMAL ENERGY STORGE (TES) SYSTEM

Thermal energy storge (TES) can be utilized in various materials in different forms (e.g., sensible heat and latent heat). The capacity of sensible heat storage is directly proportional to the specific heat, density, volume, and temperature change of the storage media. In the process of absorbing heat, no phase change occurs, and materials undergo an increase in temperature [11]. Latent heat is absorbed or released heat at constant temperature when the materials change phase from solid to liquid or liquid to solid respectively. These materials are called phase change materials (PCMs) and are classified into three categories: organic, inorganic, and eutectic. Organic PCMs can be categorized as paraffin and non-paraffin types [12]. Generally, these materials exhibit chemical stability, safety, and non-reactivity with negligible supercooling effect [13]. Paraffin wax (PAR) is a hydrocarbon with the chemical structure CnH2n+2. Commercial PAR typically melts within a range of 20°C to 70°C, depending on the number of carbon (C) atoms in its chain. The melting point increases with a higher count of C atoms. PAR is favored in concrete applications for being inert in an alkaline medium and chemically stable. However, it does have drawbacks such as flammability and low thermal conductivity in its solid state [32–34]. On the other hand, most organic non-paraffin PCMs are acids (CH3(CH2)2nCOOH) with melting points similar to those of paraffin PCMs, exhibiting excellent melting and freezing properties. However, they tend to be more expensive than paraffin PCMs [35]. Inorganic PCM are salt hydrates and metals having a rather high heat of fusion. Salt hydrates have a high latent heat value, are non-flammable, low cost, commendable thermal conductivity, and readily available [36]. Eutectic PCM consists of at least two different PCMs, resulting in a lower

phase change temperature than the parent PCMs. The heat energy stored in a latent and sensible heat thermal storage unit can be calculated using Equation (2.1) [23]:

$$E_{theortical} = m_s \cdot C_p \cdot (T_f - T_i) + J \cdot m_{PCM} \quad (2.1)$$

Where m_s is the total mass of sample (kg), C_p is the sample material specific heat (kJ/kg.^{o}C), T_f is the final temperature of sample (°C), T_i is the initial temperature of the sample at time, t = 0, (°C), J is the heat capacity of PCM (kJ/kg) and m_{PCM} is the mass of PCM inside the sample. In Equation (2.1), the first term signifies the sensible heat energy, and the second term accounts for the latent heat energy.

Due to its wide availability and high density, concrete is popular for use as sensible thermal storage media [37–39]. To enhance the energy storage capacity, PCM can be incorporated into concrete via immersion [40,41] and encapsulation [42–44]. Immersion consists of soaking the fabricated concrete component in a liquid PCM. The efficiency of this method depends on the absorption capacity of the concrete. For example, Hawes and D. Feldman studied absorption mechanisms and proposed a method for determining absorption constants in PCM. The study investigated the effect of many factors such as temperature, PCM viscosity, concrete density, and hydrogen bonding on PCM penetration. Their results showed that at 80 °C it is the optimum temperature to allow the PCM liquid to soak into the concrete blocks. The impregnation of PCM into autoclaved concrete blocks requires 1 hour, whereas the impregnation into regular concrete blocks takes 6 hours [45].

Encapsulation is achieved through (1) macro-encapsulation or (2) microencapsulation. Macro-encapsulation consists of encapsulating PCM within a chemically and physically stable shell. Integrity of the shell is critical for both preventing contamination of the PCM

and impacting the stability of the concrete hydration or the other constituents in the mix [46]. Moreover, when the PCM is in a liquid phase, the shell integrity prevents loss of PCM. Microencapsulation consists of PCM-impregnated in the pores of the aggregate. Lightweight aggregates (LWA) are used due to their high volumetric porosity. The trapped air in the pores is removed by vacuum and refilled with liquid PCM. In order to overcome PCM leakage out and to prevent any chemical reaction with surrounding media, epoxy coatings have been utilized [42,47]. Previous research investigated PCM incorporation in building materials such as masonry walls and conventional concrete. However, use of microencapsulated LWA in pervious concrete applications has not been examined.

2.3 PERVIOUS CONCRETE (PC)

Pervious Concrete (PC) is composed of coarse aggregate excluding fine aggregate and bonded together by cement paste. Consequently, the absence of fine aggregates creates open voids, facilitating substantial water infiltration and air exchange rates through interconnected macro voids [7–10]. The encouragement to use PC in pavement application due to its ability to drain rainwater [10], as well as its capacity to reduce road noise generated by tire friction against the road surface [48,49]. Moreover, namouras studies have explored that PC can be used in a different application including contaminant removal [50,51], urban heat island reduction [52], and water evaporation control from soils [53]. The porosity, water to cement (w/c) ratio, hydraulic permeability of PC made with conventional normal weight aggregate is typically in the range of 15-35%, 0.27-0.43, and 0.1-1.2 m/s, respectively [54–57]. The PC porosity has a major role in the functional and structural performance of this material, which is dependent on the cement paste content, w/c and compaction effort during fabrication [58,59]. Chindaprasit et al., [60] studied the

properties related to cement paste, revealing that its characteristics are influenced by the w/c, admixture, and mixing time. To achieve a cement paste suitable for PC, high viscosity and optimal flow are obtained with a low w/c ratio of 0.20–0.25, the inclusion of 1% superplasticizer, and thorough mixing. Their results showed PC with porosity of 15–25% and strengths ranging from 22 to 39 MPa are achieved using paste with a flow of 150–230 mm and top surface vibration lasting 10 seconds with a vibrating energy of 90 kN m/m². On the other hand the, Ibrahim et al., [61], studied the effect of aggregate size and content of the coarse aggregates on PC. Their findings indicated that properties such as permeability and porosity are notably influenced when employing either one or two coarse aggregate sizes in all concrete mixtures. In their study, the highest compressive strength reached 6.95 MPa, achieved by utilizing a single aggregate size of 9.5 mm with a cement content of 250 kg/m3. Since failure in normal weight PC occurs at the cement paste interface, Kevern et al., suggested adding a proportion of sand to enhance the interface and increase the strength of PC.

2.4 PRESSURE DROP IN THE POROUS MEDIA

The performance of PC under forced air flow differs significantly from that of water flow. This is due to incompressibility of water as compared to a compressible flow of air. A review of the literature revealed that there are very limited studies that have explored air permeability of PC. Qin et. al. [62] measured the air permeability of PC using a vacuum to create air flow. The air permeability was measured for two different sizes of normal weight aggregate (50 and 100 mm) and two w/c ratios of 0.23 and 0.25. They found out that the air permeability varies from 10^{-9} to 10^{-10} m^2 (i.e., 10^3 to 10^4 Darcy) for the range of aggregate and w/c ratios studied. It is worth noting that their study expressed the air

permeability of the PC mixes as a constant value which inherently assumes laminar flow [63]. Due to the void characteristics of PC and its Reynold's number air flow for most applications is turbulent, resulting in a quadratic relationship between velocity and pressure drop [64]. To more fully characterize the PC air permeability, a wider range of porosities and air velocities are needed [65].

Flow in a porous media is classified based on Reynold's number (R_e), with laminar flow simply referring to low R_e conditions, and turbulent flow referring to high R_e conditions due to additional drag force formed by eddies in the fluid within the porous media [64]. The modified Reynold's formula is shown in Equation (2.2).

$$\mathrm{R_{e1}} = \frac{\rho \mathrm{v}}{(1-\varepsilon)\mathrm{S_v}\mu} \tag{2.2}$$

Where $\mathrm{R_{e1}}$is the modified Reynold's number of porous media, ρ is the fluid density, ε is the porosity, v is the superficial velocity through the pores, μ is the fluid dynamic viscosity and $\mathrm{S_v}$ is specific surface which is equal to $\frac{6}{\mathrm{D_p}}$ for a packed particle bed of spheres, where $\mathrm{D_p}$ is a particle diameter. Darcy's law is valid only for laminar flow ($\mathrm{R_{e1}} < 2$) [63]. Based on Equation (2.2), for typical PC with void sizes greater than 2 mm and air velocities greater than 0.02 m/s it is improbable to get a value of $\mathrm{R_{e1}}$ less than 2.0. Ergun [66] developed an equation to predict the pressure drop of packed beds filled with regular-shaped spherical particles as a function of air flow rate for ($\mathrm{R_{e1}} > 2$) as shown in Equation (2.3).

$$\frac{\Delta \mathrm{P}}{\mathrm{L}} = \mathrm{A}\frac{(1-\varepsilon)^2}{\varepsilon^3}\frac{\mu}{\mathrm{D_p^2}}\mathrm{v} + \mathrm{B}\frac{(1-\varepsilon)}{\varepsilon^3}\frac{\rho}{\mathrm{D_p}}\mathrm{v}^2 \tag{2.3}$$

Where, ΔP is the predicted pressure drop through the packed bed, L is the bed length or height, ε is the bed porosity, v is the superficial velocity at the exit of bed, ρ is the fluid density, μ is the fluid dynamic viscosity, and D_p is the particle diameter. In Equation (2.3), the first term represents viscous energy losses that dominate during laminar flow and the second term accounts for kinetic losses that govern in the turbulent regime. A and B are empirical constants of 150 and 1.75, respectively [66]. Research was conducted to determine alternative constants to account for variation in packing material shape [67,68]. Macdonald et al. [68] revisited Ergun's equation through a detailed study of experimental results on particles of various sizes and, shapes including spherical, cylindrical, sand and gravel. They found that A is typically independent of particle roughness and B is dependent on surface roughness. They recommend an A of 180 and a B of 1.8 for smooth particles and 4.0 for rough particles [68]. This variation in the empirical constants is due to the variations in particle shape for non-spherical particles [69]. The modification had also been made by incorporating the shape factor, or particle sphericity (φ), which is a measure of the degree to which a particle's shape approaches the shape of a sphere. Ozahi et al. [67] studied packed beds of zeolite, chickpea and glass bead materials and determined particle sphericity ranges of 0.55 to 1.00 along with the empirical constants of 150 and 1.75 for A and B [67] as follows in Equation (2.4): as follows:

$$\frac{\Delta P}{L} = A\frac{(1-\varepsilon)^2}{\varepsilon^3}\frac{\mu}{\varphi^2 D_p^2}v + B\frac{(1-\varepsilon)}{\varepsilon^3}\frac{\rho}{\varphi D_p}v^2 \tag{2.4}$$

The Ergun formulation was specifically devised for spherical packed particles. This contrasts with pervious concrete, wherein air channels are created between irregularly shaped aggregates and the cement paste. Consequently, it is anticipated that estimating the

pressure drop ($\Delta P/L$) in pervious concrete using Equation (2.3) or Equation (2.4) may yield less-than-ideal results. The present study [65] explores the applicability of applying the Ergun equation to predict the pressure drop in a pervious concrete conglomerate, deviating from its conventional use in predicting pressure drop in a packed bed, and examines potential modifications to enhance its accuracy in this context.

3 PERFORMANCE OF PERVIOUS CONCRETE WITH LIGHTWEIGHT AND NORMAL WEIGHT AGGREGATES

3.1 INTRODUCTION

Pervious Concrete (PC) is a porous type of concrete made of a single-size coarse aggregate with limited to zero fine aggregate [7–10]. PC is commonly used as sustainable permeable pavement material to provide localized groundwater replenishment and manage stormwater by allowing passage of surface runoff through an interconnected void system in the hardened concrete [7]. Furthermore, the void structure of PC provides mitigation of noise pollution caused by tire–pavement interaction [48,49], allows for contaminant removal, and reduces urban heat island effects due to heat transfer through the pores [70]. Standard PC is a mixture of single-size coarse aggregate, cementitious materials, water, and admixtures. Addition of fine aggregates are sometimes used to improve strength at the expense of void content [71–73]. According to ACI Committee 522 [7], the typical range of porosity is 15 to 35%, water to cement (w/c) ratio ranges from 0.27 to 0.43, and water permeability of PC made with normal weight aggregate ranges from 0.1 to 1.2 m/s. The porosity of the PC plays a key role in the mechanical and hydraulic performance of this material and is dependent on the cement paste content, w/c ratio, and compaction effort during fabrication [74,75].

Two main categories of aggregate are examined: normal weight aggregate (NWA) and lightweight aggregate (LWA). LWAs can be utilized to produce lightweight conventional concretes (LWCs) with lower densities, reducing the overall weight of the structure, at the cost of reduced strength. Due to the high internal pore structure of LWAs they provide improved thermal and acoustic insulation performance over NWA concrete [76]. The high

porosity of LWA allows for a high absorption capacity, allowing the aggregate to be used as a reservoir to provide additional moisture for improved internal hydration [77]. Moreover, the liquid storage capacity of LWAs enables the utilization of a heat storage system by incorporating phase change materials (PCM) into the LWA. A study by Mohseni et al. 2019 [78], replaced NWA in traditional concrete with porous LWAs impregnated with liquid phase change materials (PCM) to develop a thermal heat storge concrete. This system was utilized to control indoor temperature inside commercial and residential construction projects. The PC with LWAs could be utilized in new applications including latent heat thermal energy storage systems and dry cooling applications. Particularly, some research studies investigated the use of pervious concrete without PCM for evaporative cooling applications [79–81]. While much research is conducted on normal weight PC, which exhibits high strength, only limited studies have examined the effects of LWA replacement in PC on the mechanical and thermal properties of the concrete [15–17]. However, previous studies on the utilization of lightweight aggregate in pervious concrete primarily concentrated on examining how the type of lightweight aggregate influences mechanical properties. The strength of aggregate type was qualitative.[12,13]. Furthermore, they did not propose any measures to regulate the flowability of the cement paste to achieve a measured porosity equal to the designed one. Moreover, a limited range of w/c and porosity were studied.

This study aims to achieve the optimal design for lightweight pervious concrete in terms of both strength and permeability, by investigating the following variables. The effects of aggregate type and LWA replacement ratios in terms of ACV, water-to-cement ratio (w/c) and paste to aggregate ratio (V_{PA}) ratio and flowability of cement paste. To achieve this

goal, a series of PC mixes fabricated with two types of LWAs were summarized and compared to a reference PC fabricated with NWA.

3.2 MATERIALS

3.2.1 Normal and Lightweight Coarse Aggregates Characteristics

In order to produce PC, locally available normal weight aggregate made of siliceous crushed stone (SCS), and two lightweight aggregates were used. The siliceous crushed stone (SCS) is referred to as NWA. The LWAs are an expanded clay referred to as LWA 1 and a western shale referred to as LWA 2. Ordinary Type 1 Portland cement is used in this study. PC mixtures were made using a single size aggregate passing a 9.5 mm sieve and retained on sieve No.4 (Opening size of 4.75 mm). The aggregate physical properties are listed Table 3-1. Selected photos of the normal and lightweight aggregates used in this study are shown in Figure 3-1.

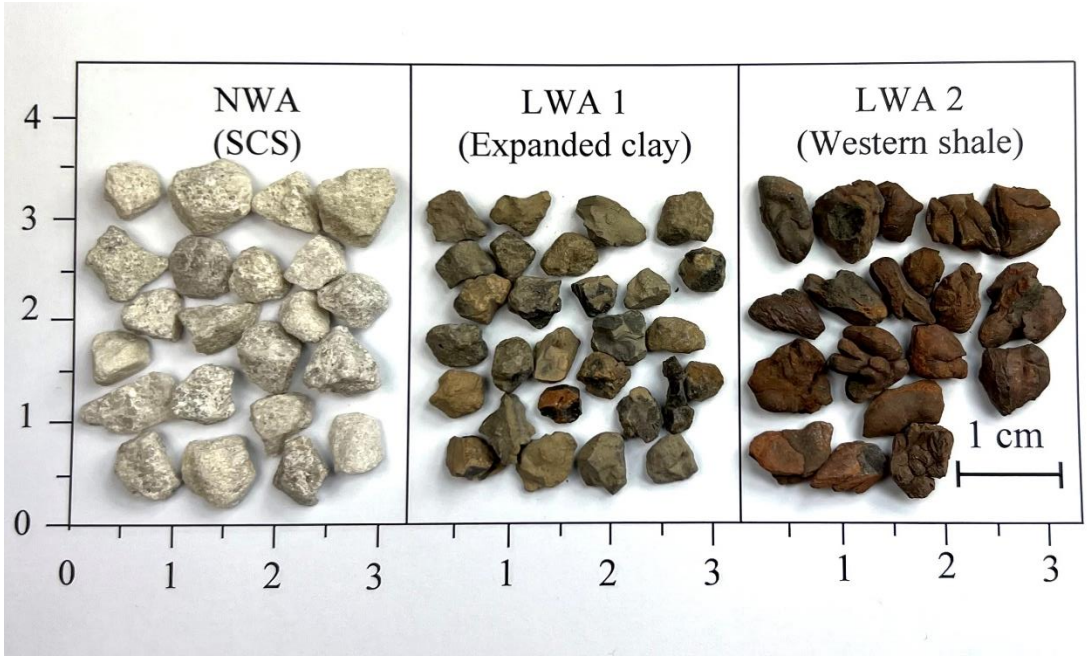
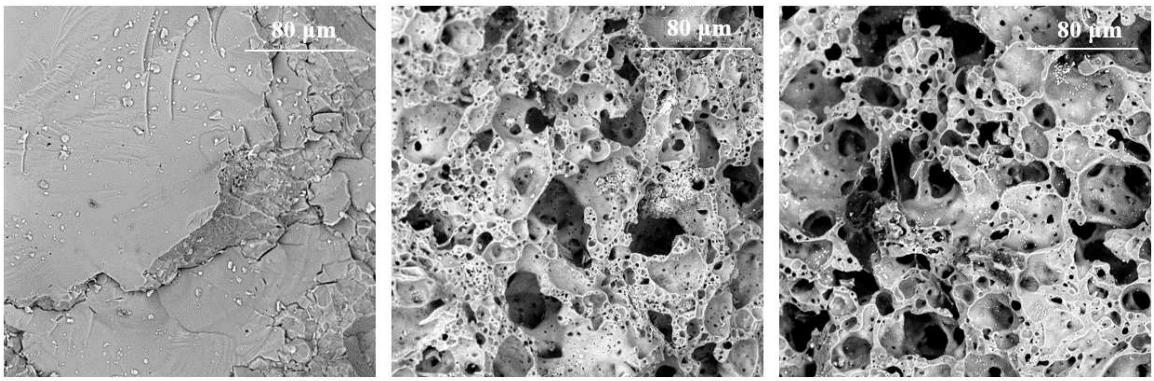


Figure 3-1: Normal weight and lightweight aggregates used, scale: cm.

Table 3-1: Properties of aggregates used in this study to prepare PC mixes.

Quantity	Aggregate Type		
	NWA (SCS)	LWA 1 (Expanded clay)	LWA 2 (Western shale)
Unit weight (kg/m^3)	1530	606	520
Void content (%)	42.9	44.2	41.4
Specific gravity (-)	2.61	1.11	1.08
Water absorption by mass (%)	0.87	16.6	15.2

The pore structure of NWA, LWA 1, LWA 2 was examined with Scanning Electron Microscope (SEM) at 1000x magnification level and selected images from the SEM analysis are shown in Figure 3-2. In these images, the dark area represents the pores while the light-colored area is the pore skeleton. It can be observed that the NWA has a solid internal structure as shown in Figure 3-2 (a), which resulted in a high specific gravity and relatively low water absorption (<1%). However, LWAs are a highly porous material with an interconnected pore structure as presented in Figure 3-2 (b) and (c), which resulted in lower specific gravity and higher water absorption (see Table 3-1). It is important to note that this difference in the internal pores structure of lightweight aggregates compared to normal weight aggregates is indicative to low strength and stiffness aggregates as will be discussed in the following subsection.



(a) NWA (SCS) (b) LWA 1 (Expanded clay) (c) LWA 2 (Western shale)

Figure 3-2**:** SEM images of different aggregate.

3.2.2 Aggregate Crushing Value

The crushing tests are used to evaluate the resistance of aggregate to crushing, allowing for the evaluation of how the characteristics of mineral aggregates impact the performance of both asphalt concrete (AC) and permeable asphalt (PA). Due to the excessive contact pressure between adjacent aggregates as a result of vehicle load, the crushing values of aggregate (especially the coarse portion) is crucial for the durability and stability of permeable asphalt (PA) mixtures [84]. For example, Reyna et al. [85] evaluated alternative test methods including Los Angeles, micro-Deval, soundness magnesium, acid insoluble, and aggregates crushing value to determine the crushing potential of aggregates and noted the impact of coarse aggregate characteristics on asphalt mixture engineering properties. In this study, the aggregate crushing value method was adopted to assess the crushing potential of the LWAs, and NWA used to fabricate PC mixes. The aggregate crushing value (ACV) test was conducted to assess strength and measure the resistance of the aggregate to crushing under a monotonic compressive load in accordance with the ISO 20290-3 [86]. The ACV test is performed on aggregate that is 100% passing through a 9.5 mm sieve and 100% retained on sieve No. 4. (4.75 mm). For the ACV test, the coarse aggregates were

filled in a cylindrical mold in three layers as shown Figure 3-3, where each layer was tamped 25 times from a height of 50 mm using the rounded end of the tamping rod. The surface of the top layer then was leveled off using the tamping rod, which was used as a straight edge. A steel plunger was placed and leveled at the top of aggregate prior to the application of a gradual compression load of 400 kN over a period of 10 min ± 30 s. The aggregate specimen then was sieved through a No. 8 (a 2.36 mm opening size sieve) sieve to determine the crushing value. The aggregate crushing value (ACV) is defined as the percentage of the mass specimen portion passing through the 2.36 mm sieve to the total mass of the specimen [86,87]. The ACV is estimated using Equation (3.1).

$$\text{ACV} = \left[\left(\frac{M_2}{M_1}\right)\right] \text{x } 100\% \tag{3.1}$$

where ACV: aggregate crushing value, %, M_1: total mass of aggregate specimen, kg, and M_2: mass of specimen portion passing 2.36 mm (No.8) sieve after compression loading, kg.



Figure 3-3: (a) Aggregate crushing value test setup, and (b) aggregate specimen during compression loading.

3.2.3 Pervious Concrete Design

A total of twelve PC mixes were fabricated to study different parameters, the effect of aggregate type and LWA volumetric replacement ratio in term of ACV, water to cement (w/c) ratio, paste to aggregate volume V_{PA} ($V_{Paste}/V_{Aggregate}$) volumetric ratio and porosity on mechanical and hydraulic properties. The concrete mix proportions and parameters are summarized in Table 3-2. The amount of cement (C), aggregate (A), lightweight aggregate (L) and/or normal weight aggregate (N) and total free water (W) is included. A standard designation is used for identifying the mixes; LWA/NWA-w/c-V_p/V_{agg} which consists of % Lightweight Aggregate, % Normal Weight Aggregate, water-to-cement ratio, and cement paste to aggregate ratio by volume. For example, 75LWA/25NW-0.32-0.36, designates 75% LW aggregate, 25% NW aggregate, 0.32 w/c ratio, and cement paste to aggregate ratio of 0.36. The design w/c ratios were 0.24, 0.28, 0.30, 0.32 or 0.34. while the V_{PA} included 0.21, 0.31, 0.36, 0.40, and 0.49. A high range water reducing (HRWR) admixture was used to achieve the appropriate flow of the paste. The HRWR used for this study consisted of polycarboxylate-based material (MasterGlenium 7500, Master Builders Solutions, Ontario, Canada). The HRWR was proportioned to achieve the same paste spread for different w/c ratios. The spread was determined in accordance with ASTM C230 [88] flow table test as will be discussed in the following subsection.

Table 3-2: Normal weight and lightweight PC mix proportions (kg/m^3).

Mix ID#	Mix code	P (%)	C	A		W	V_{PA}	Parameter change
				N	L			
M1	100NWA-0.32-0.34	30.8 ± 0.50	281	1359	0	90	0.34	Aggregate type
M2	100LWA1-0.32-0.38	30.9 ± 0.10	301	0	549	96	0.38	
M3	100LWA2-0.32-0.31	29.3 ± 0.15	258	0	595	82	0.31	
M1	100NWA-0.32-0.34	30.8 ± 0.50	281	1359	0	90	0.34	LWA replacement
M4	50LWA2/ 50NWA-0.32-0.36	32.6 ± 1.50	290	672	286	93	0.36	
M5	75LWA2/ 25NWA-0.32-0.36	29.1 ± 0.60	296	333	425	95	0.36	
M3	100LWA2-0.32-0.31	29.3 ± 0.15	258	0	595	82	0.31	
M6	100LWA2-0.24-0.31	28.3 ± 0.20	294	0	595	71	0.31	w/c ratio
M7	100LWA2-0.28-0.31	29.5 ± 1.00	274	0	595	77	0.31	
M8	100LWA2-0.30-0.31	29.6 ± 0.25	266	0	595	80	0.31	
M3	100LWA2-0.32-0.31	29.3 ± 0.15	258	0	595	82	0.31	
M9	100LWA2-0.34-0.31	31.3 ± 0.90	250	0	595	85	0.31	
M10	100LWA2-0.30-0.49	20.3 ± 1.50	427	0	595	128	0.49	Porosity
M11	100LWA2-0.30-0.40	25.3 ± 0.10	346	0	595	104	0.40	
M8	100LWA2-0.30-0.31	29.6 ± 0.25	266	0	595	80	0.31	
M12	100LWA2-0.30-0.21	37.3 ± 1.80	184	0	595	56	0.21	

To systematically investigate each parameter, it is essential to make the other parameters constant. In the case of investigating the impact of aggregate type on PC, three different aggregate types, specifically crushed limestone (NWA), clay (LWA1), and western shale (LWA2) were used. These PC mixes are denoted by M1, M2 and M3 with a constant water-to-cement ratio (w/c) of 0.32 and target porosity of 30%. The target porosity value was maintained by adjusting V_{PA}. When changing the aggregate type, it is not possible to

standardize both the volume of concrete paste or V_{PA} and porosity simultaneously because the void ratio among aggregates varies with the aggregate type as reported in Table 3-1. Therefore, adjusting the concrete paste volume is necessary to fill these voids and achieve the same porosity value of 30%. For studying the effect of LWA volumetric replacement ratio on PC, NWA and LWA 2 were selected. These PC mixes were prepared with different proportions of LWA at 0%, 50%, 75% and 100%. They are referred to as M1, M4, M5, and M3, respectively, while keeping the w/c value at 0.32 and specifying the porosity value at 30%. The effect of w/c ratio on the performance of PC was examined in four mixes, M6-M9, which were fabricated using 100% LWA 2. The mixes were designed to have porosity (P) in the range of 30 ± 1% and a w/c ratio of 0.24, 0.28, 0.30, 0.32, or 0.34 at same V_{PA} of 0.31. However, to standardize the porosity value, the flowability value was adjusted. Porosity is not solely dependent on the volume of concrete paste but also on its flowability. Since flowability is influenced by changes in w/c ratio, the High Range Water Reducer (HRWR) dosage used to achieve consistent flowability was adjusted. To study the influence of porosity and V_{PA} on PC; M8, M10, M11, and M12 PC mixes were prepared. For these mixes a w/c ratio of 0.30 was used with porosity ranging from 20 to 37%. For these mixes it was examined for LWA 2 at a w/c ratio of 0.30.

3.2.4 Mix Design and PC Fabrication

The mix design approach proposed by the National Ready-Mix Concrete Association (NRMCA) was adopted [89]. Due to the high potential absorption of the LWAs they were saturated for 24 hours to minimize the amount of water absorption during mixing and placing [90]. The excess water was drained from the aggregate for four hours. Aggregate moisture content was measured prior to batching to account for the surface water present

allowing for adjustment of the water content. A consistent procedure was used to produce aggregates with the same initial conditions in all PC mixes fabricated. A consistent mixing procedure similar to that reported by Schaefer et al. [91]. The saturated aggregate and 5% of total weight of cement were mixed in an auto mortar mixer (Collomix TMS 2000, WAYNE, NJ, USA) for 1 minute. The remaining cement, water (i.e., the amount of water according to the mix design minus the amount of water already absorbed by the aggregate), and HRWR were then mixed for three minutes. The mix was allowed to rest for two minutes before continuing for another three minutes of mixing. According to Schaefer et al. [91], this approach improves the bond between the cement paste and aggregate and has been shown to result in failure through the aggregate and an increase in the compressive strength. Next, pervious concrete mixtures were mildly compacted using a vibration table for ten seconds. Samples were allowed to cure for 24 hours in air prior to being placed in a water bath at 20 ± 1 °C for 28 days.

3.3 METHODOLOGY

3.3.1 Cement Paste Flowability

Compared to normal concrete, the volume of cement paste used in pervious concrete is minimal, consequently, the rheological characteristic of binder plays a critical role on the quality of pervious concrete [92]. The effect of paste flow on the PC mix is examined. During preliminary tests, PC mixes were prepared at different w/c ratios with same HRWR dosage of 980 ml/100kg. The results showed that samples with low water-to-cement ratio (w/c) are not sufficiently workable, ultimately resulting in larger porosity compared to the targeted porosity. Contrast, when the w/c ratio is high, workability exceeds the necessary limit, causing the cement paste to seep downward during compaction, forming a layer.

However, at a w/c ratio of 0.30, it was observed that the samples achieved the targeted porosity. Therefore, adjustments were made to the HRWR values to provide the same flowability as the sample designed with a w/c ratio of 0.30. The dosage of the HRWR needed to achieve the same paste flow for different w/c ratios was determined in accordance with ASTM C230 [88], flow table test as shown in Figure 3-4. The spread diameter for the paste prepared at a w/c of 0.30 with HRWR dosage of 980 ml/100 kg was 250 mm as shown in Figure 3-4. The HRWR dosage was adjusted (i.e., increased) for the lower w/c ratio pastes until a 250 mm flow diameter was achieved, the modified dosages then were used to fabricate PC mixes. The flow table test was performed for pastes at w/c ratios of 0.32 and 0.34. These pastes were excessively workable at a HRWR dosage of 980 ml/100kg, consequently, the HRWR amount was reduced to achieve target flow and yield design porosity. It is important to note that it was not possible to measure the spread diameter at w/c ratio of 0.32 and 0.34, the spread diameter was greater than 250 mm, which is the diameter of the flow table. The pastes with a consistent flow of 250 mm spread were used to fabricate PC mixes. The flow measurements at the initial HRWR dosage and the HRWR dosage at the target flow for all pastes used to fabricate PC mixes at different w/c ratios is summarized in Table 3-3.

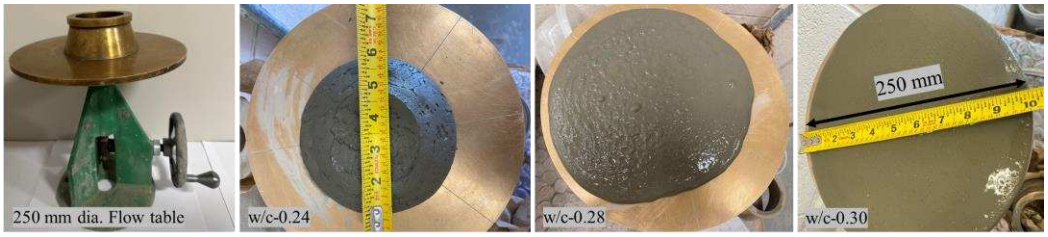


Figure 3-4: Flow measurement of recommended HRWR dosage.

Table 3-3: HRWR dosage and paste spread for varying w/c ratios.

w/c	HRWR [Initial dosage] ($ml/100kg_{cement}$)	Flow [Initial dosage] (mm)	HRWR [Modified dosage] ($ml/100kg_{cement}$)	Flow [Modified dosage] (mm)
0.24	980	150	1825	250
0.28		200	1043	
0.30		250	980	
0.32		>250	453	
0.34		>250	376	

3.3.2 Porosity of Hardened Samples

The porosity of PC specimens can be determined by calculating the weight difference between the oven dry weight and the submerged weight, as indicated in Equation (3.2). The porosity of hardened PCPC can be determined following the guidelines outlined in ASTM C1754 [93].

$$P = \left[1 - \left(\frac{W_2 - W_1}{\rho_w V_T}\right)\right] 100\% \quad (3.2)$$

Where P is the porosity (%), W_2 is the submerge sample mass (kg), W_1 is the oven dry sample mass (kg), ρ_w is the density of water (kg/mm^3) and V_T is the volume of the sample (mm^3). However, when obtaining the oven dry weight, the moisture present in the internal pores of lightweight aggregate will be evaporated. As a result, the porosity value will increase to include the voids between the aggregate particles and the internal pores of the aggregate itself. To overcome this limitation, the oven dry weight (W_1) in the oven has been adjusted to be (W_1') by incorporating the absorption value of the aggregate as indicated in Equation (3.3).

$$W_1' = W_1(1 + V_A.\omega.\rho_w) \quad (3.3)$$

Where W_1' is the modified sample oven dry mass (kg), V_A is the aggregate portion by volume in mix, and ω is the aggregate absorption by volume (%).

3.3.3 Water Permeability

To determine the coefficient of water permeability for the PC samples, a total of three representative samples from each mixture were prepared by casting them into PVC pipes with a 76.2 mm inner diameter and 100 mm length. These samples were tested using a falling head permeameter. The experimental setup for the falling head permeability test is shown in Figure 3-5. The permeability test was performed in accordance with ASTM D5084 [94]. The coefficient of permeability was determined using a 52 mm head drop from 146 mm (h_1) to 94 mm (h_2). The average k of three specimens were determined using Equation (3.4).

$$k = \frac{a \cdot L}{A \cdot t} \ln\left(\frac{h_1}{h_2}\right) \quad (3.4)$$

Where k is the coefficient of permeability (cm/sec), a is the cross-sectional area of the standpipe (mm^2), L is the length of sample (mm), A is the cross-sectional area of specimen (mm^2), t is the time for water to drop from h_1 to h_2 (seconds), h_1 is the initial water level (mm) and h_2 is the final water level (mm).

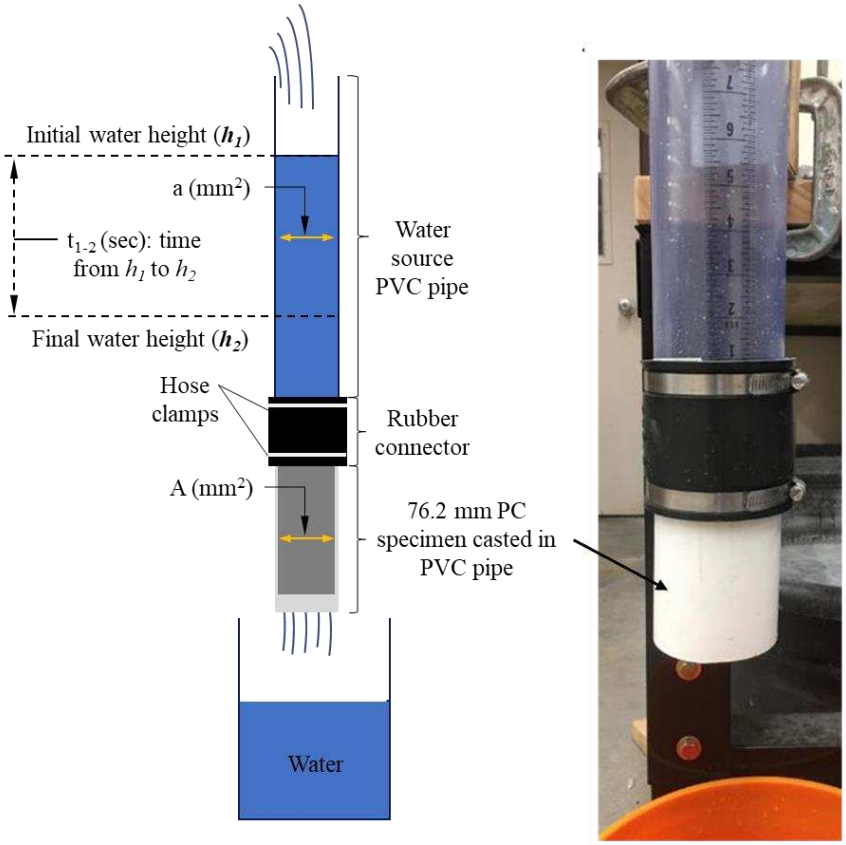


Figure 3-5**:** Falling head permeameter used to measure the water permeability of PC specimens.

3.3.4 Mechanical Properties Measurements

Compressive strength, split tensile strength and elastic modulus were determined for the materials fabricated. The tests were conducted on standard 100 mm diameter and 200 mm long cylinders. Cylinders were water cured and removed at an age of 7 and 28 days. The specimens were air dried for 24 hours at room temperature prior to testing. The tests were conducted in accordance with ASTM C39 [95], ASTM C496 [96] and ASTM C469 [97].

3.4 RESULTS AND DISSCUSION

The mechanical, physical, and hydraulic properties of pervious concrete mixes fabricated with normal and lightweight aggregates were determined in accordance with the

procedures and methods discussed in earlier sections. The measured properties of all PC mixes are summarized in

Table 3-4.

Table 3-4: Measured engineering properties of PC mixes.

Mix ID#	Mix code	Compressive strength (MPa)		Split tensile strength (MPa)	E (GPa)	k (cm/sec)
		8-day	29-day			
M1	100NWA-0.32-0.34	NM	19 ± 1.72	2.6	17.7 ± 0.70	2.6 ± 0.09
M2	100LWA1-0.32-0.38	8.5 ± 0.98	10.5 ± 1.00	1.3	4.0 ± 0.60	2.3 ± 0.03
M3	100LWA2-0.32-0.31	6.7 ± 0.40	7.4 ± 0.34	1.1	3.1± 0.30	2.5 ± 0.07
M1	100NWA-0.32-0.34	NM	19.0 ± 1.72	2.6	17.7 ± 0.70	2.6 ± 0.09
M4	50LWA2/50NWA-0.32-0.36	10.3 ± 1.17	11.2 ± 0.94	1.3	8.9 ± 0.70	3.6 ± 0.15
M5	75LWA2/25NWA-0.32-0.36	10.1 ± 0.89	10.3 ± 0.69	1.1	8.4 ± 0.30	3.3 ± 0.28
M3	100LWA2-0.32-0.31	6.7 ± 0.40	7.4 ± 0.34	1.1	3.1 ± 0.30	2.5 ± 0.07
M6	100LWA2-0.24-0.31	9.0 ± 1.08	9.4 ± 0.94	1.3	4.7 ± 0.24	2.3 ± 0.05
M7	100LWA2-0.28-0.31	8.3 ± 1.38	8.4 ± 1.14	1.0	3.4 ± 0.56	2.3 ± 0.07
M8	100LWA2-0.30-0.31	8.7 ± 0.50	10.5 ± 0.79	1.2	4.6 ± 0.40	2.4 ± 0.12
M3	100LWA2-0.32-0.31	7.8 ± 0.40	7.9 ± 0.34	1.1	3.1 ± 0.30	2.5 ± 0.07
M9	100LWA2-0.34-0.31	6.7 ± 0.62	7.4 ± 0.26	1.1	3.5 ± 0.40	3.6 ± 0.13
M10	100LWA2-0.30-0.49	6.6 ± 0.13	8.0 ± 0.44	1.0	6.4 ± 0.40	1.2 ± 0.05
M11	100LWA2-0.30-0.40	8.3 ± 0.68	11.1 ± 0.54	1.3	4.6 ± 0.20	2.4 ± 0.08
M8	100LWA2-0.30-0.31	8.7 ± 0.50	10.5 ± 0.79	1.1	4.4 ± 0.40	3.8 ± 0.12
M12	100LWA2-0.30-0.21	2.8 ± 0.10	3.2 ± 0.34	1.0	2.4 ± 0.50	6.8 ± 0.21

3.4.1 Effect of aggregate type

To investigate the impact of aggregate type on mechanical and hydraulic properties, three mixes were fabricated with NWA (M1), LWA 1 (M2), and LWA 2 (M3), respectively. The total average porosity of these PC mixes was similar and in the range of 30 ± 1% with a coefficient of variation (COV) of 2.95%. This similarity in porosity and w/c across all three

mixes enables a meaningful comparison of results. Selected photo for cuts through PC specimens made with NWA, LWA 1, and LWA 2 are shown in Figure 3-6.

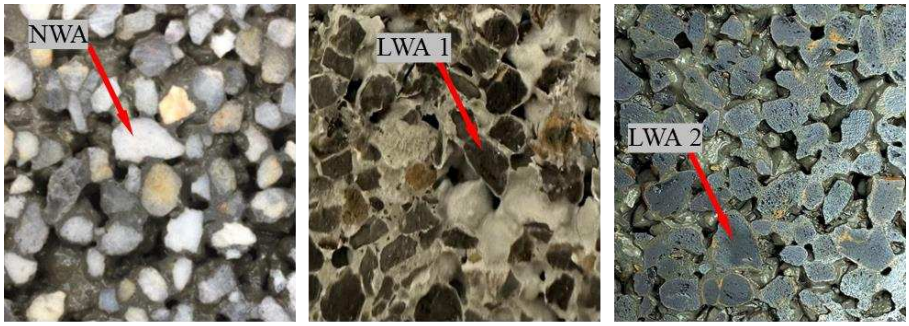


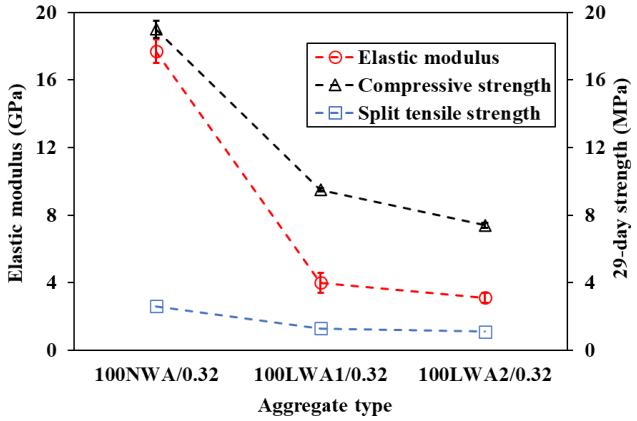
Figure 3-6: Cross sections of PC mix specimens made with different aggregate types.

The compressive strength, split strength and elastic modulus of PC incorporated with LWA1 and LWA2 were significantly lower compared to PC utilized with NWA, as indicated in

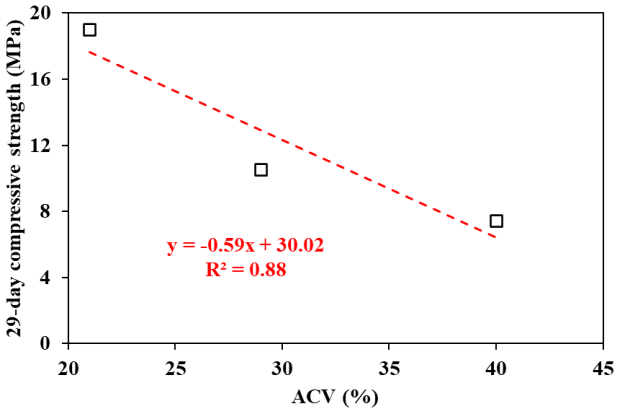
Table 3-4. Specifically, the 29- compressive strength and split strength of LWAs-PC mixes were reduced by 50% to 61% and 50% to 58% respectively, when compared the ones fabricated with NWA as shown in Figure 3-7 (a). This is attributed to the aggregate crushing value (ACV) of these aggregates. The ACV test was performed on representative samples for NWA, LWA 1, and LWA 2 to investigate the relationship between aggregate type in terms of aggregate strength or aggregate potential to crushing and the compressive strength of mixes (M1-M3). NWA aggregates showed a limited susceptibility to crushing, indicated by a low ACV of 21%. In contrast, LWA 1 displayed moderate resistance to crushing, with an ACV value of 29%, whereas LWA 2 exhibited the poorest resistance due to its high ACV value of 40%. The results demonstrate a linear decreasing of compressive strength with increasing ACV on mixes (M1-M3) as shown in Figure 3-7 (b). The percentage of

reduction in ACV for LWA1 and LWA2 was 28% and 45% when compared to ACV of the NWA, respectively. Meanwhile, the percentage of reduction in compressive strength of PC mixes M2 and M3 made with LWA 1 and LWA 2 was 45% and 61% when compared to M1, respectively.

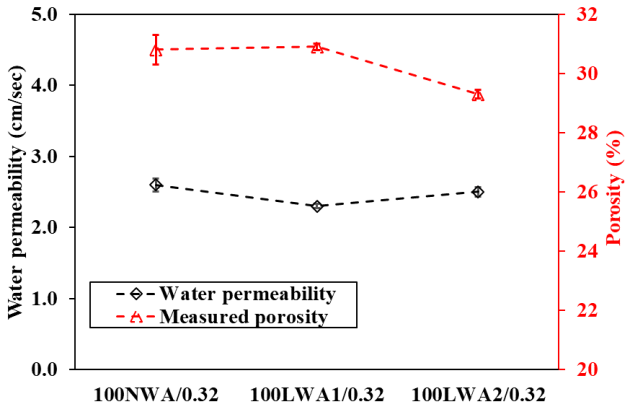
On other hand, the changes in hydraulic conductivity of these mixes [i.e., M1-M3] are not significant since the porosity and aggregate size are almost the same [98]. The relationship between the water permeability for each aggregate and the 29-day compressive strength is shown in Figure 3-7 (c).



(a)



(b)



(c)

Figure 3-7**:** (a) Mechanical performance of PC specimens with different aggregate type; (b) Relationship between aggregate crushing value and PC specimens' compressive strength; (c) hydraulic properties of PC specimens with different aggregate type.

3.4.2 Effect of LWA volumetric replacement

The impact of LWA replacement ratio on mechanical and hydraulic properties of PC were examined using M1, M3-M5 mixes. The measured porosity of M1, M3-M5 are all at 30 ± 2% with COV of 5.33%, which allows for the comparison between the fabricated specimens. The weighted average of ACVs for mixes are 0.21, 0.31, 0.35 and 0.40 respectively. Figure 3-8 shows a cut through M1, M3, M4 and M5 PC specimens at w/c of 0.32 and design porosity of 30%.

The compressive strength, split strength, and elastic modulus decrease linearly with an increase in the ACV, as illustrated in Figure 3-9 (a). This trend persists even with a complete replacement of normal aggregate with lightweight aggregate, resulting in values of 61%, 58%, and 82% for compressive strength, split strength, and elastic modulus, respectively. Figure 3-9 (b) indicates that the 25% NWA and 75% LWA exhibited the lowest porosity compared with 50% NWA/50% LWA and 100% LWA at the same w/c and V_{PA} ratios. This phenomenon is likely due to the packing density effect [99] which occurs due to the variation in aggregate shape on the blended mixes.

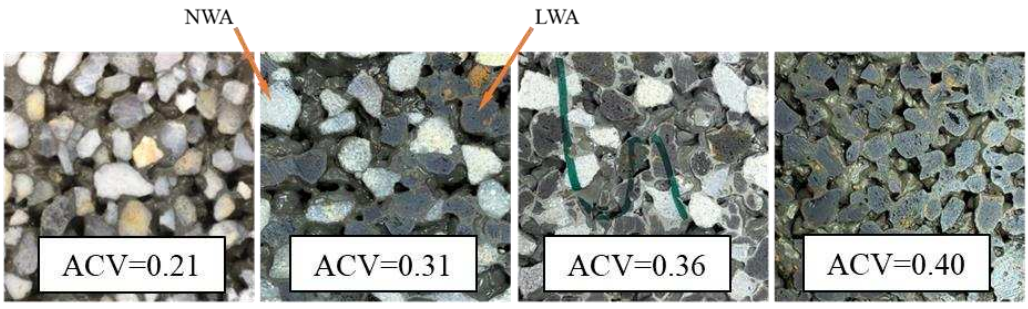
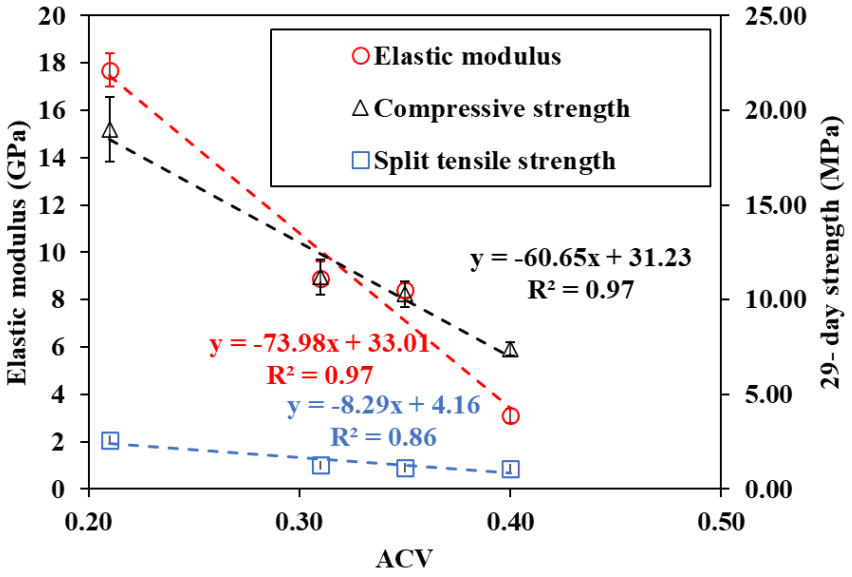
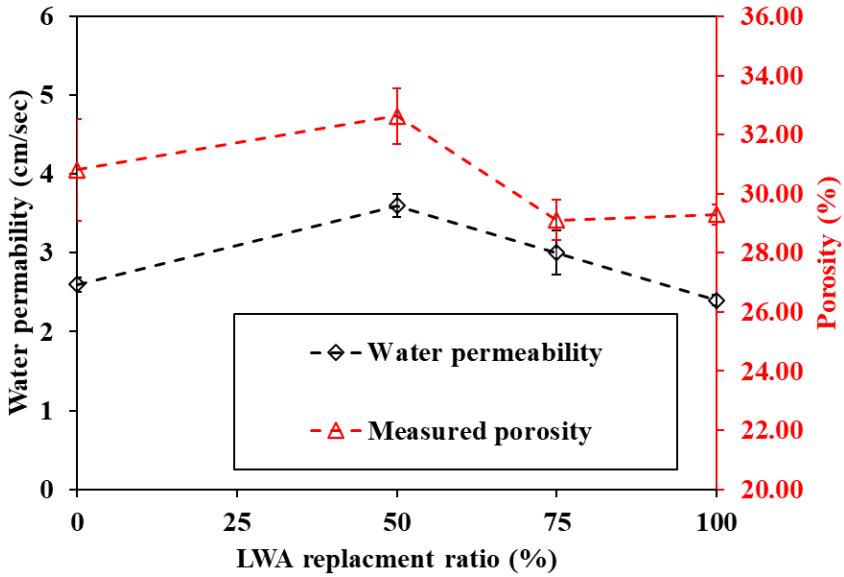


Figure 3-8**:** Cross sections of PC specimens prepared at different replacement ratios.



(a)



(b)

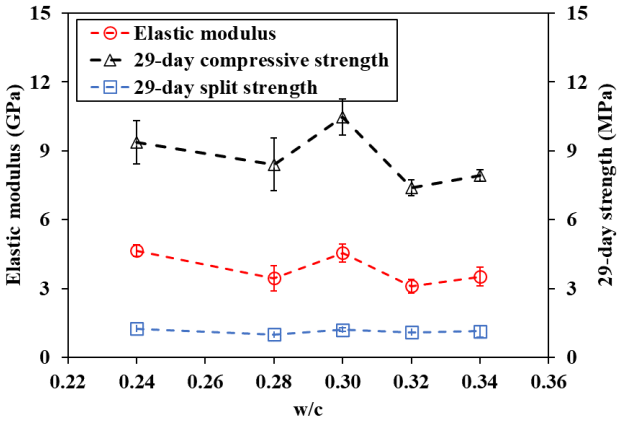
Figure 3-9: (a) Effect of aggregate replacement in term of ACV on compressive, split tensile strength, and modulus of elasticity; (b) Effect of aggregate replacement on hydraulic properties.

3.4.3 Effect of w/c ratio

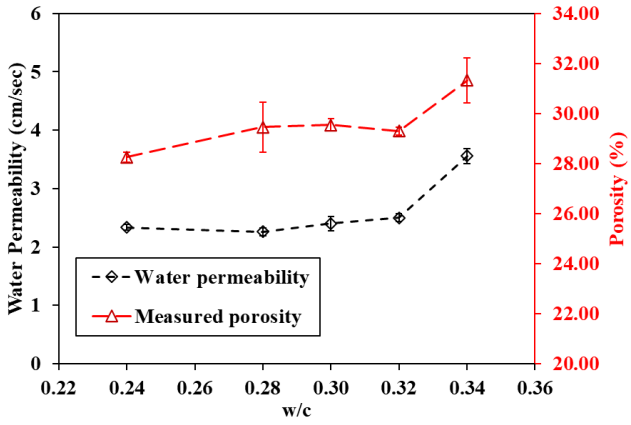
A series of PC mixes [M3, M6-M9] was fabricated with 100% LWA 2 with design porosity of 30 % to investigate the w/c effect. As reported in

Table 3-4, the measured porosity of M3, M6-M9 are all at 30 ± 2% with COV of 3.65 %, which allows for the comparison between the fabricated specimens. The strength variation with different w/c ratio is not significant as all samples consistently exhibit strengths within the range of 8 to 10 MPa as shown in Figure 3-10 (a) and this due to the failure mode in samples. Generally, in LWA concrete failure occurs within the aggregate [100]; consequently, changes in the w/c have an insignificant impact on strength when the porosity of PC mixes is equal, as the failure does not occur within the paste or interface. This contrasts with Pereira da Costa et. al. study [59], which suggests that w/c ratio does affect strength values. However, the actual impact lies in porosity changes, as the study did not account for consistent porosity amidst w/c ratio variations due to the challenge of maintaining flowability of cement paste same. As depicted in Figure 3-10 (a), the highest strength value was observed at a w/c of 0.30, whereas the lowest occurred when failure partially shifted to the interface at w/c of 0.34 as shown in Figure 3-11. Figure 3-10 (b) shows the permeability and porosity obtained for all specimens at different w/c ratios. As the dosage of HRWR is controlled, the porosity of all mixes is in good agreement. Despite the porosity falls in a narrow range, mixes have shown different permeabilities. Water permeability shows an increase with higher w/c ratios. This rise in water permeability is attributed to differences in void structure formation at varying water-to-cement ratios as shown by Li et al. [101]. PC has two forms of porosity: total porosity and interconnected porosity. The interconnected porosity consists of interconnected void channels that allow

passage of liquid (or air) through the concrete. The measured porosity in this study consists of the total porosity which includes both the interconnected voids as well as closed voids within the paste matrix. Mix M9 showed a higher permeability than mixes at lower w/c ratios due to the higher porosity which could be due to the change in pores tortuosity and pore sizes developed at high w/c ratio [59].



(a)



(b)

Figure 3-10**:** (a) Compressive, split tensile strengths, and stiffness of PC specimens fabricated with LWA 2 at different w/c ratio; (b) Porosity and permeability of PC specimens fabricated with LWA 2 at different w/c ratio.

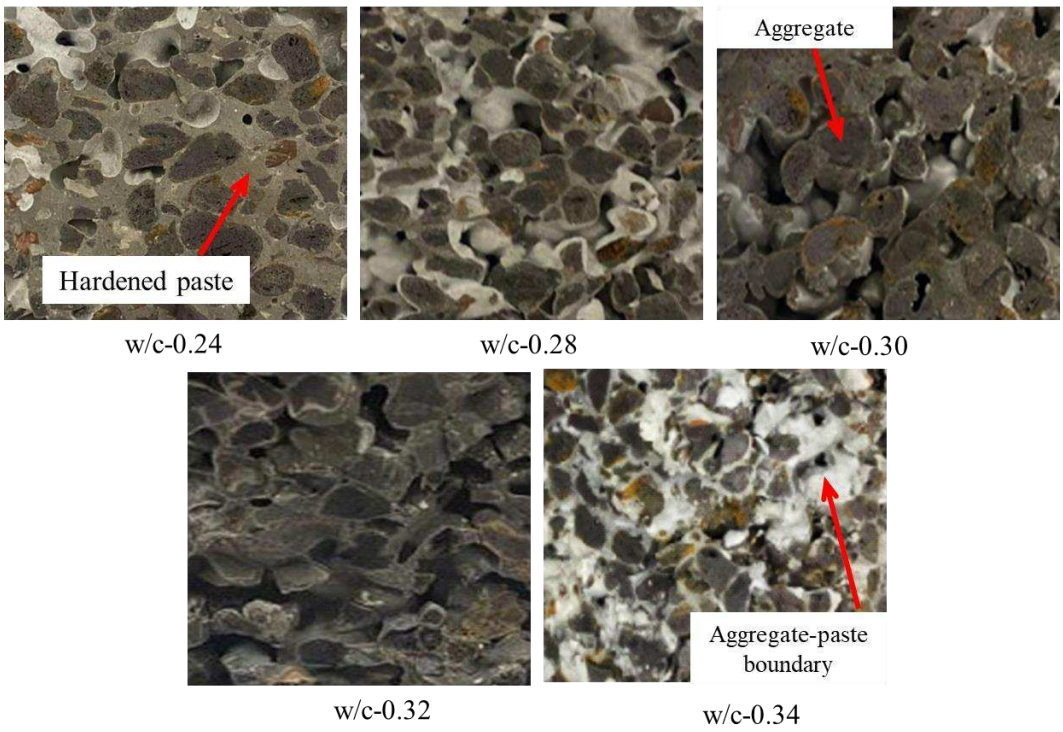


Figure 3-11**:** Failure surface of lightweight PC specimens prepared at different water to cement (w/c) ratios.

3.4.4 Effect of PC Porosity and V_{PA}

The impact of porosity of PC was evaluated through fabricating mixes M8, M10-M12 at w/c of 0.30 with 100% LWA 2 by volume. Varying mix porosity resulted in a range of paste to aggregate volume (V_{PA}) ratio. As the cement paste content (V_{PA}) decreases the porosity increases to an upper limit equal to the void content of the LWA 2 (41.40%) as shown in Figure 3-12 (a). As reported in Figure 3-12 (b), 29-day compressive strength and split tensile strength increased with porosity, the measured strength increases until reaching a maximum value in the range of 25.3 to 29.6% then decreases with porosity. The observed phenomenon can be elucidated by considering the influence of variations in the quantity of cement paste on the control of porosity within the concrete mix. At a porosity level of 20.3%, the mixture exhibits the highest amount of cement paste as shown in Figure 3-12 (c), resulting in localized failure within the cement paste itself. However, as porosity

gradually increases and the amount of cement paste decreases, the failure mechanism shifts progressively from the cement paste to the aggregate. This transition occurs within a porosity range of 25.3% to 29.6%. Beyond this optimum range, there is a reversal in the process. As porosity continues to rise and the amount of cement paste decreases, the insufficient quantity of cement paste hinders effective bonding between aggregate particles. Consequently, the strength value undergoes a decline, reaching its minimum, leading to bonding failure within the concrete structure at a porosity of 37.3%. Selected photos for PC specimens' failure at different porosity and same w/c ratio are shown in Figure 3-13. As can be seen in Figure 3-13 (a), the mix M10 failed mainly through hardened paste, which resulted in a lower strength. The PC mixes yielded higher strengths (i.e., M8 and M11), For these mixes, the amount of paste was sufficient to create a strong bond between paste and aggregate, which led to a failure mainly through aggregate, thus, higher strengths as shown in Figure 3-13 (b) and (c). However, the mix M12 mix that has the highest porosity failed mainly through interface as shown in Figure 3-13 (d). This is mainly due to the low amount cement available to coat aggregates, which resulted in a weak bond. On other hand, the modulus *E* decreases with increase porosity, since the volume aggregate is same, the stiffness increase with increase cement paste compared to voids in the PC mixes as shown in Figure 3-12 (b).

The water permeability coefficient of M8, M10-M12 was found to be increase with increase porosity linearly as shown in in Figure 3-12 (d).

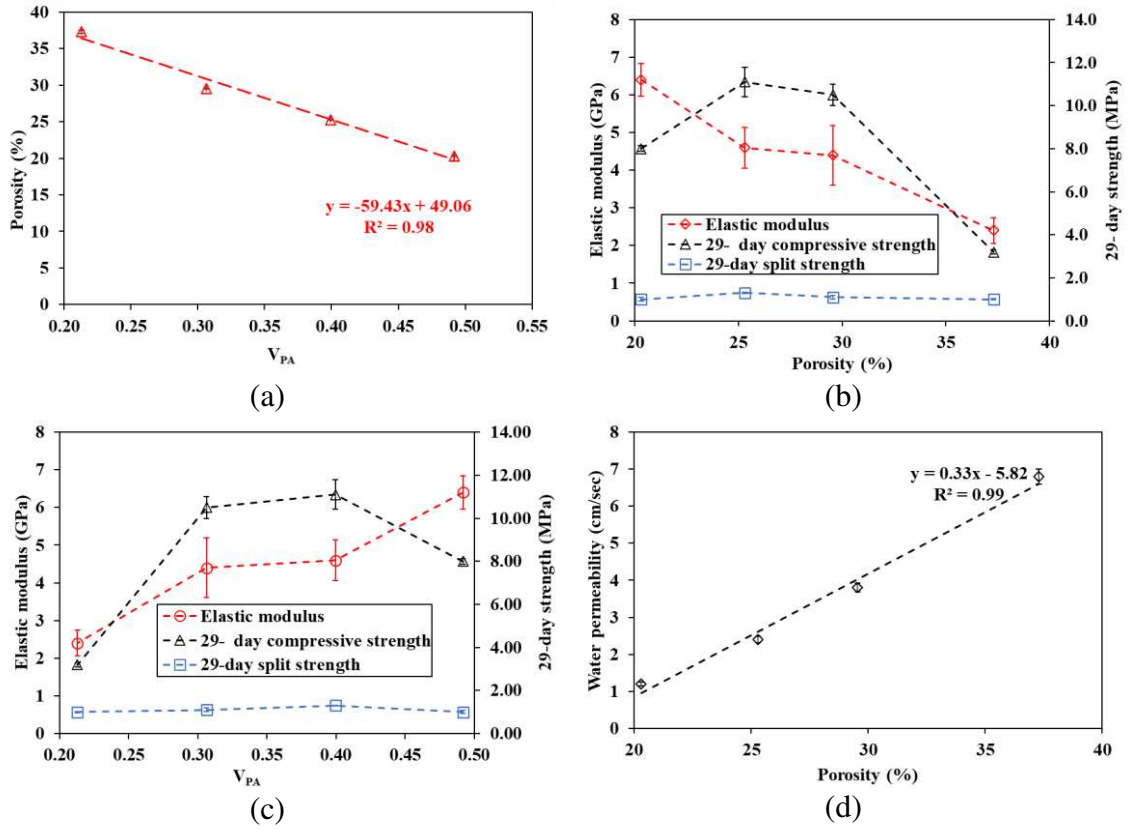


Figure 3-12: (a) Compressive, split tensile strengths, and stiffness of PC specimens fabricated with LWA 2 at different porosity; (b) permeability of PC specimens fabricated with LWA 2 at different porosity.

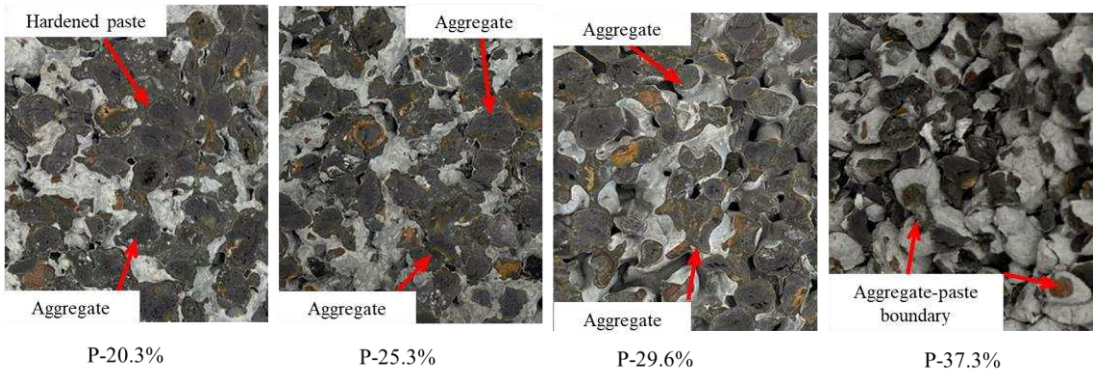


Figure 3-13**:** Failure characteristics of LWA-PC specimens fabricated at different porosity.

3.4.5 Split and Compressive Strength Relationship

The 29-day compressive strength and split tensile strength of M1-M12 mixes were plotted as shown in Figure 3-14. The data presented in Figure 3-14 depicts a linear relationship,

with the split tensile strength is 13.27% of the compressive strength. A linear relationship was also reported by Schaefer et al. [91] and Beeldens et al. [71] with fitting parameters as 12.28% and 16.92% respectively.

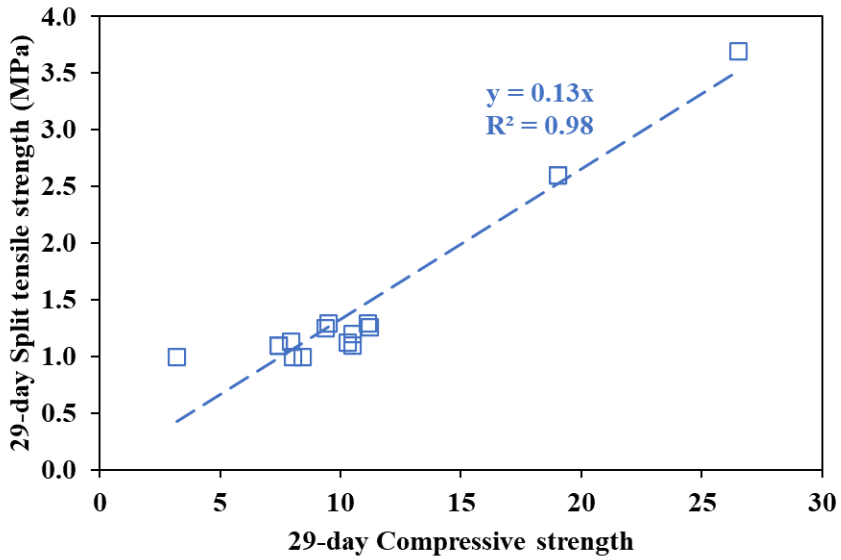


Figure 3-14: The relationship between compressive strength and split tensile strength for all PC mixes.

3.5 SUMMARY AND CONCLUSIONS

In this chapter, the goal was to evaluate the performance of PC made with lightweight aggregate (LWA) compared to conventional PC made with normal weight aggregate (NWA). This study also evaluated the influence of aggregate type, LWA replacement, water to cement ratio, V_{PA} and porosity on the mechanical properties and hydraulic properties of PC. Thus, the following conclusions can be drawn:

- The type of aggregate significantly impacts PC strength and stiffness. PC mixes with 100% LWA by volume exhibit lower compressive and split tensile strength, with reductions up to 61%, 58%, and 82% for LWAs. A linear decrease in compressive strength with an increase in Aggregate Crushing Value (ACV).

- PC strength and stiffness decrease with higher volumetric replacement of LWA. At the level of 100% LWA replacement, the compressive strength, split tensile strength and stiffness decreased about 58, 61, 82%, respectively.
- PC mixes prepared at low w/c ratios and same dosage of HRWR resulted in a less workable mix and high porosity. Adjusting HRWR dosage ensures consistent flowability leads to achieve the same porosity at different w/c.
- The effect of w/c is not significant since the failure mainly in aggregate in LWA concrete. However, at high w/c the failure shifted to be in the interface. The optimum w/c is 0.30.
- Porosity and V_{PA} ratio are controlling factors on the strength and overall performance of PC. The increase in V_{PA} ratio leads to a low porosity. As the porosity increases, the strength of PC increases until reaching a maximum value then starts to decrease due to the change in the failure mode.
- The 29-day compressive strength and split tensile strength exhibit a linear relationship, where the split tensile strength represents 13.27% of the compressive strength.

This chapter delves into the intricate process of designing concrete mixtures specifically tailored for pervious concrete. It focuses on identifying the most effective mix design, utilizing lightweight aggregates to optimize both strength and water permeability characteristics. The objective is to achieve an ideal balance that ensures superior structural integrity while facilitating efficient permeability.

Moving forward, the subsequent chapter will extensively explore the air permeability aspects of these concrete mixtures. It recognizes air as a compressible fluid, and the implications of this understanding play a crucial role in the design of cooling systems. The

analysis will delve into the intricacies of air flow within the PC and how it affects the overall performance and functionality of cooling systems integrated into the design.

Furthermore, the chapter will extend its discussion to encompass the thermal properties inherent in PC mixtures. This exploration aims to unravel the thermal conductivity and specific heat of these mixtures. The ultimate goal is to establish a comprehensive understanding of how PC can function not only as a structural component but also as an efficient cooling system.

4 PRESSURE DROP AND HEAT TRANSFER PROPERTIES FOR NORMAL WEIGHT AND LIGHTWEIGHT PERVIOUS CONCRETE

4.1 INTRODUCTION

Pervious concrete (PC) is typically produced with coarse aggregate of uniform size with little or no fine aggregate [7–10]. PC enables on-site water drainage and localized groundwater replenishment [7] and thus provides a sustainable pavement material and means for addressing stormwater requirements. PC is also useful in reducing noise pollution on roadway surfaces due to reductions in tire–pavement interaction [48,49]. To date, several studies have investigated the effect of porosity on PC strength and permeability. Based on these studies, the permeability is proportional to the porosity [101,102] and is dependent on the aggregate surface area, the pore radius, the tortuosity, and the aggregate to cement paste ratio [103–105]. In general, the water permeability of PC has been examined in detail in the literature, for stormwater drainage applications using a falling water head method [106–109].

An alternative application for pervious concrete is to utilize it for cooling tower applications. Researchers have investigated the use of pervious concrete for evaporative or wet cooling applications [110,111]. Timmer [110] employed PC in the process of evaporative cooling, conducting his experiment using a PC wall with dimensions of 0.91 x 0.91 x 0.20 m. Water was used in the cooling process, and the results indicated the following findings: during the 114-hour experiment, approximately 34 liters of water were utilized, with around 50% by volume being evaporated; and by calculating the water density and latent heat of evaporation, it is estimated that the system absorbed approximately 24 kilowatt-hours (kWh) of energy throughout the experiment. This

approach involves saturating the pervious concrete and forcing air through the panel. Rahman et. al. [111] investigated the use of PC as an evaporative cooling pad. They conducted a wind tunnel test with varying inlet air temperatures while keeping the air velocity constant at 2.5 m/s. The PC evaporative cooling pad demonstrated a higher performance than conventional cooling pad systems reported in other studies [112–114]. Dry cooling applications, which is the focus of this research, are also a viable application for PC panels. The high specific heat and thermal mass of PC provides inherent sensible heat capacity which can be used to regulate temperature within a structural system. Furthermore, utilization of lightweight porous aggregates provides the opportunity to store latent heat by infusing phase change materials (PCMs) within the aggregates prior to concrete fabrication. Determining the efficiency of dry cooling tower applications necessitates a comprehensive examination of both the magnitude of pressure drop and thermal properties. Generally, the porous medium introduces additional pressure drop, consequently reducing the airflow within the dry cooling tower, therefore compromising the overall cooling tower performance [6,115]. However, there is a trade-off between the cooling potential and pressure drop. Essentially, while the cooling potential relies on the porous medium's thermal conductivity for efficient heat exchange, the stored thermal energy is contingent upon the specific heat value of the material used in the medium [11]. To quantify the heat transfer performance of PC for dry cooling tower applications both pressure drop and the thermal characteristics are examined in this paper.

The performance of PC under forced air flow differs significantly from that of water flow. This is due to incompressibility of water as compared to a compressible flow of air. A review of the literature revealed that there are very limited studies that have explored air

permeability of PC. Qin et. al. [62] measured the air permeability of PC using a vacuum to create air flow. The air permeability was measured for two different sizes of normal weight aggregate (50 and 100 mm) and two w/c ratios of 0.23 and 0.25. They found that the air permeability varies from 10^{-9} to 10^{-10} m^2 (i.e., 10^3 to 10^4 Darcy) for the range of aggregate and w/c ratios studied. It is worth noting that their study expressed the air permeability of the PC mixes as a constant value which inherently assumes laminar flow [63]. Due to the void characteristics of PC and its Reynold's number, air flow for most applications is turbulent, resulting in a quadratic relationship between velocity and pressure drop [64]. To more fully characterize the PC air permeability, a wider range of porosities and air velocities are needed.

The thermal properties of PC have been investigated in several studies [116–118]. Researchers have investigated the use of lightweight pervious aggregates for pervious concrete road surfaces and have found that they are able to reduce the thermal conductivity but due to their low albedo tend to increase the roadway surface temperatures [116]. An increase in paste volume results in a decrease in the porosity which tends to increase thermal conductivity and use of lightweight aggregates over limestone will decrease thermal conductivity [117]. Chindaprasirt et. al [117] studied the effect of replacing the cement with fly ash or fine aggregate (by mass) on the thermal conductivity of lightweight PC. The study found that thermal conductivity increases with concrete density increases. As noted, past studies focused only on thermal conductivity, with no information on specific heat variation, over a limited range of PC porosity which investigated in the current paper.

This paper presents an experimental study that quantifies the air permeability and thermal properties of pervious concrete for use in dry cooling applications. While past studies have examined facets of the information needed to understand the cooling performance of pervious concrete no study comprehensively assessed all the facets directly. In this study a relationship between pressure drop and air velocity for PC samples under turbulent air flow conditions is determined. The measured response is compared to an analytical approach based on the work of Ergun, who established a means of estimating pressure drop due to air flow through a packed bed composed of spherical particles [16]. The thermal characteristics, specifically the conductivity and specific heat of the PC and sensible heat energy capacity were determined for normal and lightweight aggregate at water/cement ratios from 0.24 to 0.34 and at porosities ranging from 20% to 37%. Control tests were performed to understand the effects of particle shape or sphericity with packed beds of spherical-shaped steel beads, 20/30 Ottawa sand, and river gravel samples. Using these developed relationships and properties, the performance of pervious concrete for cooling applications is detailed.

4.2 EXPERIMENTAL PROGRAM

4.2.1 Materials

The present study investigates the pressure drop values with variation in the bed material. For this purpose, six different types of bed materials were used as shown in Figure 4-1. steel beads, 20/30 Ottawa sand (Sand), normal weight river gravel (RG), Western Shale lightweight aggregate (LWA), Siliceous normal weight aggregate (NWA), and 30 samples of pervious concrete (PC). Steel beads with a diameter of 4.37 mm were used to verify the test setup. The steel beads are spherical and have a smooth surface, consequently it is

expected that the measured response would correlate with the Ergun equation. The Ottawa sand is a standard uniformly round-grained quartz sand [119–121], while river gravel is rounded stone with a relatively smooth surface. The gravel and lightweight aggregate consist of a limited particle size with 100% passing through U.S. sieve size with opening size 9.5 mm (3/8 in.) and 100% retained on U.S. sieve opening size 4.75 mm (No.4). The limited size was chosen to facilitate fabrication of the pervious concrete as a wide gradation reduces the permeability of the matrix. Standardizing the size across all coarse aggregate types also ensured consistency and comparability within the study. The sand and gravel were utilized as a control to investigate the effect of particle shape on the difference between measured pressure drop and predicted pressure drop by Ergun equation.

Ordinary Type 1 Portland cement is used in this study. PC mixtures were made using a single size aggregate passing a 9.5 mm sieve and retained on sieve No.4 (Opening size of 4.75 mm). The aggregate physical properties are listed in Table 4-1.

Table 4-1: The physical properties of granular materials.

Granular Type	**Sand**	**LWA**	**RG**	**NWA**
Material Type	Quartz	Western Shale	Crushed-River Stone	Crushed Limestone
Bulk Density (kg/m^3)	1980	520	1920	1530
Void ratio (%)	34.06	41.40	38.85	42.87
Specific gravity	2.65	1.08	2.62	2.61
Size range (mm)	0.60-0.85	4.75-9.50	4.75-9.50	4.75-9.50
D_p (mm)	0.73	7.10	7.10	7.10

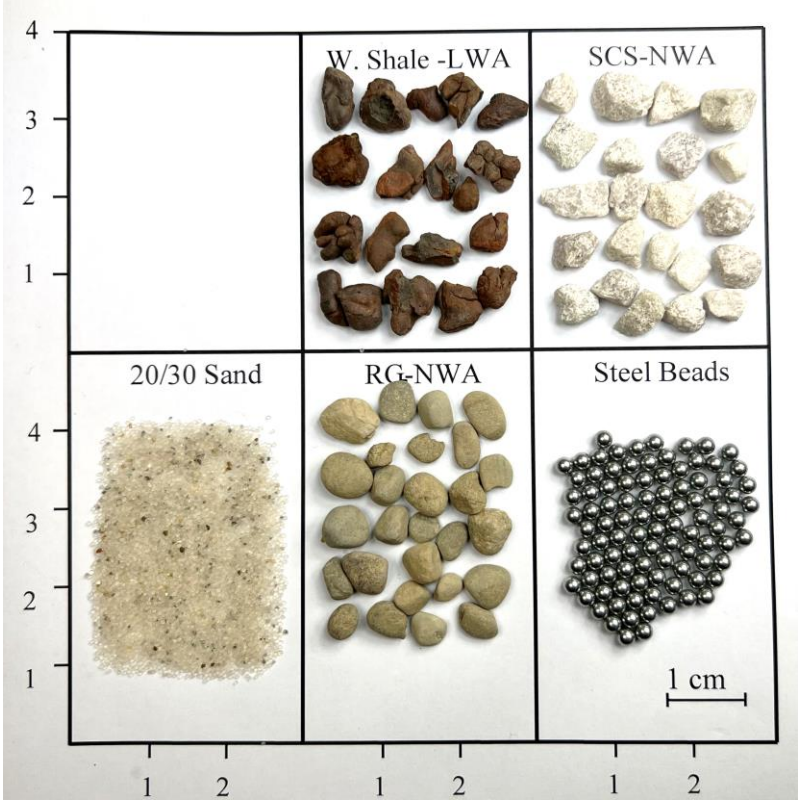


Figure 4-1: Bed materials.

4.2.2 Test Equipment and Methods

4.2.2.1 Air permeability

The air permeability test setup used in this experiment is shown in Figure 4-2. The setup consists of a rigid PVC pipe with a length of 152 mm and inner diameter (*D)* of 76 mm. The PVC pipe is placed between two metal caps that are sealed by grease. The top metal cap has a hole that connects to a pitot tube which allows the airflow generated from the central laboratory pump to pass through the sample that is placed in the PVC pipe. A flow meter, which measures the airflow coming from the central pump, is used between the central pump and the top metal cap. The bottom metal cap allows airflow to exit the sample. PC sample with length (L) of 102 mm is cast in the PVC pipe. In order to measure the static pressure drop ($\Delta P_M = P_2 - P_1$) induced by the resistance of the sample to the air passing

through, two pitot tubes are connected with electronic pressure gauges located at 12.7 mm above (P_2) and below (P_1) the sample to measure the pressure drop at inlet and outlet [122]. The experimental data was collected at atmospheric pressure and at temperature of 20 ˚C.

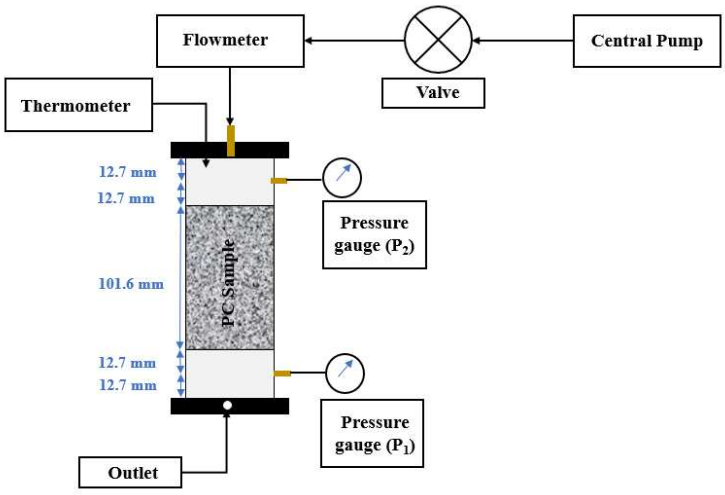


Figure 4-2: Air permeability test setup.

4.2.2.2 Thermal Conductivity and Specific Heat

The transient plane source (TPS) method was used to measure thermal conductivity and specific heat at room temperature of the PC specimens. The PC samples were prepared at different volumetric LWAs replacement ratios at 0 (all normal weight aggregate, no LWA), 50, 75, and 100% (all LWA). The principles of the TPS has been described by several researchers [123,124], and used to measure the thermal properties of materials including wood (spruce) and concrete from room temperature to temperatures up to ~700 ℃ [125]. The TPS system (Hot Disk® Instrument TPS 2500, Gotenborg, Sweden) utilizes a flat thermal sensor inserted between two 100 mm diameter disks of concrete specimens with thickness of 25 mm. The flat thermal sensor serves as both a heater as well as detector of temperature change [125]. The TPS setup illustrating the concrete samples and a thermal sensor is shown in Figure 4-3. The frequency and intensity of the electrical current flowing

through the sensor can be varied to generate a wide temperature range. The heat accumulated in the sensor propagates through the disk. The temperature of the samples over time is recorded and used to calculate thermal conductivity, thermal diffusivity, and specific heat. For this study, the thermal conductivity and specific heat are measured at room temperature.

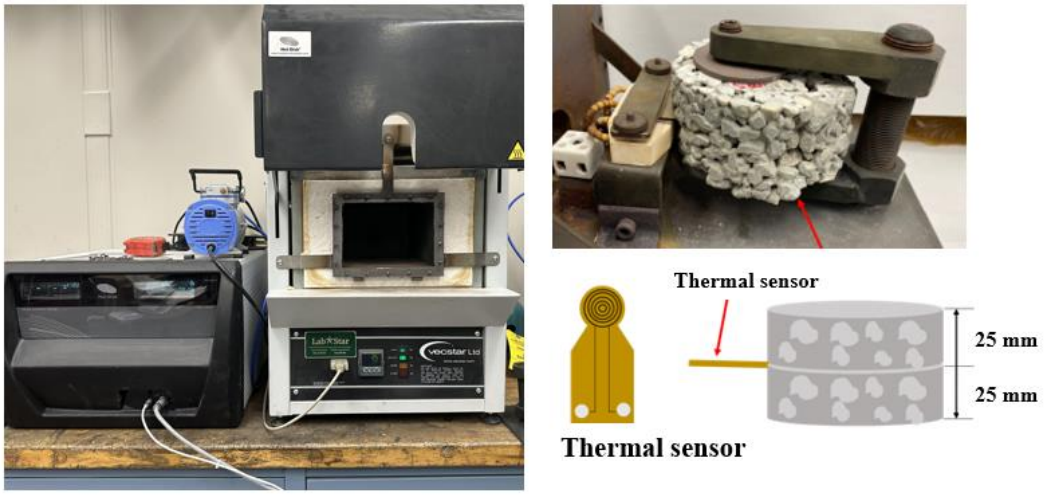


Figure 4-3: Transient plane source (TPS) setup used to determine thermal properties of PC.

4.2.2.3 Heat Transfer Apparatus and Method

Multiple PC samples were experimentally tested to understand the heat transfer performance with temperatures ranging from 23°C to 32 °C at an air velocity of approximately 0.36 m/s. The stored heat energy from the hot air was quantified and compared with the theoretical energy stored of the PC. Figure 4-4, shows a schematic (without the thermal insulation layer) of the experimental setup which consists of a cylindrical PC sample, electrical heater, and a vacuum. The PC is cast in a PVC pipe with length (L) of 152 mm and inner diameter, (D), of 76 mm. An anemometer by (PCE-423, PCE Americas Inc., Jupiter, FL, USA) was used to measure the air velocity and type K thermocouples are installed to measure the one-dimensional temperature differential.

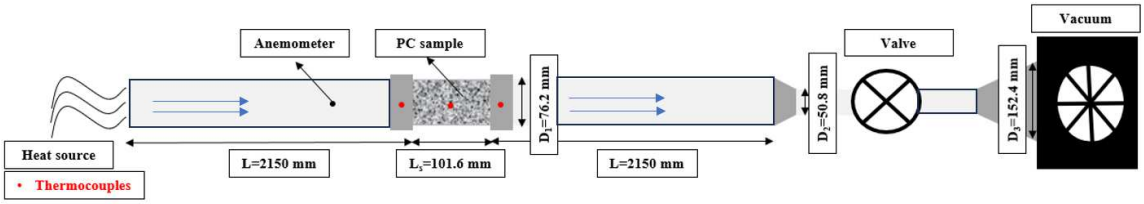


Figure 4-4: Heat transfer setup.

In the initial stage, a 3450 RPM, (Century AC Motor) vacuum is used to create negative pressure (i.e., suction) to force the airflow through the PVC pipe. During the first hour, the heater is off allowing the sample to achieve thermo-equilibrium with the lab (23 °C). At one hour, the heater is set to 32 °C and the charging phase starts. The hot air passes through the pervious concrete horizontally from left to right as shown in Fig 3. During the test, temperatures are measured using K-type thermocouples with an accuracy of ±0.5 °C. Data is collected at 1 Hz using a Measurements Computing^{TM}, USB-TC acquisition system. The air velocity/flow rate is measured by the PCE-423 anemometer at an accuracy of 0.05 m/s at the same sampling rate of 1 Hz.

The theoretical sensible energy stored in the PC can be calculated using Equation (4.1) [23,41]:

$$E_{theortical} = m_s \cdot C_p(T_f - T_i) \quad (4.1)$$

Where m_s is the mass of sample (kg), C_p is PC specific heat (kJ/kg·°C), T_f is the final temperature of the PC (°C) and T_i is the initial temperature of the PC (°C).

During charging, the amount of energy stored in the PC over a time period can be obtained by the following Equation (4.2) [126]:

$$E_{stored} = \sum_{i} \dot{m}_i \cdot C_{pair} \cdot (T_{in} - T_{out})_i \cdot \Delta t \quad (4.2)$$

Where $\dot{m}$ is the mass flow rate (kg/s), C_{pair} is the air specific heat (kJ/kg. °C), T_{in} and T_{out} are the temperature at inlet and outlet of the PC storage (°C) at each time step, respectively, and Δt is time step duration. The mass flow rate of air at each step can be calculated by the following Equation (4.3):

$$\dot{m}_i = v_i \cdot A \cdot \rho_{air} \quad (4.3)$$

Where v_i is the air velocity in the pipe at each time step i, m/s, A is the internal cross-sectional area of the pipe, m^2 and ρ_{air} is the air density, kg/m^3.

4.2.3 Pervious Concrete Design

The mix formulations used in this study are listed in Table 4-3. Each mix formulation is designated by a specific mix code; LW/NW-w/c-V_p/V_{agg}, which consists of % Lightweight Aggregate, % Normal Weight Aggregate, water-to-cement ratio, and cement paste to aggregate ratio by volume. For example, 75LW/25NW0.32V0.36, designates 75% LW aggregate, 25% NW aggregate, 0.32 w/c ratio, and cement paste to aggregate ratio of 0.36. The design w/c ratios were 0.24, 0.28, 0.30, 0.32 or 0.34. The cement paste-to-aggregate by volume ratios included 0.21, 0.31, 0.36, 0.40, and 0.49. A high range water reducing (HRWR) admixture was used to achieve the appropriate flow of the paste. The HRWR used for this study consisted of polycarboxylate-based material (MasterGlenium 7500, Master Builders Solutions, Ontario, Canada). The HRWR was proportioned to achieve the same paste spread for different w/c ratios. The spread was determined in accordance with

ASTM C230 [88] flow table test. The HRWR dosage was adjusted for each w/c ratio until a 250 mm flow was achieved in the paste as summarized in Table 4-2.

Table 4-2: HRWR dosage for varying w/c ratios.

w/c	HRWR Dosage (ml/100 kg $_{cement}$)
0.24	1825
0.28	1043
0.30	983
0.32	440
0.34	350

All batches were mixed as recommended by Schaefer et al. [91]. First, the aggregate was soaked in water for twenty-four hours to saturate the aggregate and prevent water absorption during mixing. This is necessary for lightweight aggregates due to their high-water absorption capacity. The excess water was drained from the aggregate for four hours. Three moisture content and absorption samples were taken to determine the amount of free water on the aggregate, allowing for appropriate adjustment of the total water needed. The saturated aggregate and 5% of total weight of cement were mixed in an auto mortar mixer (Collomix TMS 2000, WAYNE, NJ, USA) for 1 minute. The remaining cement, water (i.e., the amount of water according to the mix design minus the amount of water already absorbed by the aggregate), and HRWR were then mixed for three minutes. The mix was allowed to rest for two minutes before continuing for another three minutes of mixing. Next, pervious concrete mixtures were mildly compacted using a vibration table for ten seconds. Samples were allowed to cure for 24 hours in air prior to being placed in a water

bath at 20 ± 1 ℃ for 28 days. For the density and porosity, three samples from each batch were cast in a 75 mm diameter and 150 mm height molds and tested according to ASTM C1688 [21]. To perform the air permeability test (i.e., pressure drop measurements), three samples from each batch were cast in a 76 mm diameter and 102 mm long PVC pipes.

Table 4-3**:** PC mix proportions

Mix ID#	**Mix code**	**Cement**	**Aggregate**		**Water**	**w/c**	**V_P/V_{Agg} (%)**	**Porosity (%)**
			NWA	**LWA**				
M1	50LW/50NW0.32V0.36	259	703	301	83	0.32	0.36	32.6
M2	75LW/25NW0.32V0.36	259	351	452	83	0.32	0.36	29.1
M3	100LW0.24V0.31	294	0	595	71	0.24	0.31	28.3
M4	100LW0.28V0.31	275	0	595	77	0.28	0.31	29.5
M5	100LW0.30V0.31	266	0	595	80	0.30	0.31	29.6
M6	100LW0.32V0.31	258	0	595	82	0.32	0.31	29.2
M7	100LW0.34V0.31	250	0	595	85	0.32	0.31	30.1
M8	100LW0.30V0.49	428	0	600	128	0.30	0.49	20.3
M9	100LW0.30V0.40	347	0	600	104	0.30	0.40	25.3
M10	100LW0.30V0.21	185	0	600	56	0.30	0.21	37.3

4.3 EXPERIMENTAL RESULTS

4.3.1 Porosity Measurement

For the river gravel, sand, shale, siliceous aggregate, and steel beads, the porosity of the packed bed is determined by the formulas as shown in Equation (4.4) and Equation (4.5).

$$\varepsilon = \frac{V_v}{V_T} = \frac{V_T - V_m}{V_T} \tag{4.4}$$

$$V_m = \frac{W_m}{SG \cdot \gamma_W} \tag{4.5}$$

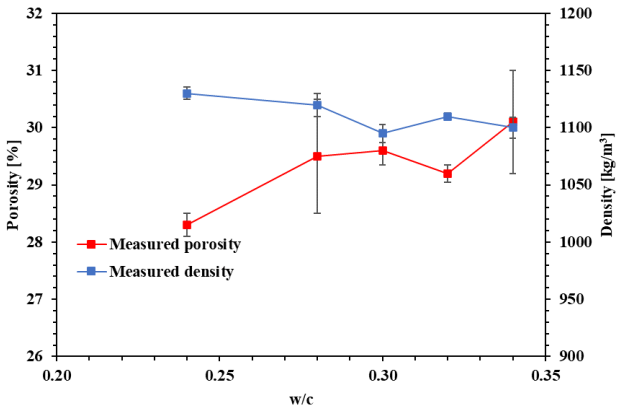
Where ε is the bed porosity, V_v is the volume of voids, V_T is the volume of sample, $V_m$is the volume of bed material, SG is the specific gravity of bed material and ρ_W is the density of water. The porosity of PC specimens can be determined by taking the difference in weight between the dry weight and the submerged weight as shown in Equation (4.6). The porosity of the hardened PC can be determined according to ASTM C1754 [93].

$$\varepsilon = \left[1 - \left(\frac{W_2 - W_1}{\rho_w V_T}\right)\right] 100\% \tag{4.6}$$

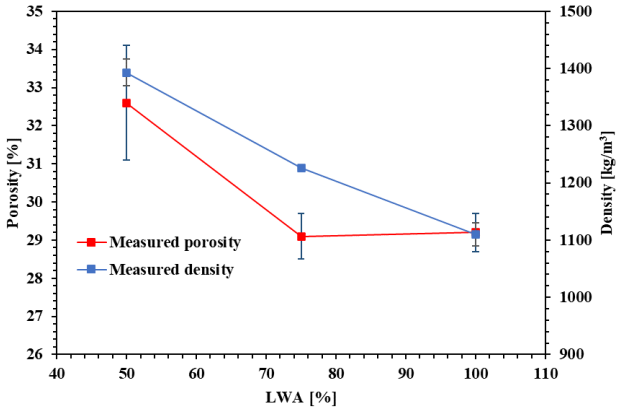
Where ε is the bed porosity, W_2 is the submerged sample mass and W_1 is the dry sample mass. The porosity and density results are listed in Table 4-3. As observed in Table 4-1, the two aggregates with angular shapes (shale and the siliceous) have a higher void ratio than the river gravel and the sand which have a rounder particle shape.

Five PC mixes were designed with different w/c ratios but the same target porosity of 30%. Utilizing the aforementioned HRWR dosages resulted in a consistent measured porosity and density as shown in Figure 4-5. Three LWA replacement levels (50%, 75%, and 100%) were designed to have a target porosity of 30%. The aggregates were proportioned by using the weighted void ratio of the two aggregates. The resulting measured porosities were consistent with the 30% target with an observed variation from 29.1% to 32.6% Figure 4-5 (a). Figure 4-5 (b) indicates at 25% NWA and 75% LWA achieved the lowest porosity compared with 50% NWA/50% LWA and 100% LWA at the same w/c and V_P/V_{Agg}, this is attributed to packing density effect due to the inconsistency of the aggregate distribution as well as the shape of aggregate [99]. Four mixes were made with different variations in

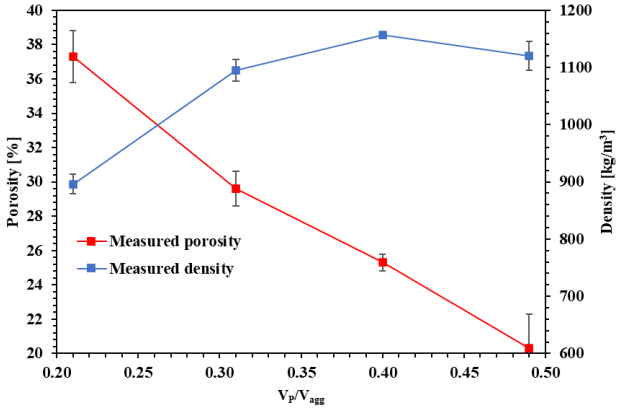
volume of paste to volume of aggregate. Figure 4-5 (c) demonstrates the effect of cement paste to aggregate ratio by volume (V_P/V_{Agg}). As the cement paste content decreases the porosity increases to an upper limit equal to the void content of the aggregate (41.40%). An increase in density occurs with an increase in the volume of cement paste content. However, at the highest value of V_P/V_{Agg} of 0.49, a slight decrease in density is observed compared to 0.40 and it could be attributed to water evaporation.



(a)



(b)



(c)

Figure 4-5: (a) Effect of w/c ratio measured porosity, (b) Effect of normal weight aggregate replacement ratio on measured porosity and (c) Effect of V_P/V_{Agg} on the measured porosity.

4.3.2 Validation of Air Permeability Setup

The air permeability setup was verified using air flow through a packed bed of spherical particles. The measured pressure drop through a packed bed of uniform diameter steel beads were compared to the theoretical formulation developed by Ergun [66]. Figure 4-6, presents the normalized pressure drop measured for steel beads. This comparison illustrates a noteworthy alignment between the experimental data and the predicted values. The calculated Root Mean Square Error (RMSE) is 3%, RMSE can be calculated using Equation (4.7):

$$\mathrm{RMSE} = \frac{100}{\mathrm{N}} \sqrt{\sum_{\mathrm{i}=1}^{\mathrm{N}} \left(\frac{\Delta \mathrm{P} - \Delta \mathrm{P_M}}{\Delta \mathrm{P}}\right)^2} \ \% \tag{4.7}$$

In Figure 4-7, the pressure drop through the natural materials are compared to values predicted by the Ergun equation. In order to use the Ergun equation, the authors assumed D_p is equal to the average of each particle size range as shown in Table 4-1. The LWA and NWA are not predicted well by the Ergun equation (15 % and 21 % RMSE, respectively) as shown in Figure 4-7. The large error can be attributed to the roughness and angularity of the coarse aggregates and size gradation. As the particle shape becomes smoother and rounder the RMSE decreases. The river gravel has a RMSE of 9% whereas 20/30 Ottawa sand particles is well predicted with a RMSE of only 4% ,since the particle of sand is smooth and round [119].

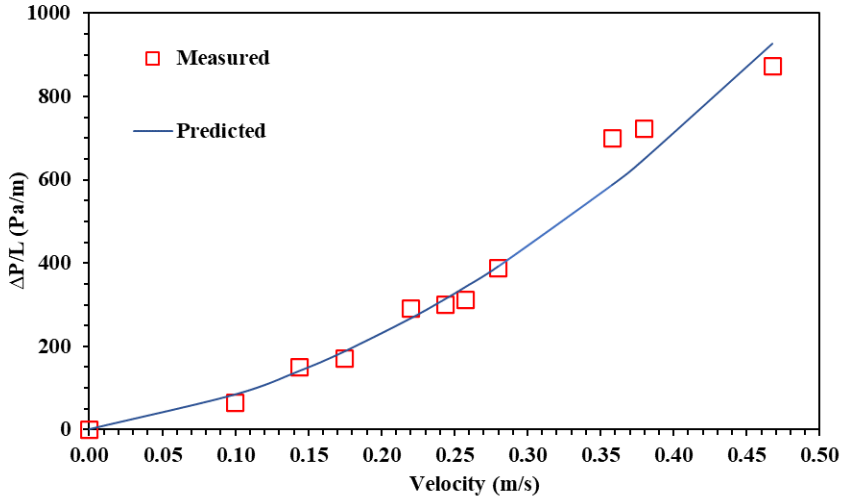


Figure 4-6**:** Normalized pressure drop for steel beads.

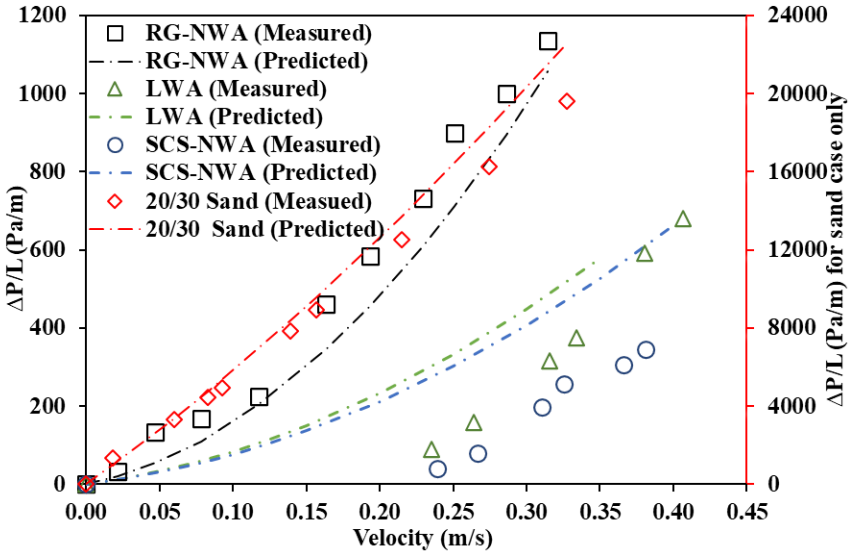


Figure 4-7**:** Normalized pressure drop for different granular materials.

4.3.3 Air Permeability Results for Pervious Concrete

In this subsection the effect of w/c, V_P/V_{Agg} and the normal weight aggregate replacement ratio on the air pressure drop through pervious concrete were studied and compared the measured results with the predicted values using Ergun equation. To predict the pressure

drop of air when it flows through regular porous medium (e.g., spherical particles), the Ergun equation is used. This equation does not consider the shape of voids between aggregate and is not ideally applicable for irregular aggregate shapes of pervious concrete. Therefore, a less-than ideal estimation for the pressure drop ($\Delta P/L$) in pervious concrete is expected.

4.3.3.1 Effect of w/c

The effect of w/c was investigated by preparing mixes with different w/c at constant volume of cement paste to volume of aggregate. Figure 4-8 presents the pressure drop versus velocity of the air flow for all mixes. The experimental pressure drop measurements were accurately predicted using quadratic least squares fit with an R^2 greater than 0.99. As expected, the 100LW0.24V0.31 mix has the highest pressure drop since it possessed the lowest porosity. Although 100LW0.28V0.31, 100LW0.30V0.31 and 100LW0.32V0.31 have similar porosity, the pressure drop increases with decreases in w/c. This increase in pressure drop can be attributed to the variation in the type of void structure formed at different water-to-cement ratios. As shown by Li et al. [101], PC has two forms of porosity: total porosity and interconnected porosity. The interconnected porosity consists of interconnected void channels that allow passage of liquid (or air) through the concrete. The measured porosity in this study consists of the total porosity which includes both the interconnected voids as well as closed voids within the paste matrix. The results showed while total porosity remains constant the interconnected porosity decreases with increasing w/c ratio.

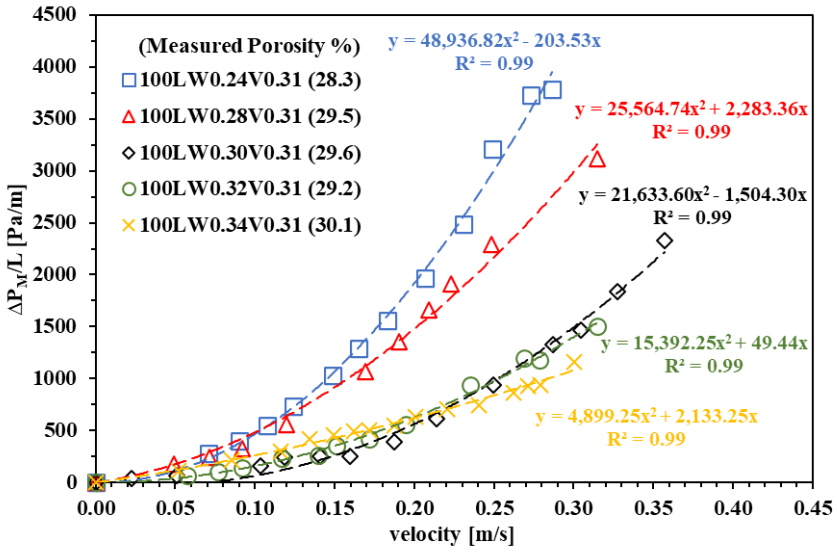


Figure 4-8**:** The normalized pressure drop for mixes with different w/c ratios.

4.3.3.2 Effect of V_P/V_{Agg}

To study the effect of V_P/V_{Agg} on the pressure drop of PC, a total of four PC mixes were prepared at different V_P/V_{Agg} ratios as shown in Figure 4-9. Since all the mixes have the same w/c and the type of aggregate, the void content is controlled only by the amount of the cement paste in each mix (i.e., V_P/V_{Agg}). Figure 4-10 presents the results of pressure drop versus air flow velocity along with the quadratic best fit. An inverse relationship is observed between the pressure drop and the cement paste content. For example, the pressure drop for 100LW0.30V0.21, which has a porosity of 37.3 %, is approximately 90 % less than the pressure drop for 100LW0.30V0.49 which has a porosity of 20.3 %. This can be attributed to the difference in the cement paste volume between the two mixes. The cement paste content has a direct impact on the porosity and reduces the average diameter of channels within the sample.

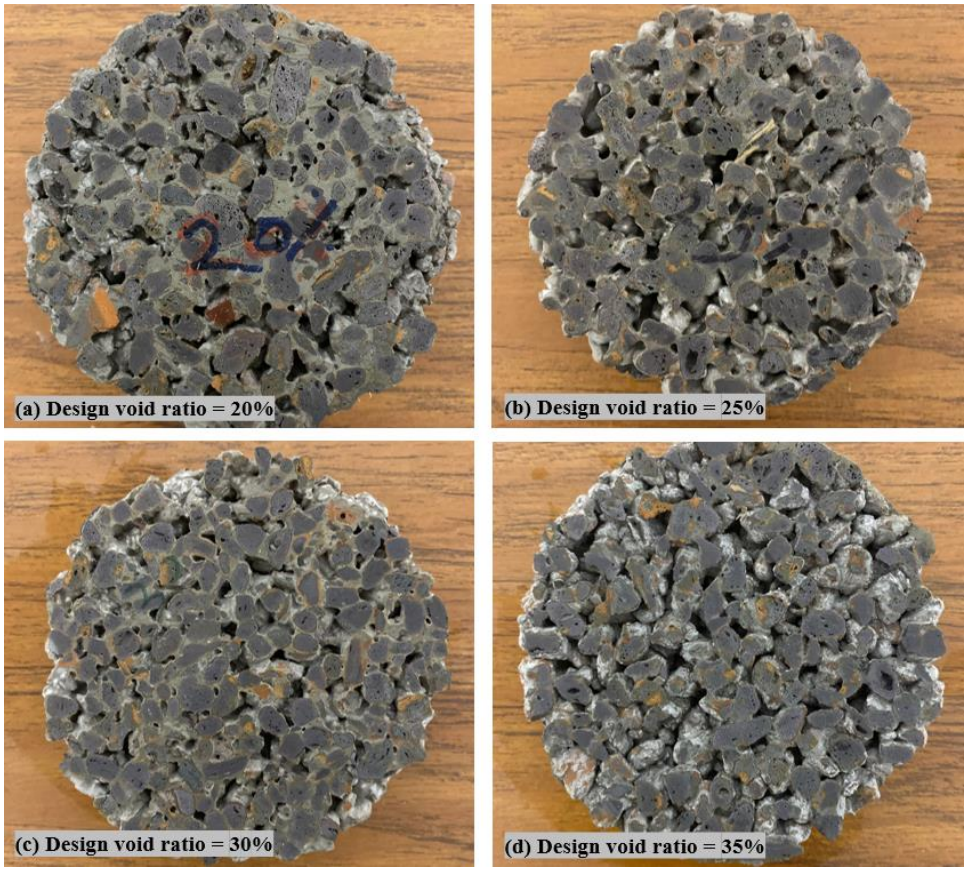


Figure 4-9: The cross section of PC samples with different V_P/V_{Agg} ratios.

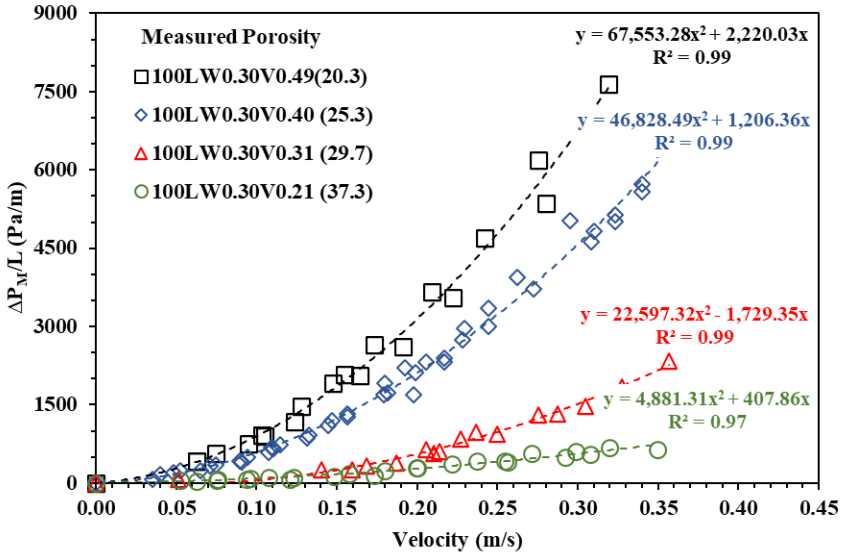


Figure 4-10 : The normalized pressure drop for mixes with different design void ratios.

4.3.3.3 Effect the Replacement Ratio

To study the effect of the amount of normal weight aggregate on the pressure drop in PC, PC mixes were prepared at different replacement ratios, 25% and 50% NWA with w/c of 0.32. Figure 4-11, presents the pressure drop versus air flow velocity for the mixes with different replacement ratios along with a quadratic best fit. During fabrication of the PC the aggregates are coated with cement paste thus decreasing the influence of aggregate shape. Consequently, no significant difference in pressure drop was observed due to changes in the proportion of lightweight aggregate replacement in the mix. Similarly, for the NWA and LWA studied, the type of aggregate has negligible effect if the quantity of cement paste and water-cement ratio w/c remain constant.

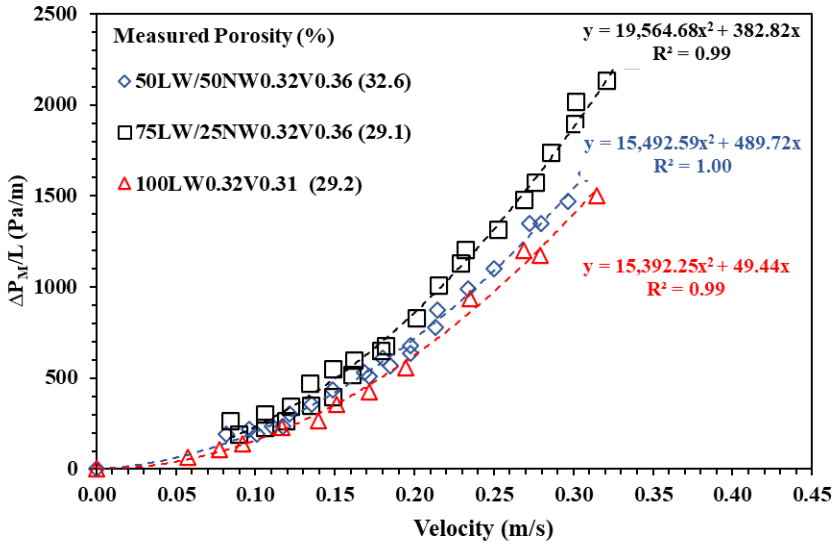


Figure 4-11: The normalized pressure drop for mixes with different LWA replacement ratios.

4.3.3.4 Pressure Drop Estimation Approach

In this study, the expected pressure drop was evaluated using the Ergun equation, assuming that the particle diameter represents the aggregate size. This assumption, however, ignores the cement paste content that coats the aggregate and influences the diameter of the void

channel. Ergun derived his equation from the pressure drop equation for a flowing fluid through any pipe channel. The predicted pressure drop in the pipe can be calculated using Kozeny-Carman and Burke-Plummer equation as described in Equation (4.8):

$$\frac{\Delta P_1}{L} = C_1 \frac{\mu}{D_{eq}^2} \mathrm{v} + C_2 \frac{\rho}{2\, D_{eq}} \mathrm{v}^2 \tag{4.8}$$

Where, ΔP_1 is the predicted pressure drop through the pipe, L is the length or height of the pipe, C_1 and C_2 friction factors, v is the superficial velocity, which is equal to the interstitial velocity divided by the porosity $\left(\frac{v}{\varepsilon}\right)$, and D_{eq} is the diameter of an equivalent pipe, m. Ergun transformed the interconnected voids in the packed bed into pipe channels with an equivalent diameter and determined that the equivalent diameter of these channels is directly related to the porosity value and the diameter of the spherical particles. The packed bed and equivalent pipe model are illustrated in Figure 4-12.

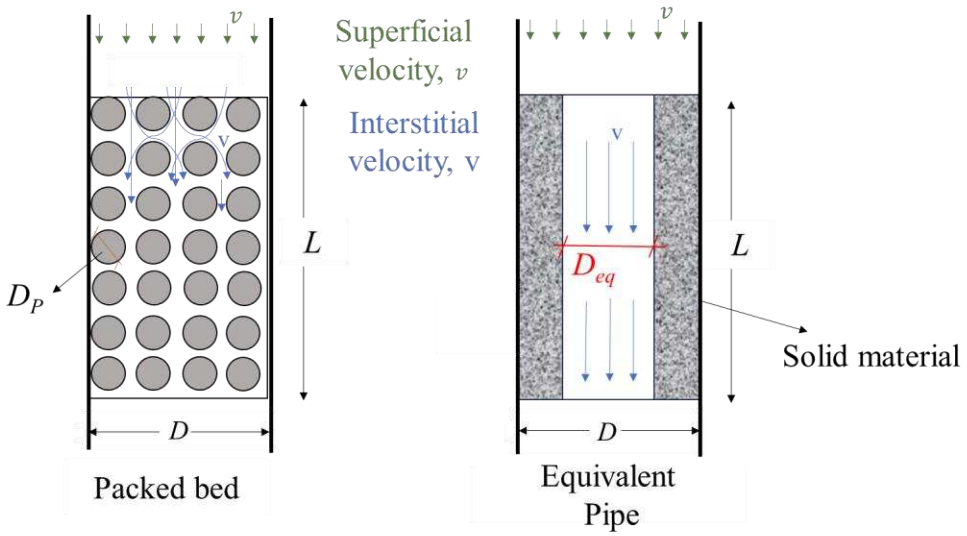


Figure 4-12: Ergun packed bed and equivalent pipe model.

The equivalent diameter (D_{eq}) can be calculated using Eq. (4.9):

$$D_{eq} = \frac{2D_p\,\varepsilon}{3\,(1-\varepsilon)} \tag{4.9}$$

There is no standard laboratory method to determine the effective void channel diameter in PC. When using the average particle diameter as shown in Table 4-1, a noticeable disparity is observed between the experimental outcomes for pressure drop and those predicted by the Ergun equation using the recommended values of *A* and *B*. In order to minimize this disparity, the equivalent diameter in Kozeny-Carman and Burke-Plummer equation were modified to be function of w/c and cement paste content, via an optimization process that minimized RMSE between the experimental results and the prediction. The C_1 and C_2 terms used in Equation (4.8) correspond to the *A* and *B* values of 150 and 1.75 used in Equation (2.3). The values of C_1 and C_2 are dependent on roughness values and path geometry, requiring a more detailed study for development of a first principles determination. The empirical fit resulted in C_1 of 67 and C_2 equal to 2.33. As depicted in Figure 4-13, the optimized D_{eq} values decrease with a decrease in the water-to-cement ratio (w/c) or increase cement paste (V_P/V_{Agg}). A relationship between D_{eq} and the water to cement content and V_p/V_{Agg} was developed and is presented in Equation (4.10).

$$D_{eq} = 0.10\exp\left(8.40\frac{\mathrm{w}}{\mathrm{c}}\right) + 195.26\exp\left(-24.85\frac{V_p}{V_{Agg}}\right)\,[m], \mathrm{R}^2 = 0.83 \tag{4.10}$$

Figure 4-14 displays the normalized measured pressure drop and the predicted values based on both the original Ergun equation and the modified Kozeny-Carman and Burke-Plummer prediction. Table 4-4 reports the RMSE between the normalized measured pressure drop and the predicted values for the original Ergun equation (Equation (2.3)), Ozahi modified Ergun equation (Equation (2.4)) with an assumed shape factor $\boldsymbol{\varphi}$ of 0.82 (similar to what

was used in his study), and the modified version of Kozeny-Carman and Burke-Plumme equation (Equation (4.8) and (4.10)). The observed error using the equivalent pipe approach provides the best overall fit and unlike the two other approaches no outlier predictions are observed. The error is still moderate when using Equation (4.10) ranging from 20 to 35%. This remaining error can be attributed to the assumption of constant values for C_1 and C_2 in Equation (4.8). These values are more likely variable as they are dependent on the friction factor of the channels which is derived from the Moody chart. Determining this value requires the roughness value of the concrete and the Reynolds number, which, in turn, depends on the equivalent diameter. The current formulation is fit to aggregate examined consequently, the use of this equation for other aggregate sizes may not be accurate. Achieving more accurate results thus requires a deeper exploration into the values of both C_1 and C_2 and aggregate size and shape.

.

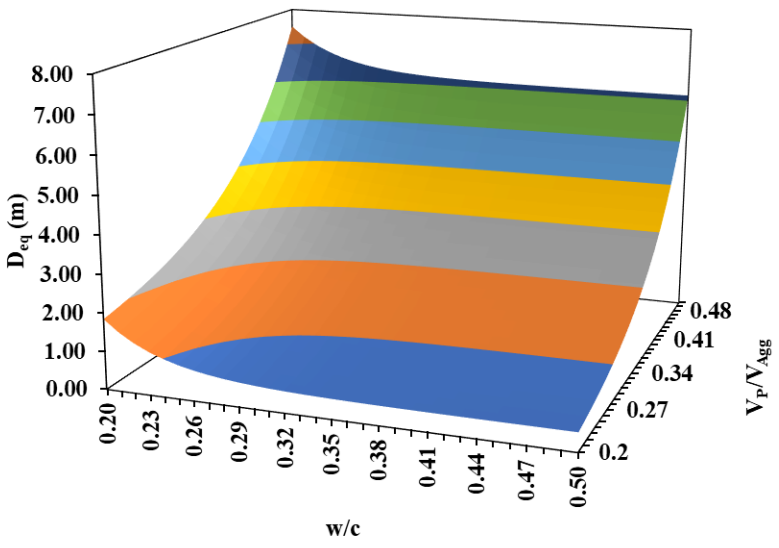


Figure 4-13: Optimized equivalent diameter.

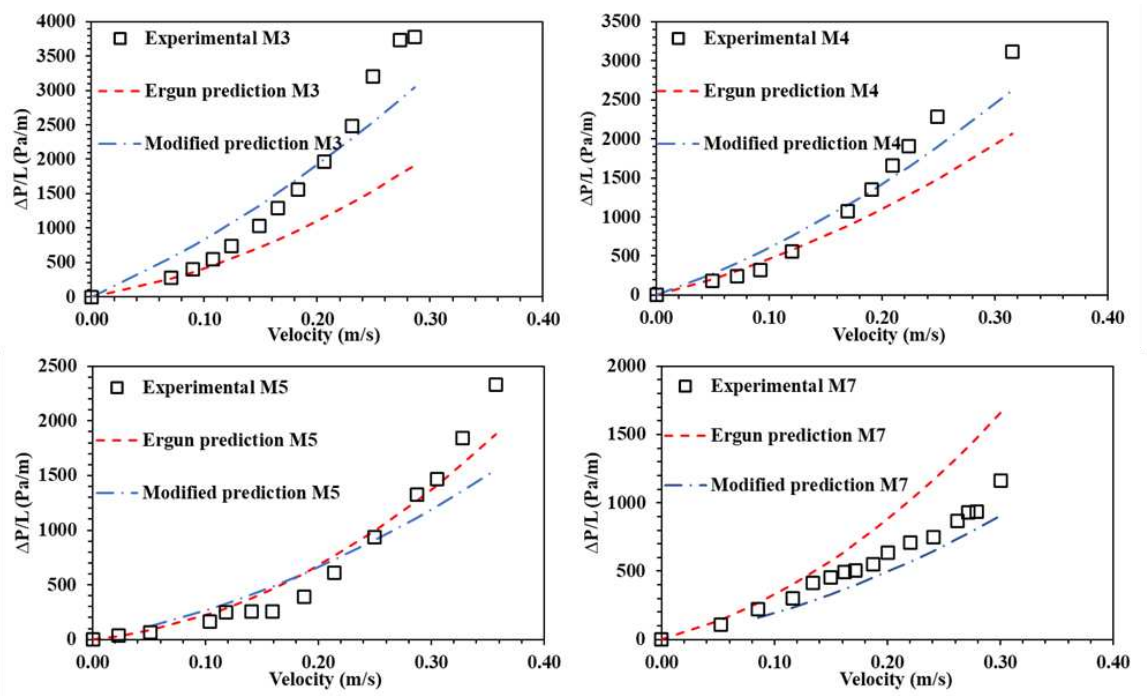


Figure 4-14: The comparison between the measured normalized pressure drop and predicted values.

Table 4-4**:** The mean square error between measured pressure drop and predicted values based on the Ergun equation.

Mix code	RMSE (%)		
	Equation (2.3)	**Equation (2.4)**	**Equation (4.10)**
50LW/50NW0.32V0.36	19.9	17.1	20.6
75LW/25NW0.32V0.36	44.0	17.5	23.6
100LW0.24V0.31	194.5	123.5	29.2
100LW0.28V0.31	164.9	99.5	35.0
100LW0.30V0.31	364.0	213.9	38.2
100LW0.32V0.31	21.0	28.2	31.6
100LW0.34V0.31	36.8	10.7	25.9
100LW0.30V0.49	54.8	23.0	33.7
100LW0.30V0.40	118.1	66.9	32.6

4.3.4 Thermal Properties Results for Pervious Concrete (PC)

Previous research by Zaetang et al. [118] focused on thermal conductivity, highlighting its significance in determining the applicability of PC for pavement applications. However, measurements of specific heat, which is a fundamental factor in calculating sensible heat in cooling applications, were not addressed, and is examined here. The PC made with LWAs showed lower thermal conductivity than that of PC containing normal weight aggregates. For PC mixes prepared at different LWAs replacement ratios, the thermal conductivity of 100% LWA-PC was ~20% of 100 NW PC mix (0.5 vs. 2.4 W/m·K). Figure 4-15 illustrates the relationships between the thermal conductivity and specific heat of PC containing different amount of LWAs by volume. The results showed the thermal conductivity and specific heat is mainly influenced by the type of aggregate. This difference in thermal conductivity is attributed to the porous structure of the LWAs since the thermal properties of air voids are less than solid materials.

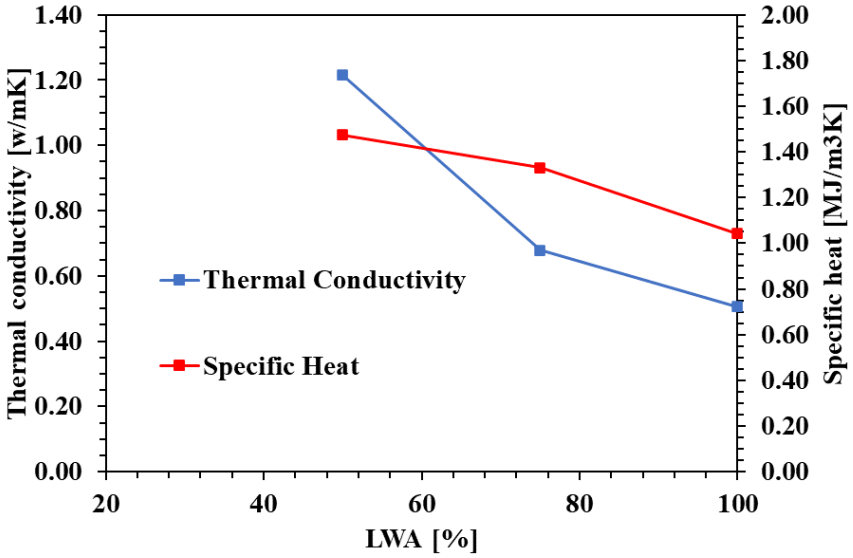


Figure 4-15: The relationship between % of LWA replacement ratio with the measured thermal conductivity and specific heat of PC mixes prepared with different LWA replacement ratios.

Similarly, the 100% LWAs PC possessed a thermal conductivity of 0.50 W/m K and specific heat of 1.05 MJ/M^3 K, which represents a reduction of 60% and 30%, respectively, when compared to the thermal conductivity and specific heat of the 50NW/50LW PC mix. Moreover, Figure 4-16 shows the relationships between the thermal conductivity and specific heat of PC with different amount of cement paste by volume V_P/V_{Agg}. The results show the thermal conductivity and specific heat is mainly influenced by the amount of cement paste. This difference in thermal conductivity is attributed to the porosity of PC itself as discussed in the introduction. The 100LW0.30V0.21 PC possessed a thermal conductivity of 0.34 W/m·K and specific heat of 0.70 MJ/M^3·K, which represents a reduction of ~40% and ~50%, respectively, when compared to the thermal conductivity and specific heat of the 100LW0.30V0.49 mix.

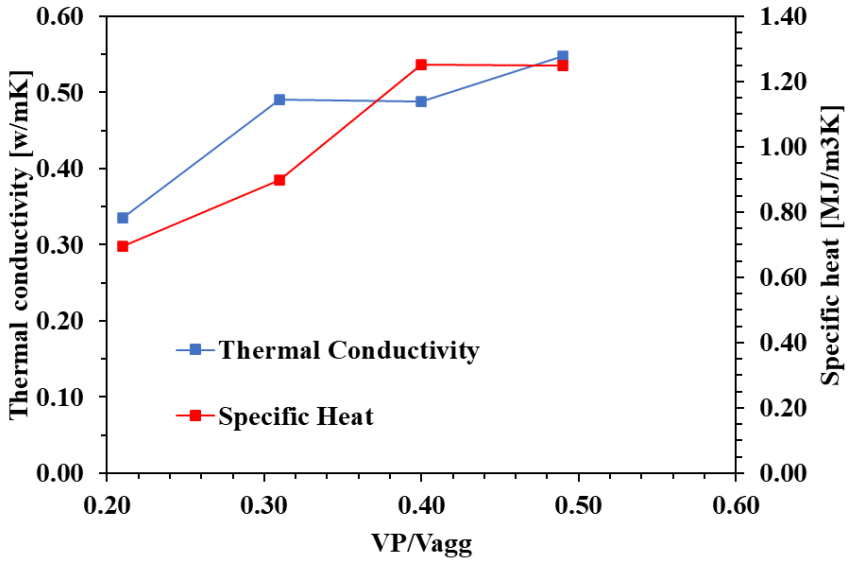


Figure 4-16: The thermal properties of PC samples with different V_P/V_{Agg} ratios.

4.3.5 Heat Transfer for Pervious Concrete (PC)

Three PC were examined: 100LWA, 75LW/25NW and 50LW/50NW for heat transfer

properties. The samples were initially brought to room temperature ranging from 22 to 23°C and then subjected to heat of 30 to 32°C until the inlet and outlet temperatures were equal at an air velocity of 0.36 m/s. The temperature differences are summarized in Figure 4-17. The sensible heat in 100LW PC was the lowest of the three samples at 12300 kJ/m^3. The 50LW/50NW sample with the highest weight possesses the highest heat capacity (26,700 kJ/m^3) and provides thermal transfer heat transfer for approximately two hours. The measured heat capacity was accurately estimated using Equation (2.1) and Equation (4.2). The theoretical and experimental heat energy are presented in Table 4-5. The error range is (-5.7% to 3.18 %). The results indicate that the NWA is an effective means of providing thermal energy.

Table 4-5: Heat capacity for PC

Sample	**ΔT (°C)**	**Sample weight (kg)**	**Theoretical stored energy (kJ/m^3)**	**Air velocity (m/s)**	**Measured stored energy (kJ/m^3)**	**Error (%)**
100LW0.32V0.36	10.63	0.514	12300	0.34	13000	-5.70
75LW/25NW0.32V0.36	9.73	0.568	15900	0.38	15600	1.67
50LW/50NW0.32V0.36	10.97	0.765	26700	0.39	25900	3.18

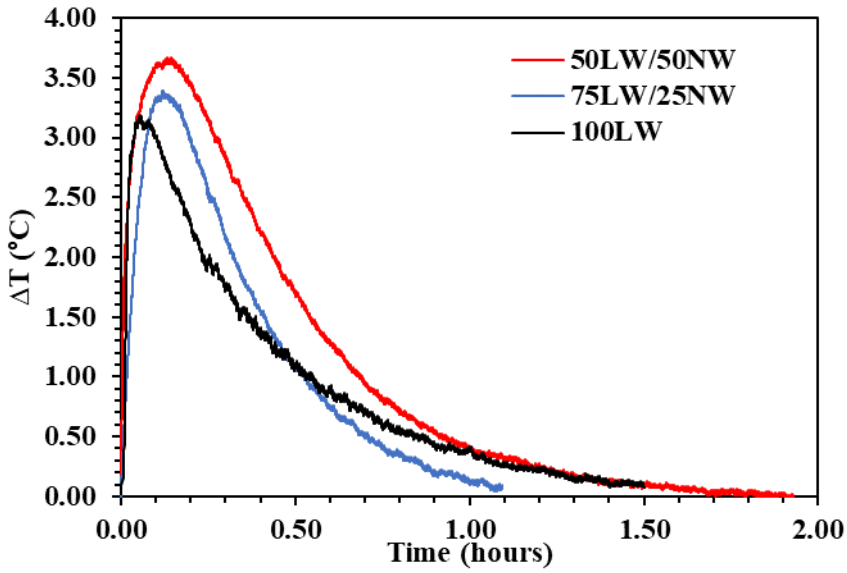


Figure 4-17: Temperature difference between inlet and outlet in charging phase for different replacement ratio.

4.4 SUMMARY AND CONCLUSIONS

An experimental program was conducted to examine the use of pervious concrete for forced air cooling applications. Pervious concrete samples were fabricated from light weight and normal weight aggregates were fabricated at different w/c ratios, paste to aggregate volume ratios, and porosities. The samples were evaluated for pressure drop due to forced air flow, cooling performance, and thermal properties. The following conclusions can be drawn from the study.

- Pressure drop due to forced air flow can be accurately predicted for round grain sand (20/30 Ottawa sand) and coarse aggregate (river gravel) packed beds using the Ergun equation. Typical lightweight concrete aggregates and crushed coarse aggregates are not predicted well using the Ergun equation due to the roughness of the media.

- Ergun equation provides a poor estimate for determination of pressure drop in pervious concrete (i.e., RMSE up to 368 %) due to interconnected pore structure of the matrix.

- A modified Kozeny-Carman and Burke-Plummer formulation is developed to determine the relationship between pressure drop and air velocity in pervious concrete. The approach creates an equivalent pipe diameter as a function of the water/cement ratio and the volume of paste to volume of aggregate ratio. This approach provides a good estimate of pressure drop and results in a RMSE error of 20 % to 38 %.

- The thermal conductivity and specific heat of pervious concretes are mainly influenced by the type of aggregate and paste volume. The thermal conductivity is found to increase from 0.55 to 1.20 W/m·K and the specific heat increases from 1.00 to 1.40 $MJ/m^3 \cdot K$ when normal weight aggregate to lightweight aggregate increases 0 to 50%. Low conductivity lightweight aggregates decrease the conductivity of pervious concrete.

- The heat transfer characteristics of pervious concrete can be accurately estimated using standard principles of thermodynamics along with the measured specific heat and thermal conductivity of the concrete.

In summary, this chapter investigated the pressure drop readings, specifically within the context of PC. The discussions culminated in the successful development of a predictive model, enhancing the capacity to anticipate pressure readings during the design phase of PC. This accomplishment is deemed essential for ensuring the performance of PC in cooling application. Furthermore, an investigation was extended to the thermal properties of PC, with a focus on its ability to store sensible energy. This aspect assumes significance in contemplating the potential use of PC in thermal storage systems. The findings contribute valuable insights into the thermal behavior of the PC, establishing the groundwork for its cooling application. With these fundamental properties examined and

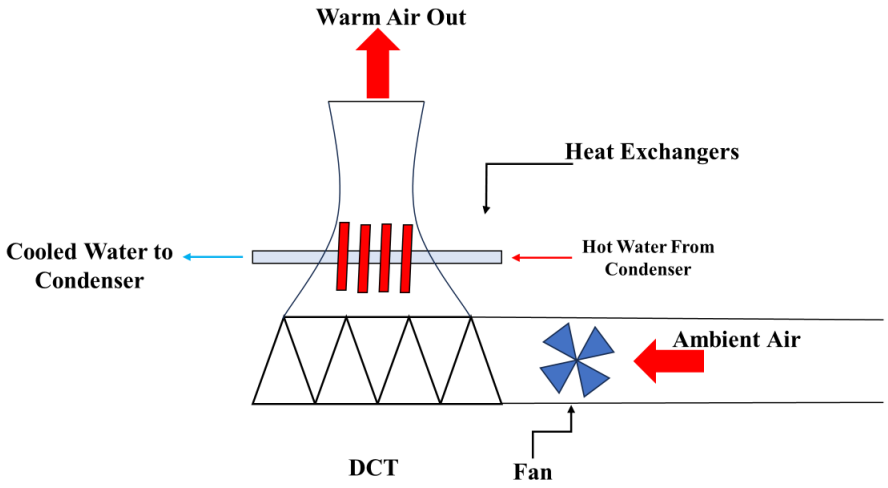
comprehended, the groundwork for the development of a cooling system utilizing PC has been concluded. The subsequent chapter will advance our exploration by delving into the behavior of porous concrete integrated with Phase Change Materials (PCM). This integration introduces a new dimension to the material's capabilities, and the study will encompass both theoretical considerations and practical applications. Additionally, the concrete mixtures developed in chapter three will play a crucial role in the upcoming investigations. These mixtures are carefully formulated to optimize the performance of PC, taking into account factors such as porosity, strength, and thermal conductivity. The choice of porosity will be informed by the pressure readings developed in the fourth chapter, ensuring a comprehensive and data-driven approach to the design process.

Upcoming chapter promises a deeper exploration into the potential of PC with PCM, developing and designing cooling system using PC.

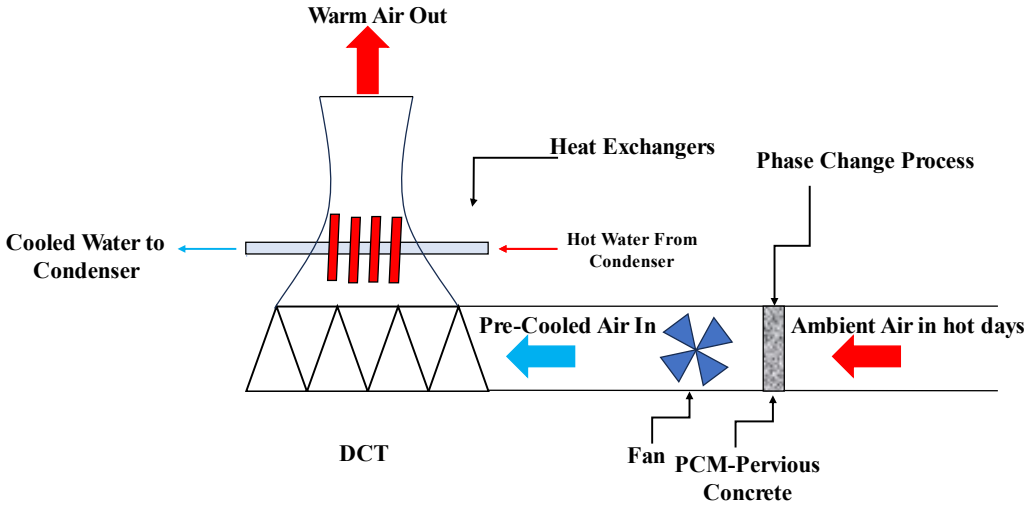
5 ENERGY STORAGE IN LIGHTWEIGHT AGGREGATE AND PERVIOUS CONCRETE INFUSED WITH PHASE CHANGE MATERIALS

5.1 INTRODUCTION

Population growth and energy demand are increasing significantly, leading to a rise in the consumption of freshwater resources. Power plants in the U.S. account for approximately 40% of all freshwater withdrawal, with 90% of it used in condenser cooling [1]. The most common cooling technology used in coal-fired power plants requires water withdrawal rates of 75 to 150 m^3/MWh after which most of it is returned but at an elevated temperature leading to thermal pollution of the water source [2]. Cooling tower technology is categorized based on the contact between the working fluid (e.g., hot water) and the airflow and consists of wet cooling towers (WCTs) and dry cooling towers (DCTs). WCTs are recirculation water systems that carry out cooling by providing direct contact between the hot water and inlet air. The hot water flows from the condenser in the power plant through pipes to the cooling tower and over the tower's fill material. The fill material provides a large contact surface to improve evaporation and heat transfer. After the water-cooling process, involving evaporation and convective heat transfer, the water is collected by a water tank under the fill material and pumped to the condenser in a continuous circuit [3]. DCTs on the other hand, rely only on convection heat transfer to release heat from the working fluid by indirect contact between the air and the working fluid through heat exchangers [4]. DCTs do not require freshwater withdrawal or issues with thermal pollution of water sources. Moreover, the DCTs are categorized based on the draft method to natural draft and mechanical draft (i.e., fan) [127,128]



(a)



(b)

Figure 5-1: (a) dry cooling tower (DCT); (b) improved dry cooling tower.

The efficiency of the DCT is dependent on the inlet air temperature as shown in Figure 5-1 (a). Hot days create unfavorable conditions by raising the ambient air temperatures, reducing the effectiveness of the cooling process. To address this issue pre-cooling of the inlet air via fogging, wet-media, and spray cooling has been examined. The main shortcomings of fogging and spray cooling are the risk of corrosion and the additional costs

associated with water use and water demineralization. In wet-media pre-cooling, the water quality and corrosion of the heat exchanger are not significant [5,6]; However, water loss by evaporation in all these pre-cooling methods is a major obstacle. This chapter focuses on the development of a dry cold thermal energy storage system (CTESS) using inorganic phase change material (PCM) encapsulated in pervious concrete (PC) as shown in Figure 5-1 (b). PC is a porous concrete that is fabricated from a uniform size coarse aggregate with minimal to no fine aggregate [7–10]. PC has been studied by researchers for its applications in evaporative or wet cooling [110,111]. Examine the inherent sensible heat capacity of pervious concrete and the latent heat storage potential using PCM infused lightweight porous aggregates were presented in this study. The heat transfer performance of PC for dry cooling applications is assessed through the determination of both the air permeability and thermal characteristics of the concrete.

5.2 MATERIALS

5.2.1 Phase Change Material (PCM)

The inorganic PCM used in this work was calcium chloride hexahydrate ($CaCl_2 \cdot 6H_2O$). It was synthesized in the laboratory by mixing a commercial anhydrous calcium chloride ($CaCl_2$) with deionized water based on the stoichiometric ratio of $CaCl_2 \cdot 6H_2O$. The melting point of this inorganic PCM was observed to be 25 ± 0.6 °C. The physical and thermal properties of PCM are summarized in Table 5-1. Past research has shown that this PCM has a stable latent heat of 150 kJ/kg over 1,000 freeze-thaw cycles and the supercooling is minimized by the rough inner surface of the lightweight aggregate [23].

Table 5-1: Physical and thermal properties of PCM

Property	Inorganic PCM
Specific gravity (liquid)	1.33
Melting point (°C)	25.0
Heat storage capacity (J/g)	150
Specific heat, liquid (J/g·K)	2.54
Specific heat, solid (J/g·K)	1.68

5.2.2 Lightweight Aggregate (LWA)

To produce PCM-PC, commercially available lightweight aggregates, and siliceous crushed stone (SCS) normal weight aggregate were used. Table 5-2 shows the physical and thermal properties of the LWAs. To fabricate a consistent pervious concrete the aggregates were sieved to ensure all materials passed a 9.5 mm sieve and were retained on sieve No. 4 sieve (4.75 mm opening). The sieved lightweight aggregates used in this study are shown in Figure 5-2 (a). The SEM images of porous LWAs are shown in Figure 5-2 (b). In these images, the dark area represents the pores while the light-colored area is the pore skeleton. Clearly, LWAs are a highly porous material with an interconnected pore structure.

Table 5-2: Physical and thermal properties of the aggregates

Material type	Shale	Clay	Glass	SCS
Unit weight (kg/m^3)	520	610	300	1530
Void content (%)	41.4	44.2	51.1	42.9
Specific gravity (-)	1.08	1.16	0.63	2.61
Specific heat (kJ/kg·°C)	1.10	0.85	0.84	0.91
Absorption (%) by wt.	13.6	24.8	48.8	0.87

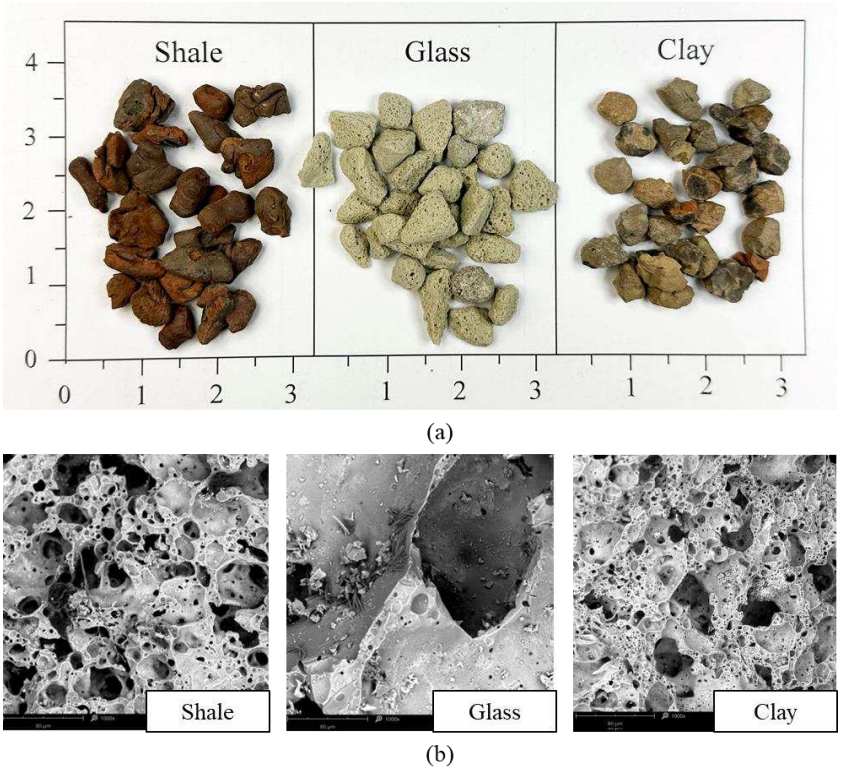
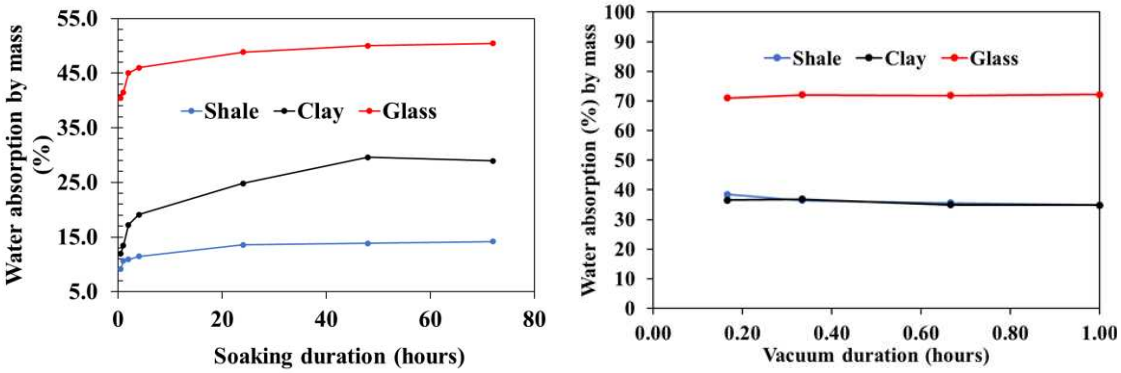


Figure 5-2: (a) Real image of LWAs (scale in cm); (b) SEM images of LWA.

5.2.3 PCM-LWA

To provide the greatest amount of latent heat, the mass of PCM within the LWA must be maximized. Infusion was first examined by soaking the LWA in water. Due to the high internal pore structure of the LWA the material was soaked for a period of 72 hours. The measured water absorption was 14.2, 28.9, and 50.5% by weight for the shale, clay and

glass, respectively, as summarized in Figure 5-3 (a). To improve the rate of absorption and the amount of material impregnated within the LWA a vacuum method was also deployed. The water absorption by weight increased to 36.4% for shale and 36.8% for clay under a 20-minute vacuum (i.e., absolute pressure of 18.3 kPa) as shown in Figure 5-3 (b). Consequently, to maximize impregnation and minimize time, the PCM infused LWA were prepared by oven-drying the LWA and placing them under vacuum for ten minutes as shown in Figure 5-4. The melted PCM (i.e., liquid PCM) then was fed into the chamber until the aggregates were submerged. The submerged LWA is kept under vacuum for twenty minutes. During the infusion process, the LWA and $CaCl_2 \cdot 6H_2O$ (PCM) must be heated (above the PCM melting point of 25 °C) to maintain the liquid state of the PCM. Following infusion, the excess PCM was drained, and the aggregate was refrigerated at 4 °C to solidify. The PCM impregnation was found to be 40, 44 and 120% by weight for shale, clay, and glass, respectively.



(a) (b)

Figure 5-3: Water absorption of LWA (a) by soaking, (b) by vacuum method.

The coating concepts cited in literature [42] were utilized to introduce adequate coating materials and methods to avoid/minimize infused PCM leakage and to prevent any chemical reaction with surrounding media. Omitting an epoxy coating and directly mixing

the infused aggregate particles with the concrete paste is not feasible due to the hydrophilic nature of the inorganic PCM. Direct contact of the PCM with the cement paste would result in absorption of water from the paste. This would impact the performance of the PCM and would prevent the formation of cement hydrate compounds and bonds, ultimately resulting in concrete failure. Hence, a dual-layer approach was implemented. This involved immersing the infused aggregates in a liquid epoxy for 15 minutes to establish an initial coating layer as shown in Figure 5-5. The wet epoxy covered aggregates are subsequently coated with dry cement (Type II Portland Cement) in order to separate the aggregate particles. This process allows each aggregate to remain separate and cure the epoxy prior to addition into the concrete mix. This is achieved by mixing the wet aggregates with the dry cement powder for 2 minutes in a drum mixer. The coated aggregates were sieved on a No.4 sieve to remove the excess cement. The dual-layer coated PCM-LWA was allowed to air dry for 24 hours at 23 °C ± 2 °C followed by oven curing at 40 °C for 24 hours to accelerate the epoxy curing. The coated PCM-LWA was soaked in water for 3 days to allow for surface cement (second coating layer) to hydrate before being used in PC fabrication. This also removed uncertainty in the final water to cement ratio of the pervious concrete mixes. Images of the coated PCM-LWA and an SEM image of a sectioned coated aggregate are shown in Figure 5-6. Note that the melting point of the cured epoxy is 90°C which is well above melting point of the PCM and operation conditions for the PC system. Consequently, failure of the epoxy shell during thermal operations was not observed. The physical and thermal properties of the PCM encapsulated coated LWAs are summarized in Table 5-3.

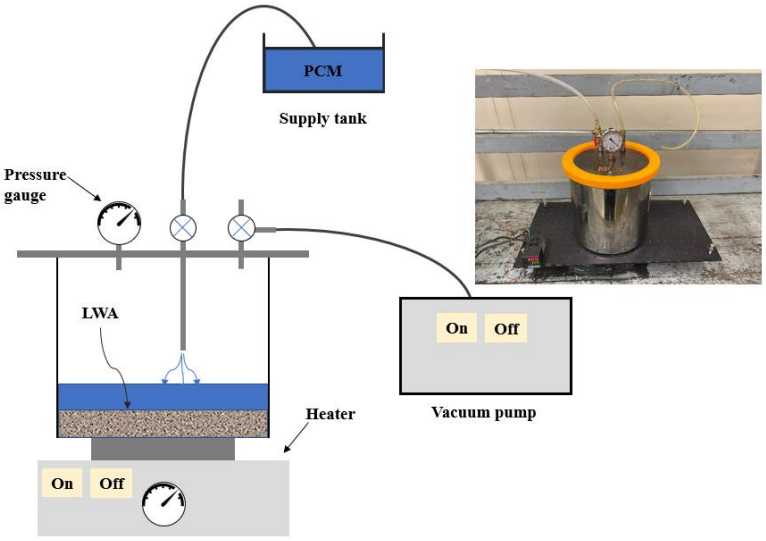


Figure 5-4: Infusion vacuum setup.

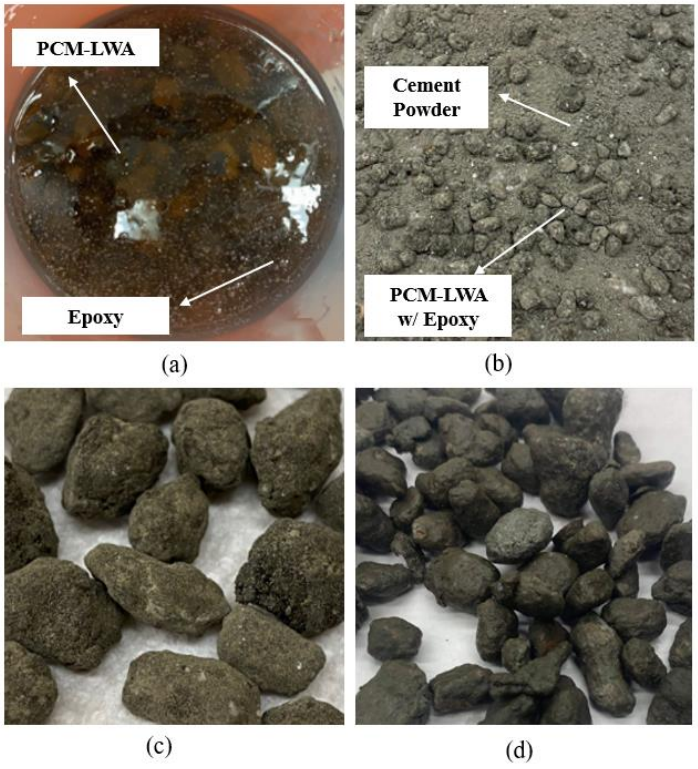


Figure 5-5: Microencapsulation coating procedure: (a) LWA immersion in epoxy; (b) cement coating of epoxy; (c) air curing of coated LWA; (d) PCM-LWAs following water curing.

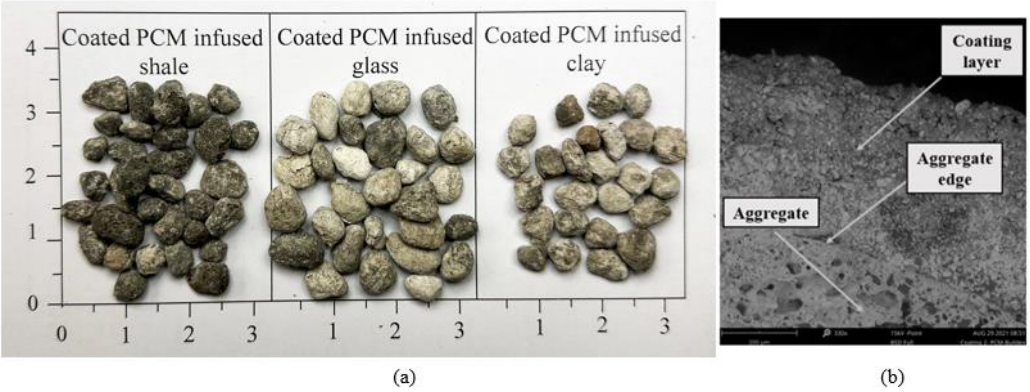


Figure 5-6: (a) Coated encapsulated LWAs (scale in cm); (b) SEM image of coated encapsulated shale.

Table 5-3: Physical and thermal properties of the encapsulated LWAs.

	Coated encapsulated Shale	**Coated encapsulated Clay**	**Coated encapsulated Glass**
Specific gravity	1.45	1.29	1.01
Bulk density [kg/m^3]	867	768	595
Void content [%]	40.10	38.90	40.90
Absorption (%) by weight	3.0	12.0	17.0
Specific heat [kJ/kg·°C]	1.32	1.29	1.38
PCM impregnation rate (%) by weight	40	44	120
PCM impregnation rate (%) by volume	32.5	36.4	57.0

5.2.4 Macro-Encapsulated PCM

Alternative macro-encapsulation methods were examined. The goal was to explore if an alternative procedure could be used to store PCM in small containers without the need to infuse them into the aggregate. Plastic balls of various sizes and wall thickness were examined but the cost of the balls and time required to manually inject PCM into each ball

was found to be prohibitive. An alternative method was examined which consisted of freezing the liquid PCM in 28-mm diameter sphere-shaped ice molds. The solid PCM spheres were then coated to provide an impermeable shell. The same dual-layer coating approach used for the microencapsulated aggregates was used as shown in Figure 5-7.



Figure 5-7: Macro-Encapsulated PCM: (a) Solid PCM balls; (b) Coated PCM balls.

5.3 METHODOLOGY

5.3.1 Pervious Concrete Design

The mix design approach proposed by the National Ready-Mix Concrete Association (NRMCA) was adopted [89]. According to ACI Committee 522 [7], pervious concrete has a porosity ranging from 15 to 35%, water to cement (w/c) ratio from 0.27 to 0.43, and permeability of 0.1 to 1.2 m/s when made from normal weight aggregates. Lower porosity leads to decreased permeability, which negatively impacts cooling applications. Conversely, higher porosity, above 35%, significantly diminishes compressive strength, rendering the concrete unsuitable for non-structural purposes. Hence, a porosity level of 30% was chosen to strike an optimal balance between strength and permeability. Type II Portland cement is used in this study with w/c ratio of 0.30 to achieve a porosity of $30\pm1\%$.

PC mixtures were made from non-encapsulated LWA and encapsulated PCM-LWAs. A blended PC is also fabricated consisting of siliceous crushed stone (SCS) normal weight aggregate and Macro-encapsulated PCM. Baseline mixes without PCM were also made for each mix design. The physical and thermal properties of SCS are listed in Table 5-2Table 5-2: Physical and thermal properties of the aggregates. The mix proportions used in this study and measured porosity and bulk density are listed in Table 5-4Error! Reference source not found.. The mixes are formulated assuming that the micro and macro encapsulated PCM do not absorb any water.

Table 5-4: Pervious concrete proportions

Mix code	Cement (kg/m3)	Aggregate (kg/m3)	Water (kg/m3)	PCM (kg/m3)	Epoxy (kg/m3)	Measured Porosity (%)	Bulk Density (kg/m3)
Shale w/ PCM	226	460	68	180	100	29.9 ±0.48	1120
Shale w/o PCM	266	595	71	0	0	29.6 ± 0.25	1100
Glass w/ PCM	290	167	87	310	100	29.8 ± 0.17	850
Glass w/o PCM	334	280	100	0	0	30.6 ± 0.29	690
Clay w/ PCM	293	359	88	200	100	31.4 ± 0.49	1150
Clay w/o PCM	310	564	93	0	0	30.6 ± 0.10	1110
SCS w/o PCM	281	1360	85	0	0	30.8 ± 0.50	NM
75% Macro-encapsulated PCM-25% SCS PC	372	435	112	292	148	Not measured	NM

5.3.2 PC w/o PCM

A consistent mixing procedure similar to that reported by Kevern et al. [8] was adopted to prepare the conventional PC (without PCM). The samples were batched using the following steps. The aggregates were soaked for twenty-four hours to ensure that the aggregate pores were saturated prior to concrete batching. This is necessary as LWAs typically have very high absorption capacity which can complicate determination of water content during batching. The excess water was drained for four hours prior to batching. Three moisture contents and three absorption samples were taken and averaged to

determine the amount of additional water needed to meet the target w/c ratio. The batching initiated by mixing the saturated aggregate and 5% of the required cement in an auto mortar mixer for 1 minute. The remaining amount of cement, water, and superplasticizer were added and mixed for three minutes followed by a two-minute rest before continuing for another three minutes of mixing.

5.3.3 Microencapsulated PCM PC

Micro-encapsulated LWA was used for the PCM-PC fabrication. The batching procedure followed the steps used for the baseline pervious concrete with the exception that pre-soaking of the aggregate was not required. The micro-encapsulated LWAs were used in a dry condition. Since the aggregates were epoxy coated and included a light coating of hydrated cement these aggregates were assumed to have no surface moisture and zero water absorption.

5.3.4 Macro-Encapsulated PCM PC

Macro-encapsulated PCM-PC consisted of a combination of 75% macro-encapsulated PCM balls and 25% normal weight aggregate, measured by volume. The macro-encapsulated PCM balls and the normal weight aggregate were carefully placed into the rotating mixer. After the PCM balls and aggregate were added, cement and water were introduced into the mixer according to the proportions specified in Table 5-4. Once all the components were in the mixer, the rotating action was initiated, allowing for thorough mixing and distribution of the PCM balls, aggregate, cement, and water as shown in Figure 5-8. The mixing process continued for a duration of three minutes, ensuring a homogenous

mixture was achieved. The PCM-based concrete mixture was promptly cast into plastic molds and then compacted for 10 seconds using a vibration table.

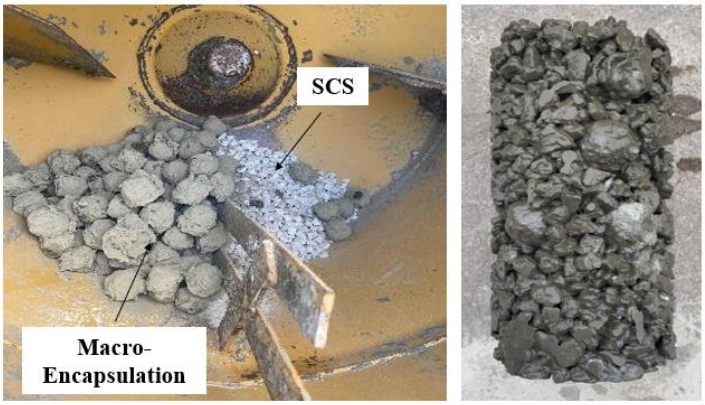


Figure 5-8: (a) Macro-encapsulated PCM prior to mixing; (b) Macro-encapsulated PCM PC sample.

5.4 TESTING PROCEDURE

5.4.1 Mechanical Properties

Cylinders were molded and were compacted using a vibration table for ten seconds. The samples were cured in a water bath at 19 ± 1 °C for 7 and 28 days. The cylinders were air dried for 24 hours at room temperature prior to testing resulting in compressive strength measurements at 8- and 29-days after fabrication. The tests were conducted on standard 100 mm diameter and 200 mm long cylinders. The tests were conducted in accordance with ASTM C39-21[129].

5.4.2 Porosity and Permeability Measurements

For consistency, all PCM mixes were designed to have a volumetric porosity of 30%. Due to the natural shape and surface characteristics of the aggregates and the thixotropic properties of the plastic paste the in-situ porosity varies. The measured porosity varied from 29.6% to 31.4% as shown in Table 5-5. The porosity of the hardened PCM samples was measured in accordance with ASTM C1754 [93]. For the porosity measurements, 100 mm diameter and 200 mm long cylinders were used. Three representative specimens from each PC mix were cured in water overnight then weighed in water. The dry weight of the sample and the volume of the samples were obtained. The porosity of PC specimens is determined by taking the difference in weight between dry weight and submerged weight as shown in Equation (5.1).

$$P = \left[1 - \left(\frac{W2 - W1}{\rho_w \cdot V_s}\right)\right] 100\% \tag{5.1}$$

Where P is the porosity (%); W1is the weight of sample in water (kg); W2 is the dry weight of sample (kg); V_s is the volume of sample (mm^3); and ρ_w is the density of water (kg/mm^3).

In order to determine the coefficient of water permeability, k, for the PC samples, a total of three representative samples from each mixture were prepared by casting them into PVC pipes with a 76.2 mm inner diameter. These samples were tested using a falling head permeameter. The experimental setup for the falling head permeability test is shown in Figure 5-9**.** The permeability test was performed in accordance with ASTM D5084 [130]. The coefficient of permeability was determined using a 50 mm head drop from 146 mm (h_1) to 94 mm (h_2). The average k of three specimens were determined using Equation (5.2).

$$k = \frac{a \cdot L}{A' \cdot t} \ln\left(\frac{h_1}{h_2}\right) \tag{5.2}$$

Where, k: coefficient of permeability, cm/sec; a: cross-sectional area of the standpipe, cm^2; L: length of sample, mm; A': cross-sectional area of specimen, mm^2; t: time for water to drop from h_1 to h_2, mm; h_1: initial water level, mm; h_2: final water level, mm.

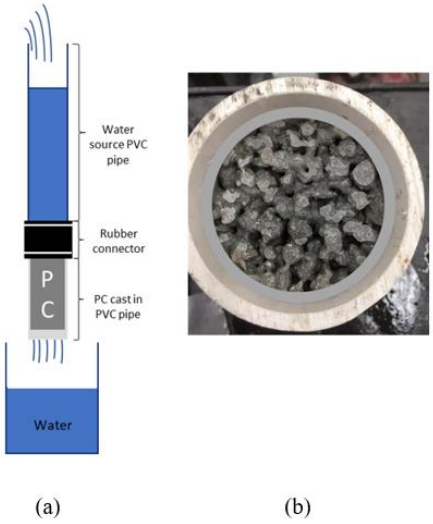


Figure 5-9: (a) Schematic model of water permeability setup; (b) Top view of water permeability sample.

The air permeability test setup used in this study is shown in Figure 5-10. The setup of the air permeability test consists of a rigid PVC pipe with a length of 152.4 mm and an inner diameter (D) of 76.2 mm. The PVC pipe is positioned between two metal plates, which are sealed at the junction with grease to ensure a tight seal. The top metal plate features a hole connected to a pitot tube, allowing airflow from a central laboratory pump to pass through the sample inside the PVC pipe. A flow meter is installed between the central pump valve and the top metal cup to measure the airflow rate. The bottom metal cup facilitates the exit of airflow from the sample. The pervious concrete sample of length, L, 101.6 mm is cast at the middle of PVC pipe. In order to measure the static pressure drop, $\Delta P_M = P_2 - P_1$,

induced by the resistance of the sample to the air passing through, two pitot tubes connected with electronic pressure gauges located at 12.7 mm above and below the sample were installed. Experimental data was collected at standard atmospheric pressure of 100 kPa and temperature of 20 °C.

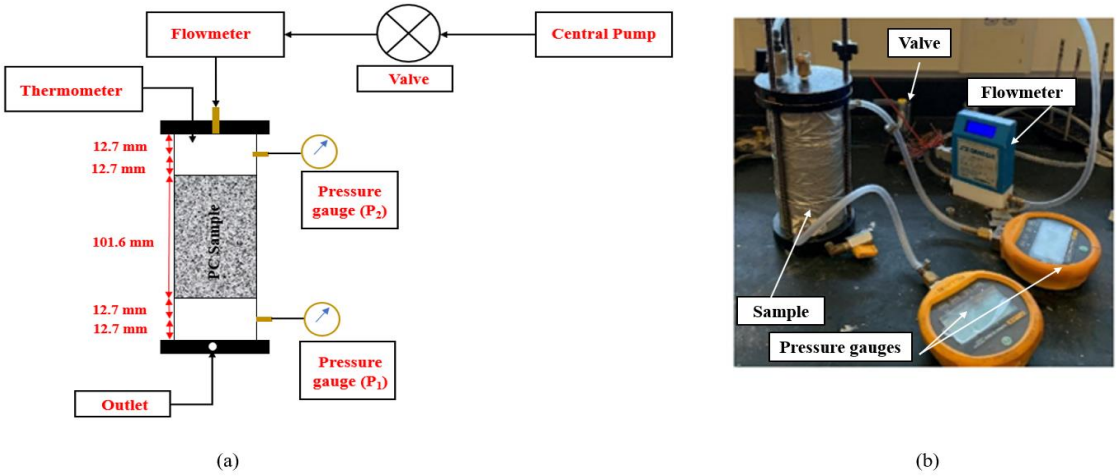


Figure 5-10: (a) Schematic model; (b) Pressure drop setup.

5.4.3 Heat Capacity Measurements

The heat transfer testing is conducted on one PC sample from each batch to investigate their thermo-fluid flow and charging performance across a temperature range of 23 °C to 32 °C with air velocity range of 0.36 to 0.44 m/s. Additionally, the heat energy stored within the PC samples is measured and compared with the theoretical energy storage capacity of the PC material. Figure 5-11 shows a schematic (without the thermal insulation layer) of the experimental setup which consists of a cylindrical PC sample, electrical heater, and a vacuum. The PC is cast in PVC pipe with length of 152.4 mm and inner diameter, D, of 76.2 mm. Moreover, an anemometer is used to measure the air flow velocity and type T thermocouples are installed to measure the one-dimensional temperature difference.

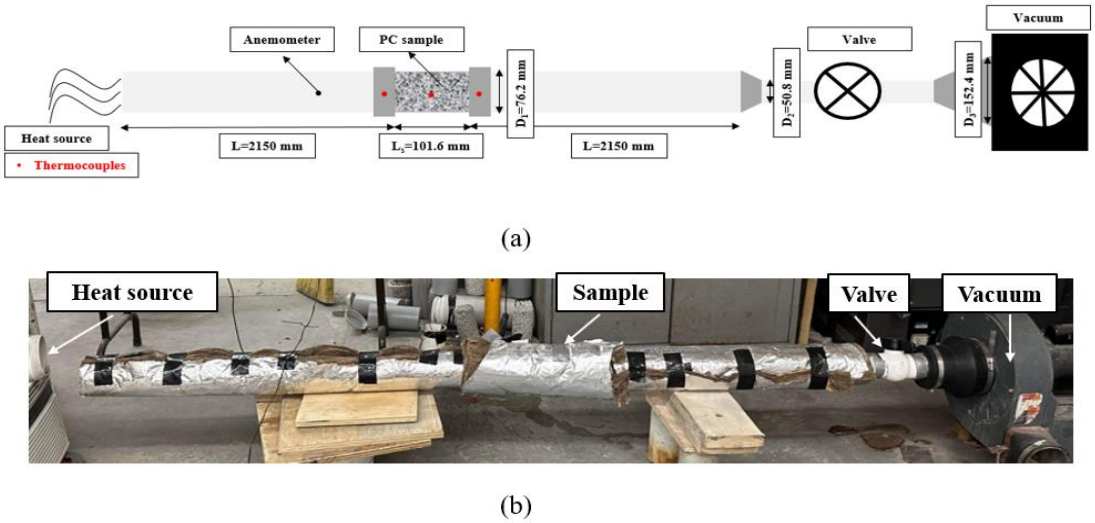


Figure 5-11**:** (a) Schematic model; (b) Thermal heat transfer setup.

During the initial stage, a vacuum is employed to create a negative pressure, leading to airflow through the PVC pipe. To establish thermo-equilibrium, the heater is turned off for the first hour, allowing the specimen to stabilize at the room temperature of approximately 23°C. After the first hour, the charging phase commences, and the heater is activated setting the input airflow to approximately 32°C. The heated air flows through the setup shown from left to right. Throughout the airflow process, temperatures are monitored using T-type thermocouples with an accuracy of ±0.5 °C. Data is collected at 1 Hz with air velocity and mass flow rate measured concurrently using a PCE-423 anemometer, which has an accuracy of 0.05 m/s and a sampling rate 1Hz. During the charging phase, the instantaneous amount of energy stored in the PC can be determined using the following Equation (5.3) [126]:

$$E_{stored} = \sum \dot{m} \cdot C_{pair} \cdot (T_{in} - T_{out}) \cdot \Delta t \tag{5.3}$$

Where $\dot{m}$ is the mass flow rate (kg/s), C_{pair} is the air specific heat (1 kJ/kg·°C), T_{in} is the temperature at inlet of storage tank °C and T_{out} is the temperature at the outlet of storage tank °C and Δt is time step duration. The mass flow rate of air can be calculated by the following Equation (5.4):

$$\dot{m} = v \cdot A \cdot \rho_{air} \tag{5.4}$$

Where v is the air velocity in the pipe, m/s, A is the internal cross-sectional area of the pipe, m^2, and $\rho_{air}$is air density, kg/m^3.

5.5 RESULTS AND DISSCUSION

5.5.1 Mechanical and Hydraulic Properties

The compressive strengths of PCM Lightweight Aggregates (LWAs) incorporated with shale, glass, and clay mixes were significantly lower compared to the PC mix without PCM, as indicated in

Table 5-6. Specifically, the 8-day and 29-day compressive strengths of the PCM LWAs-PC mixes were reduced by 5% to 65%. It is essential to note that these reductions are relative to the strengths of the respective aggregates. To provide clarity, please refer to Table 5-5 Table 5-5: Mechanical and hydraulic concrete properties for a detailed breakdown of the strengths for each mix. In terms of mechanical properties, the addition of epoxy had a notable impact, particularly in the cases of clay and shale mixes. The introduction of epoxy significantly improved the strength of the aggregates, causing a shift in the failure mechanism from the aggregate to the interface with the cement paste.

However, it's important to mention that this improvement came at the expense of bond strength, leading to a sharp deterioration in overall strength, decreasing to approximately 5 MPa, as demonstrated in Figure 5-12. Conversely, due to the inherent weakness of glass aggregates, the addition of epoxy did not have a significant impact, and the strength values remained relatively unchanged. The failure continued to occur primarily at the aggregate level, indicating that the epoxy addition did not substantially enhance the overall strength of the material. The compressive strength of the glass-PC mix was the lowest among the different types of aggregates. This can be attributed to the high porosity of glass LWA which allows for high PCM impregnation but also results in a fragile aggregate that is prone to breakage even during the mixing process.

Although all samples were designed to achieve identical porosity the values vary slightly depending on the aggregate types as illustrated in Table 5-5. The measured porosity of all mixes is in good agreement (with a total coefficient of variation of 1.07% for all samples tested) which allows for the comparison between the fabricated mixes. A compressive strength test was conducted on a PC mixture containing 75% by volume of PCM balls. The test was conducted in two phases as shown in Figure 5-13. A liquid phase when the sample temperature exceeded 25 °C, with the PCM being in a liquid state within the balls, and a solid phase when the sample temperature was below 25 °C. A noticeable difference in values was observed, where the solidification of the PCM significantly improved the compressive strength by up to 67%. The failure occurring during freezing happens at the interface. However, when the PCM transitions to a liquid state, the encapsulated PCM spheres become weaker, leading to a failure plane through the shell of the spheres. These

values were compared to those of PC containing 100% SCS without PCM, revealing a deterioration in strength by up to 85%.

Table 5-5: Mechanical and hydraulic concrete properties

Mix ID#	Mix code	Compressive strength (MPa)		Water permeability (cm/s)
		8-day	29- day	
1	Shale PC w/ PCM	5.00 ± 0.21	5.20 ± 0.42	3.10 ± 0.09
2	Shale PC w/o PCM	8.70 ± 0.50	10.50 ± 0.79	2.64 ± 0.12
3	Glass PC w/ PCM	2.00 ± 0.31	2.40 ± 0.34	6.19 ± 0.08
4	Glass PC w/o PCM	1.90 ± 0.24	3.20 ± 0.32	5.40 ± 0.04
5	Clay PC w/ PCM	4.90 ± 0.16	5.00 ± 0.12	1.92 ± 0.10
6	Clay PC w/o PCM	9.20 ± 0.28	14.30 ± 0.34	1.57 ± 0.03
7	SCS PC w/o PCM	17.50 ± 1.20	19.00 ± 1.72	2.60 ± 0.09
8	75% Macro-encapsulated PCM-25% SCS PC (>25°C)	0.87	0.92	Not measured
9	75% Macro-encapsulated PCM-25% SCS PC (<25°C)	1.19	2.79	Not measured

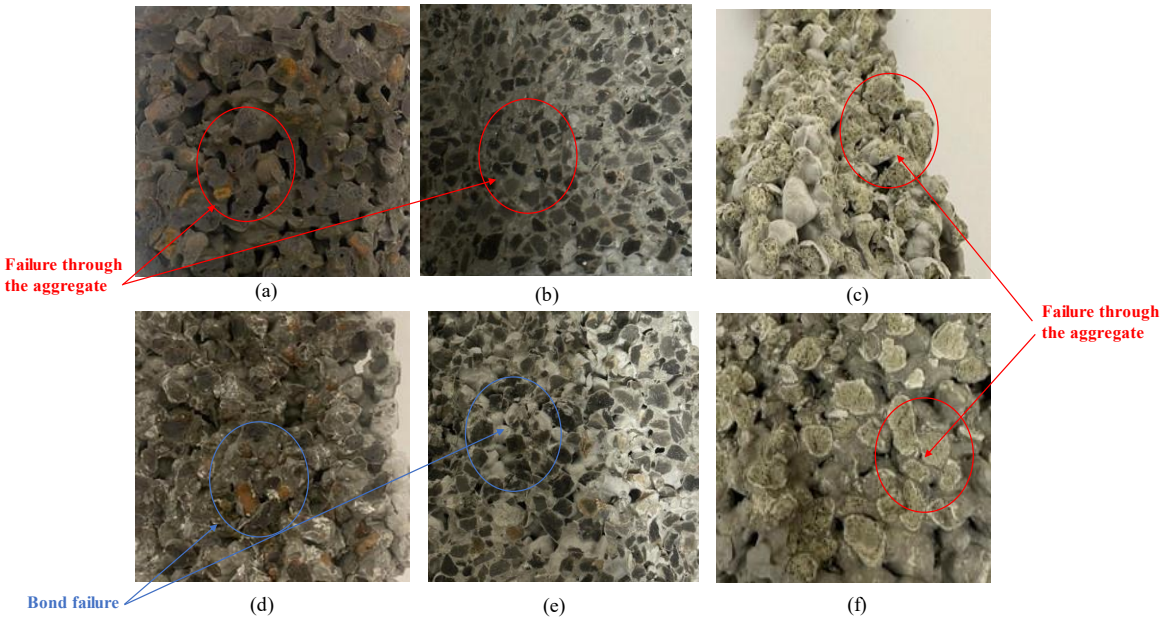


Figure 5-12: failure mode of PCM-PC samples: (a) Shale PC w/o PCM; (b) Clay PC w/o PCM; (c) Glass PC w/o PCM; (d) Shale PC w/ PCM; (e) Clay PC w/ PCM; (f) Glass PC w/ PCM.

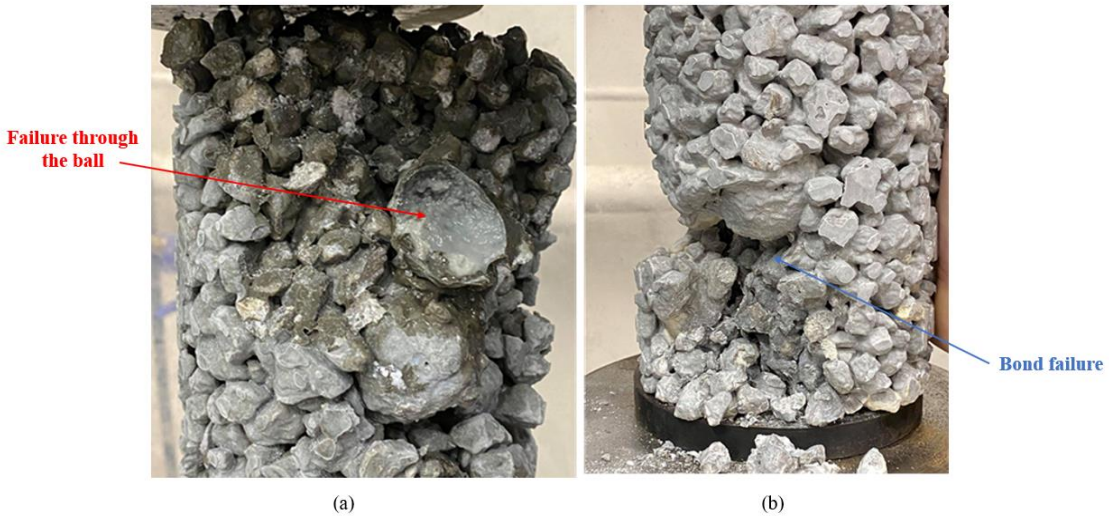


Figure 5-13: Failure mode in PCM macro-encapsulated PC: (a) liquid phase; (b) solid phase.

5.5.2 Water and Air Permeability

The resistance to water and air flow were quantified by measuring the water permeability and pressure drop through the fabricated mixes. The water permeability coefficient of PCM LWAs-PC with shale, glass, and clay mixes was found to be higher compared to the PC mix without PCM as summarized in Table 5-5. In the process of coating, particle diameter increases, consequently enlarging the internal voids and enhancing permeability. This behavior was demonstrated in a study by Joshi where larger aggregate diameter resulted in higher water permeability [98]. The increase in diameter due to the epoxy cover thickness was determined using the SEM apparatus and was found to range from 600 to 800 micrometers. The water permeability coefficient of the PCM LWAs-PC mixes increased by 11% for shale, 15% for glass, and 22% for clay mixes when compared to the PC mix.

Similarly, the larger diameter PCM-PC samples produced lower pressure drop due when compared to the uncoated PC aggregates. Air pressure drop through particle media is generally a function of particle diameter as shown by Ergun [66]. Figure 5-14 presents the pressure drop versus velocity of the air flow for all mixes. The experimental pressure drop measurements for each mix can be fitted by the quadratic curve presented in dashed lines with a high accuracy level (i.e., regression factor higher than 0.98 for all mixes). This quadratic relationship arises from the turbulent airflow that occurs when passing through the pervious concrete even at low velocities [65]. Moreover, it can be observed that the variations in pressure drop are greater in the samples without coating compared (i.e., No PCM) to the samples with coating (i.e., with PCM). This may be attributed to the different shapes of the aggregate particles which are more pronounced in the uncoated stones. In

general, the coating results in a smoother and uniform shape as shown in Figure 5-2 and Figure 5-6.

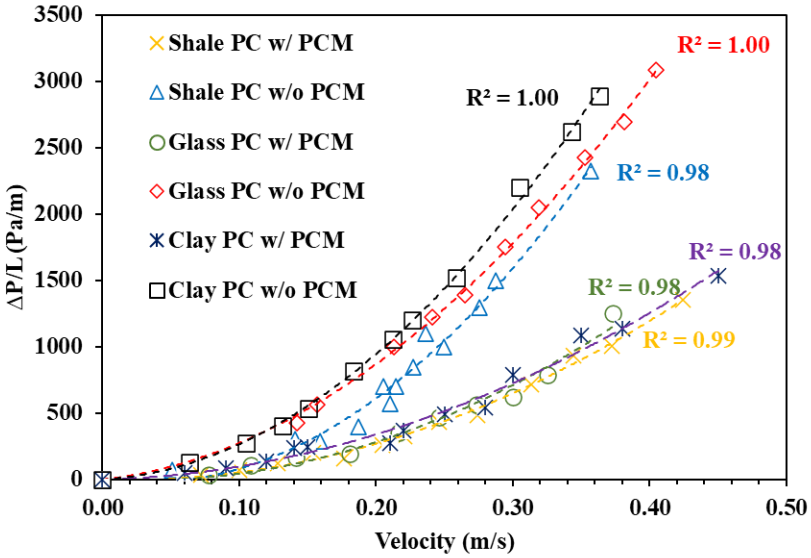


Figure 5-14: Pressure drop for all mixes.

5.5.3 Heat Transfer of Pecked Bed and PC

The energy storage capacity of the infused Lightweight Aggregates (LWAs) was assessed in this study by preparing packed beds of these infused aggregates or utilizing the infused aggregates in PC mixtures. The macro-encapsulated samples were not evaluated for their heat transfer performance due to their significantly lower strength characteristics. Nine samples were prepared, three packed beds consisting of PCM infused shale, glass, and clay, and the remaining six were PC specimens using the same aggregate types in both PCM infused and non-infused conditions. Note that the packed bed and pervious concrete made from the same materials have different proportions of cement paste and PCM due to differences in the void characteristics of each aggregate type. For example, the packed bed of glass and clay have a higher expected heat capacity than pervious concrete while the

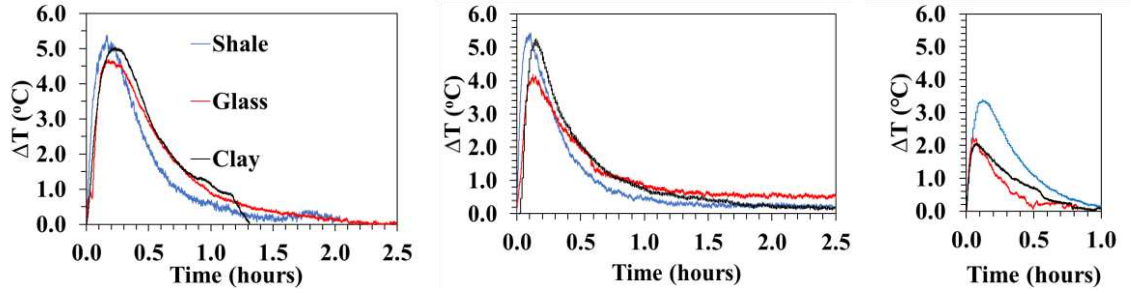
opposite is true for the shale. The estimated mass of the sample and mass of PCM used in each case is summarized in

Table 5-6. The samples were initially brought to room temperature ranging from 20 to 23°C and then subjected to airflow at 32 to 38 °C until the inlet and outlet temperatures were equal. The measured heat capacity was estimated using the approaches previously summarized in Equation (2.1) and Equation (5.3). The theoretical and experimental heat energy are presented in

Table 5-6. The theoretical values were determined from the measured mass of materials used in each case. The error between the measured and theoretical values varies from 2.2 to 13.3 % with the glass aggregate samples having a greater deviation. This is likely attributed to the low strength of the glass aggregate which can result in damage to the material during fabrication. The temperature differences are summarized in Figure 5-15. Both PCM infused packed bed and PC samples are capable of providing a shift in thermal outlet temperatures for at least 2 hours. This duration may be insufficient for large cooling applications and realistic daily thermal temperature ranges due to the relatively small size of the samples and the associated limited amount of PCM infused in them. Nevertheless, the information provided lays the groundwork for the development of larger-scale panels that can accommodate longer duration thermal variations. The PCM infused samples are able to decrease the outlet temperatures by more than 2 °C for 30 minutes for shale and clay PCM infused and 43 minutes for glass PCM infused. This duration decreases to only 10 to 16 minutes with the non-infused concrete sample. The results showed that the glass PCM infused LWAs exhibited the highest latent heat capacity due to the higher volume of PCM infused, leading to a slow equilibrium process taking up to 4 hours.

Table 5-6: Heat capacity for PC

Sample name	Mass of sample [kg]	Mass of PCM [kg]	ΔT [°C]	Total Heat Capacity [kJ/m^3]	Measured Total Heat Capacity [kJ/m^3]	Error [%]
Shale PCM infused	0.400	0.094	10.10	40100	41000	-2.24
Glass PCM infused	0.300	0.165	11.70	63000	57300	9.04
Clay PCM infused	0.400	0.113	9.30	47000	51200	-7.50
Shale PC w/ PCM	0.520	0.094	14.93	45420	44700	1.60
Shale PC w/o PCM	0.514	0	10.60	9800	10500	-7.14
Glass PC w/ PCM	0.400	0.143	11.70	60650	51250	13.34
Glass PC w/o PCM	0.320	0	12.30	7200	8000	-11.15
Clay PC w/ PCM	0.532	0.100	14.53	46600	45800	1.71
Clay PC w/o PCM	0.513	0	12.50	9400	10100	-7.44

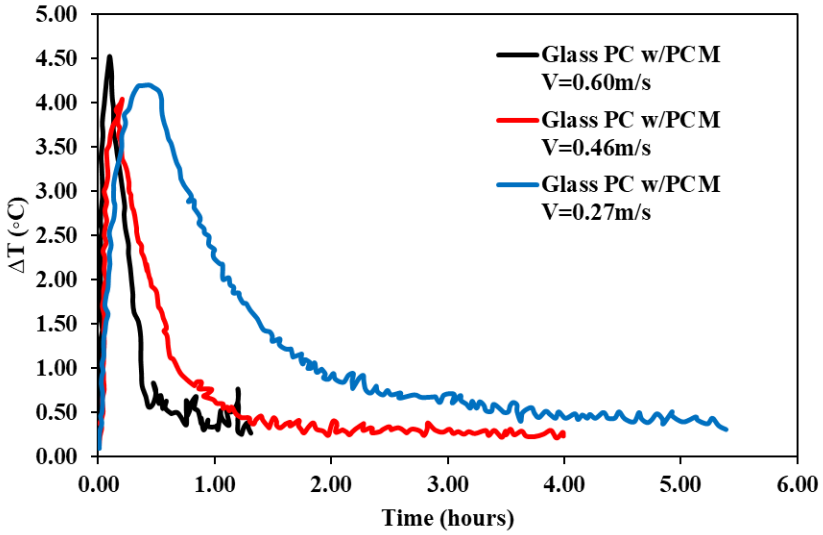


(a) (b) (c)

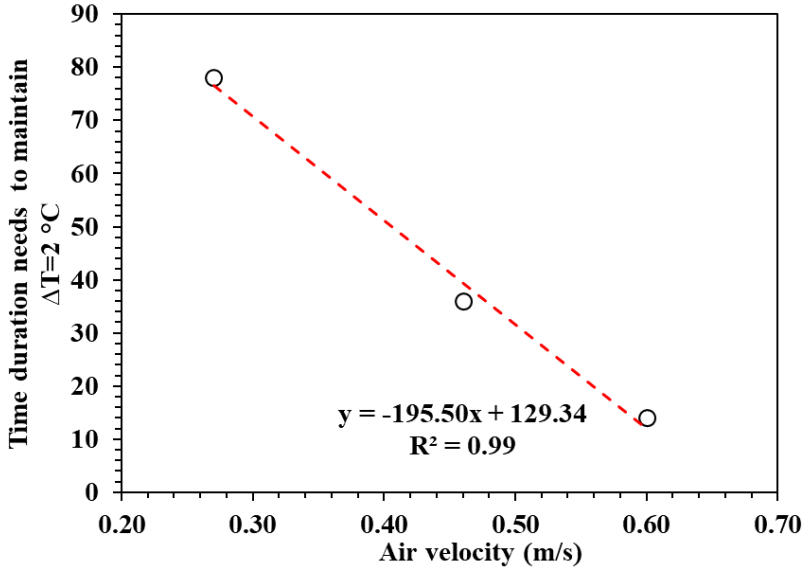
Figure 5-15: Temperature difference between inlet and outlet in charging phase: (a) PCM infused packed bed; (b) PCM infused PC; (c) PC w/o PCM.

In order to determine the required air velocity in designing a cooling system, a study was conducted to examine the impact of air velocity on the duration during which a PCM-PC cooling system can maintain a temperature difference of 2°C. Figure 5-16 (a) illustrates the

impact of varying air velocity on the duration required for the glass PCM-PC in the phase change process. As noted in Equation (5.3) the energy is linearly related to time and mass flow with mass flow linear related to velocity. Since the total energy transferred remains constant across the three trials and equals the integration of time for the area under the curve, it follows that energy and time are linearly proportional. Consequently, time and velocity are expected to be linearly proportional as demonstrated in Figure 5-16 (b). To maintain a temperature change of 2 °C the time needed decreases linearly from 1 hour and 20 minutes at a velocity of 0.27 m/s to less than 15 minutes at a velocity of 0.60 m/s as shown in Figure 5-16 (b).



(a)



(b)

Figure 5-16: (a) Temperature difference between inlet and outlet in charging phase for glass PCM-PC at different velocities; (b) a time duration needs to maintain a temperature change of 2 °C.

5.6 DESIGN RECOMENDATIONS

For effective design, selecting the right type of aggregate, determining porosity, and water-to-cement ratio (w/c) are essential to meet the criteria of strength, stored energy, and

pressure drop. This study focused mainly on types of aggregates. Strength of the fabricated panel is a function of the crushing strength of each aggregate type. It was noted that the strength of concrete containing either clay or shale aggregates are comparable and higher than that of the glass aggregate. The choice of aggregate type does not significantly affect the pressure drop since the study was conducted using aggregates of nearly the same size and it did not appear that surface characteristics significantly impact the air flow channels when used in pervious concrete.

The type of aggregate impacts the strength and the amount of stored energy as shown in Figure 5-17. The three PC w/ PCM have the same porosity of 30%. Both shale and clay aggregates provide favorable strength and heat capacity. The shale has a marginally higher strength with marginally lower heat capacity than the clay. Both materials have almost double the strength compared to glass aggregate. Due to the high absorption capacity of the glass, however, the heat capacity of the glass is higher. If strength is not an issue, glass can be used to maximize heat capacity.

The strength requirements for this concrete are dependent on the application for which it will be used. For a use as a non-structural panel element a criterion can be defined that the panel must be capable of supporting their self-weight without experiencing any cracking. This can be determined in accordance with standard design codes such as ACI 318-19 [131]. As an example, if the panel is spanning horizontally the section must resist flexural demands. Cracking can be prevented by providing adequate panel depth or concrete strength to ensure that the self-weight flexural demand is less than the flexural capacity of the panel. This can be accomplished using standard principles of structural engineering along with recommended factors of safety. For a panel that is simply supported (i.e., pin –

roller support) the flexural moment demand due to self-weight can be determined as shown in Equation (5.5). The flexural resistance can be determined based on the flexural cracking moment as calculated using the Equation (5.6).

$$M = \frac{WL^2}{8} \tag{5.5}$$

$$M_{cr} = \frac{2f_r I}{d} \tag{5.6}$$

Where W is the weight per length of panel *x* factor of safety of 1.4 (kN/m), L is the span length of panel (m), f_r is the modulus of rupture capacity of the concrete material, I is the moment of inertia of the cross-section (m^4), and d is the depth of the panel (m). In case the moment from the self-weight is higher than cracking moment, the panel will fail. The modulus of rupture is related to the concrete compressive strength ($f'c$) as shown in Equation (5.7). Consequently, lower strength concrete or a smaller moment of inertia or depth will yield a lower cracking moment and therefore be prone to cracking on smaller panel dimensions.

$$fr \approx Constant\ x\ \sqrt{f'c} \tag{5.7}$$

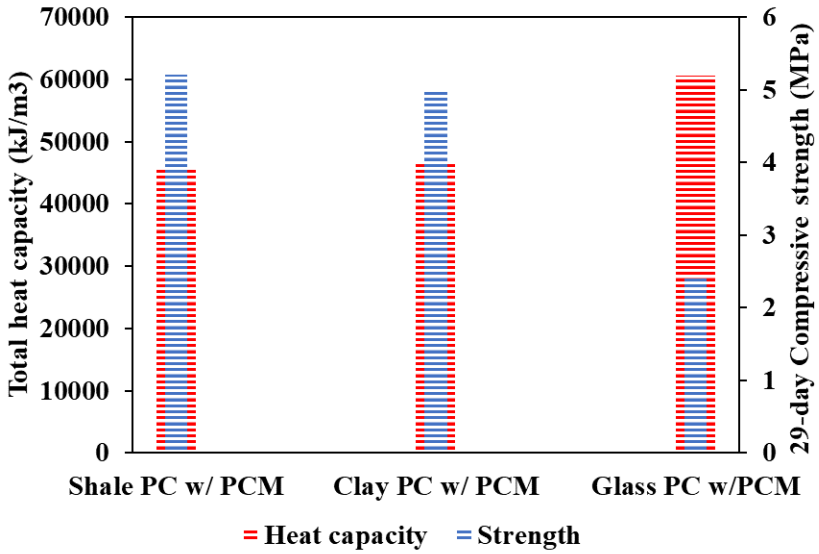


Figure 5-17: The compressive strength and total heat capacity of PC w/ PCM for different types of aggregate at the same porosity (30%).

5.7 SUMMARY AND CONCLUSION

An experimental investigation assessed the applicability of pervious concrete (PC) integrated with phase-change materials for dry cooling application. The study primarily centered on examining various material characteristics, including porosity, water permeability, pressure drop, PCM absorption capacity, and compressive strength. These evaluations were carried out for different types of lightweight aggregates (LWAs) and at different ages. The following conclusions can be drawn from the study:

- SEM analysis indicates that LWAs exhibit a highly porous structure with interconnected pores, enabling volumetric PCM infusion ranging from 36% to 64%.
- The compressive strengths of PCM LWAs-PC with shale, glass, and clay mixes were significantly lower compared to the PC no PCM mix due to a change in the failure plane from through the aggregate to the interface between the coated

aggregate and the paste. Strengths were reduced by 42 to 65% for the stronger clay and shale aggregates but remained less than 25% for the weaker glass aggregates.

- The macro-encapsulation process is influenced by PCM phase changes. Above 25°C, PCM transforms into a liquid within the balls, and below 25°C, it solidifies. Solidification significantly enhances compressive strength by up to 67%. The compressive strength is less than 1 MPa making it unsuitable even for non-structural concrete.
- The water and air permeability of PCM-PC is greater than conventional LWA PC due to the increase in aggregate size from the coating process.
- PCM infused LWAs packed bed and PC are able to transfer sensible and latent heat, as expected. Notably, the PCM-infused samples demonstrate the ability to sustain a shift in thermal outlet temperatures for a minimum of 2 hours.
- Shale and clay have similar strength and heat capacity; Glass has lower strength but higher heat retention due to its absorption capacity. If strength is not a priority, glass aggregate provides the greatest heat capacity.
- Increasing air velocity in a PCM-PC cooling system reduces linearly the time required to maintain a 2°C temperature difference. This linear relationship emphasizes the potential for establishing a standardized performance metric in cooling system design.

In summary, the PCM-PC composites exhibit a relatively high porosity of approximately 30% alongside a moderate 28-day compressive strength of 5.0 MPa. Moreover, they demonstrate the capability to maintain a shift in thermal outlet temperatures for a minimum

of 2 hours. Further research is warranted to fully assess the thermal energy storage performance of PCM-impregnated PC for larger-scale dry cooling applications.

6 SUMMARY AND CONCLUSIONS

This doctoral dissertation research was dedicated to the advancement of dry cooling tower efficiency by mitigating the consumption of fresh water in the pre-cooling process through the development of an innovative dry pre-cooling system. The approach involved the design and development of a Cold Thermal Energy Storage System (CTESS), incorporating phase change material (PCM) encapsulated within pervious concrete.

Furthermore, the study explored a novel application of pervious concrete by integrating PCM into concrete for use in thermal storage systems and cooling applications. The research aimed to establish an optimum pervious concrete mix design that not only met the requirements for strength but also facilitated permeability. The investigation also involved the development of an empirical model, modifying the Ergun equation, to predict the pressure drop within the pervious concrete structure. This multifaceted approach aimed to contribute valuable insights to the field of sustainable and efficient dry cooling systems.

6.1 RESEARCH CONTRBUTIONS

The research presented in this dissertation contributes significantly to the advancement of pervious concrete (PC) technology, focusing on key aspects such as aggregate utilization, air flow characteristics, and the integration of phase change materials (PCM) for dry cooling applications. This section synthesizes the findings and insights derived from three interconnected studies, each addressing crucial facets of PC performance and applications.

- **Aggregate Utilization in Pervious Concrete**

The initial study delves into the potential of lightweight aggregates (LWAs) to enhance the absorption properties of PC, especially in applications like dry cooling and thermal energy storage. By replacing normal weight aggregate (NWA) with leighweight aggregates (LWA). by using three types of aggregate: Siliceous crushed stone, lightweight expanded clay (LWA 1), and lightweight western shale (LWA 2)), the investigation systematically explores the effects of aggregate type, LWA replacement ratio, water-to-cement ratio (w/c), and paste to aggregate ratio (V_{PA}) on mechanical and hydraulic properties. The study provides essential insights for optimizing PC mix design to meet strength and permeability requirements.

- **Air Flow Characteristics and Thermal Properties**

The second study investigates the performance of PC in heating and cooling applications under forced air conditions. Experimental evaluation of ten mixes explores the influence of aggregate type, water-cement ratio, and paste volume on air flow characteristics. The study reveals nuanced relationships, demonstrating how pressure drop varies with different parameters, such as paste to aggregate ratio and water/cement ratio. Additionally, a modified pressure drop formulation is proposed, facilitating accurate prediction of air flow characteristics in pervious concrete. The assessment of thermal properties and sensible heat energy storage offers essential insights into the energy dynamics of PC systems, contributing to the broader understanding of its applicability.

- **Integration of Phase Change Materials in Pervious Concrete**

The third study addresses the feasibility of incorporating diverse LWAs and PCM into PC for dry cooling applications. Utilizing macro- and microencapsulation techniques, the

investigation evaluates PCM impregnation rates, compressive strength, and pressure drop under air flow. The findings highlight the effectiveness of microencapsulation in reducing pressure drop and showcase the sensitivity of macro-encapsulated PCM to phase transitions. The study systematically explores the comprehensive laboratory experiments, including porosity, water permeability, PCM absorption capacity, compressive strength, and microstructure of LWAs. This research offers valuable insights into the performance of LWAs and PCM in pervious concrete, providing a comprehensive understanding of their interaction in dry cooling applications.

Collectively, these studies contribute to the evolving landscape of pervious concrete technology, offering essential knowledge for sustainable and efficient applications in dry cooling and thermal energy storage systems.

6.2 FUTURE RESEARCH

This study primarily focused on investigating the use of PCM-PC for cooling applications in power plants, such as coal power plants. However, it can also find applications in residential or commercial cooling, where it can be integrated into Heating, Ventilation, and Air Conditioning (HVAC) systems. Almost half of the building energy demand is consumed by the HVAC system to maintain the ventilation requirements. Air handling units (AHUs), as one of the HVAC components, consume a lot of energy. AHUs are composed of coils and designed to supply clean air with proper thermodynamic properties. Particularly, PCM-PC can be added to the AHU of the HVAC system to enhance efficiency by creating a pre-cooling system before the cooling coils. This innovative approach aims to reduce electrical consumption by improving the HVAC system's effectiveness.

To ensure optimal performance and energy conservation, it is necessary to conduct an energy analysis of the AHU, determining the energy content of the supply air before its distribution to the conditioned space. The integration of pervious concrete with PCM into the HVAC system represents a strategic step towards achieving energy efficiency and sustainability in both power plants and various cooling applications.

7 REFERENCES

[1] R. Goldstein, Water Use for Electric Power Generation, EPRI, Palo Alto, CA, 2008.

[2] US Code, Federal Water Pollution Control Act, 2002.

[3] S. Taghian Dehaghani, H. Ahmadikia, Retrofit of a wet cooling tower in order to reduce water and fan power consumption using a wet/dry approach, Applied Thermal Engineering 125 (2017) 1002–1014. https://doi.org/10.1016/j.applthermaleng.2017.07.069.

[4] M.M. Ehsan, X. Wang, Z. Guan, A.Y. Klimenko, Design and performance study of dry cooling system for 25 MW solar power plant operated with supercritical CO2 cycle, International Journal of Thermal Sciences 132 (2018) 398–410. https://doi.org/10.1016/j.ijthermalsci.2018.06.024.

[5] A. Alkhedhair, H. Gurgenci, I. Jahn, Z. Guan, S. He, Numerical simulation of water spray for pre-cooling of inlet air in natural draft dry cooling towers, Applied Thermal Engineering 61 (2013) 416–424. https://doi.org/10.1016/j.applthermaleng.2013.08.012.

[6] S. He, H. Gurgenci, Z. Guan, A.M. Alkhedhair, Pre-cooling with Munters media to improve the performance of Natural Draft Dry Cooling Towers, Applied Thermal Engineering 53 (2013) 67–77. https://doi.org/10.1016/j.applthermaleng.2012.12.033.

[7] ACI Committee 522, American Concrete Institute, Report on pervious concrete, American Concrete Institute, Farmington Hills, MI, 2010.

[8] J. Kevern, K. Wang, M. Suleiman, V. Schaefer, Mix Design Development for Pervious Concrete in Cold Weather Climates, in: Proceedings of the 2005 Mid-

Continent Transportation Research Symposium, Iowa State University, Ames, Iowa, 2005.

[9] Y. Chen, K. Wang, X. Wang, W. Zhou, Strength, Fracture and Fatigue of Pervious Concrete, Construction and Building Materials 42 (2013) 97–104. https://doi.org/10.1016/j.conbuildmat.2013.01.006.

[10] J. Yang, G. Jiang, Experimental study on properties of pervious concrete pavement materials, Cement and Concrete Research 33 (2003) 381–386. https://doi.org/10.1016/S0008-8846(02)00966-3.

[11] A.J. Carrillo, J. González-Aguilar, M. Romero, J.M. Coronado, Solar Energy on Demand: A Review on High Temperature Thermochemical Heat Storage Systems and Materials, Chem. Rev. 119 (2019) 4777–4816. https://doi.org/10.1021/acs.chemrev.8b00315.

[12] S. Wonorahardjo, I. Sutjahja, D. Kurnia, Z. Fahmi, W. Putri, Potential of Thermal Energy Storage Using Coconut Oil for Air Temperature Control, Buildings 8 (2018) 95. https://doi.org/10.3390/buildings8080095.

[13] B. Nie, A. Palacios, B. Zou, J. Liu, T. Zhang, Y. Li, Review on phase change materials for cold thermal energy storage applications, Renewable and Sustainable Energy Reviews 134 (2020) 110340. https://doi.org/10.1016/j.rser.2020.110340.

[14] A.E. Conradie, D.G. Kröger, Performance evaluation of dry-cooling systems for power plant applications, Applied Thermal Engineering 16 (1996) 219–232. https://doi.org/10.1016/1359-4311(95)00068-2.

[15] J. Smrekar, J. Oman, B. Širok, Improving the efficiency of natural draft cooling towers, Energy Conversion and Management 47 (2006) 1086–1100. https://doi.org/10.1016/j.enconman.2005.07.012.

[16] S.A. Leeper, Wet cooling towers: rule-of-thumb design and simulation, 1981. https://doi.org/10.2172/5281927.

[17] N. Milosavljevic, P. Heikkilä, A comprehensive approach to cooling tower design, Applied Thermal Engineering 21 (2001) 899–915. https://doi.org/10.1016/S1359-4311(00)00078-8.

[18] G. Davis, Comparison of Alternate Cooling Technologies for California Power Plants Economic, Environmental and Other Tradeoffs, (n.d.).

[19] X. Li, H. Gurgenci, Z. Guan, X. Wang, L. Xia, A review of the crosswind effect on the natural draft cooling towers, Applied Thermal Engineering 150 (2019) 250–270. https://doi.org/10.1016/j.applthermaleng.2018.12.147.

[20] A. Liqreina, L. Qoaider, Dry cooling of concentrating solar power (CSP) plants, an economic competitive option for the desert regions of the MENA region, Solar Energy 103 (2014) 417–424. https://doi.org/10.1016/j.solener.2014.02.039.

[21] Z. Zou, Z. Guan, H. Gurgenci, Y. Lu, Solar enhanced natural draft dry cooling tower for geothermal power applications, Solar Energy 86 (2012) 2686–2694. https://doi.org/10.1016/j.solener.2012.06.003.

[22] H. Deng, R.F. Boehm, An estimation of the performance limits and improvement of dry cooling on trough solar thermal plants, Applied Energy 88 (2011) 216–223. https://doi.org/10.1016/j.apenergy.2010.05.027.

[23] L. Yan, E. Yaghmour, D. Scott, M.I. Abu Qamar, J. Fox, C. Naito, S. Neti, C.E. Romero, N. Sarunac, M. Suleiman, Experimental investigation of the thermal performance of pervious concrete integrated with phase change material for dry cooling applications, Applied Thermal Engineering 236 (2024) 121749. https://doi.org/10.1016/j.applthermaleng.2023.121749.

[24] Y. Sun, Z. Guan, H. Gurgenci, X. Li, K. Hooman, A study on multi-nozzle arrangement for spray cooling system in natural draft dry cooling tower, Applied Thermal Engineering 124 (2017) 795–814. https://doi.org/10.1016/j.applthermaleng.2017.05.157.

[25] Y. Sun, Z. Guan, H. Gurgenci, K. Hooman, X. Li, L. Xia, Investigation on the influence of injection direction on the spray cooling performance in natural draft dry cooling tower, International Journal of Heat and Mass Transfer 110 (2017) 113–131. https://doi.org/10.1016/j.ijheatmasstransfer.2017.02.069.

[26] L. Xia, H. Gurgenci, D. Liu, Z. Guan, L. Zhou, P. Wang, CFD analysis of pre-cooling water spray system in natural draft dry cooling towers, Applied Thermal Engineering 105 (2016) 1051–1060. https://doi.org/10.1016/j.applthermaleng.2016.03.096.

[27] A. Alkhedhair, I. Jahn, H. Gurgenci, Z. Guan, S. He, Parametric study on spray cooling system for optimising nozzle design with pre-cooling application in natural draft dry cooling towers, International Journal of Thermal Sciences 104 (2016) 448–460. https://doi.org/10.1016/j.ijthermalsci.2016.02.004.

[28] H. Ma, F. Si, K. Zhu, J. Wang, Quantitative research of spray cooling effects on thermo-flow performance of the large-scale dry cooling tower with an integrated

numerical model, International Journal of Heat and Mass Transfer 141 (2019) 799–817. https://doi.org/10.1016/j.ijheatmasstransfer.2019.06.085.

[29] M.H. Sadafi, I. Jahn, K. Hooman, Cooling performance of solid containing water for spray assisted dry cooling towers, Energy Conversion and Management 91 (2015) 158–167. https://doi.org/10.1016/j.enconman.2014.12.005.

[30] Y. Sun, Z. Guan, H. Gurgenci, J. Wang, P. Dong, K. Hooman, Spray cooling system design and optimization for cooling performance enhancement of natural draft dry cooling tower in concentrated solar power plants, Energy 168 (2019) 273–284. https://doi.org/10.1016/j.energy.2018.11.111.

[31] X. Li, L. Xia, H. Gurgenci, Z. Guan, Performance enhancement for the natural draft dry cooling tower under crosswind condition by optimizing the water distribution, International Journal of Heat and Mass Transfer 107 (2017) 271–280. https://doi.org/10.1016/j.ijheatmasstransfer.2016.11.046.

[32] W. Huang, J. Zhang, J. Wang, Y. Zheng, J. Ma, F. Ding, Performance analysis of paraffin microcapsules and phase change concrete based on microporous cenospheres, Construction and Building Materials 409 (2023) 134030. https://doi.org/10.1016/j.conbuildmat.2023.134030.

[33] Y. Qu, J. Chen, L. Liu, T. Xu, H. Wu, X. Zhou, Study on properties of phase change foam concrete block mixed with paraffin / fumed silica composite phase change material, Renewable Energy 150 (2020) 1127–1135. https://doi.org/10.1016/j.renene.2019.10.073.

[34] P. Suttaphakdee, N. Dulsang, N. Lorwanishpaisarn, P. Kasemsiri, P. Posi, P. Chindaprasirt, Optimizing mix proportion and properties of lightweight concrete

incorporated phase change material paraffin/recycled concrete block composite, Construction and Building Materials 127 (2016) 475–483. https://doi.org/10.1016/j.conbuildmat.2016.10.037.

[35] D. Zhang, Z. Li, J. Zhou, K. Wu, Development of thermal energy storage concrete, Cement and Concrete Research 34 (2004) 927–934. https://doi.org/10.1016/j.cemconres.2003.10.022.

[36] M. Hunger, A.G. Entrop, I. Mandilaras, H.J.H. Brouwers, M. Founti, The behavior of self-compacting concrete containing micro-encapsulated Phase Change Materials, Cement and Concrete Composites 31 (2009) 731–743. https://doi.org/10.1016/j.cemconcomp.2009.08.002.

[37] V.A. Salomoni, C.E. Majorana, G.M. Giannuzzi, A. Miliozzi, R. Di Maggio, F. Girardi, D. Mele, M. Lucentini, Thermal storage of sensible heat using concrete modules in solar power plants, Solar Energy 103 (2014) 303–315. https://doi.org/10.1016/j.solener.2014.02.022.

[38] S. Ayyappan, K. Mayilsamy, V.V. Sreenarayanan, Performance improvement studies in a solar greenhouse drier using sensible heat storage materials, Heat Mass Transfer 52 (2016) 459–467. https://doi.org/10.1007/s00231-015-1568-5.

[39] D. Laing, D. Lehmann, C. Bahl, Concrete Storage For Solar Thermal Power Plants and Industrial Process Heat, (2008).

[40] D.W. Hawes, D. Feldman, D. Banu, Latent heat storage in building materials, Energy and Buildings 20 (1993) 77–86. https://doi.org/10.1016/0378-7788(93)90040-2.

[41] M.I. Abu Qamar, E. Yaghmour, X. Wang, C. Naito, M. Suleiman, P. Bocchini, J. Fox, C. Romero, L. Yan, Use of 3D printed concrete components for thermal energy

storage, Construction and Building Materials 411 (2024) 134240. https://doi.org/10.1016/j.conbuildmat.2023.134240.

[42] S.A. Memon, H.Z. Cui, H. Zhang, F. Xing, Utilization of macro encapsulated phase change materials for the development of thermal energy storage and structural lightweight aggregate concrete, Applied Energy 139 (2015) 43–55. https://doi.org/10.1016/j.apenergy.2014.11.022.

[43] A.M. Thiele, G. Sant, L. Pilon, Diurnal thermal analysis of microencapsulated PCM-concrete composite walls, Energy Conversion and Management 93 (2015) 215–227. https://doi.org/10.1016/j.enconman.2014.12.078.

[44] Y. Shen, S. Liu, C. Zeng, Y. Zhang, Y. Li, X. Han, L. Yang, X. Yang, Experimental thermal study of a new PCM-concrete thermal storage block (PCM-CTSB), Construction and Building Materials 293 (2021) 123540. https://doi.org/10.1016/j.conbuildmat.2021.123540.

[45] D.W. Hawes, D. Feldman, Absorption of phase change materials in concrete, Solar Energy Materials and Solar Cells 27 (1992) 91–101. https://doi.org/10.1016/0927-0248(92)90112-3.

[46] J.S. Baruah, V. Athawale, P. Rath, A. Bhattacharya, Melting and energy storage characteristics of macro-encapsulated PCM-metal foam system, International Journal of Heat and Mass Transfer 182 (2022) 121993. https://doi.org/10.1016/j.ijheatmasstransfer.2021.121993.

[47] H. Cui, S.A. Memon, R. Liu, Development, mechanical properties and numerical simulation of macro encapsulated thermal energy storage concrete, Energy and Buildings 96 (2015) 162–174. https://doi.org/10.1016/j.enbuild.2015.03.014.

[48] H. Bendtsen, L.E. Larsen, Two-Layer Porous Pavements and Noise Reductions in Denmark, in: Copenhagen, Denmark, 2002: p. 17. https://trid.trb.org/view/733423 (accessed August 31, 2021).

[49] H.K. Kim, H.K. Lee, Influence of cement flow and aggregate type on the mechanical and acoustic characteristics of porous concrete, Applied Acoustics 71 (2010) 607–615. https://doi.org/10.1016/j.apacoust.2010.02.001.

[50] H. Shang, Z. Sun, PAHs (naphthalene) removal from stormwater runoff by organoclay amended pervious concrete, Construction and Building Materials 200 (2019) 170–180. https://doi.org/10.1016/j.conbuildmat.2018.12.096.

[51] P. Wijeyawardana, N. Nanayakkara, C. Gunasekara, A. Karunarathna, D. Law, B.K. Pramanik, Improvement of heavy metal removal from urban runoff using modified pervious concrete, Science of The Total Environment 815 (2022) 152936. https://doi.org/10.1016/j.scitotenv.2022.152936.

[52] J. Chen, R. Chu, H. Wang, L. Zhang, X. Chen, Y. Du, Alleviating urban heat island effect using high-conductivity permeable concrete pavement, Journal of Cleaner Production 237 (2019) 117722. https://doi.org/10.1016/j.jclepro.2019.117722.

[53] Y. Qin, J.E. Hiller, Water availability near the surface dominates the evaporation of pervious concrete, Construction and Building Materials 111 (2016) 77–84. https://doi.org/10.1016/j.conbuildmat.2016.02.063.

[54] ACI Committee 522, American Concrete Institute, Report on pervious concrete, American Concrete Institute, Farmington Hills, MI, 2010.

[55] N. Neithalath, M.S. Sumanasooriya, O. Deo, Characterizing pore volume, sizes, and connectivity in pervious concretes for permeability prediction, Materials Characterization 61 (2010) 802–813. https://doi.org/10.1016/j.matchar.2010.05.004.

[56] P.D. Tennis, M.L. Leminy, D.J. Akers, Pervious Concrete Pavements, (2004) 36.

[57] Y. Zaetang, A. Wongsa, V. Sata, P. Chindaprasirt, Use of lightweight aggregates in pervious concrete, Construction and Building Materials 48 (2013) 585–591. https://doi.org/10.1016/j.conbuildmat.2013.07.077.

[58] W. Goede, L. Haselbach, Investigation into the Structural Performance of Pervious Concrete, Journal of Transportation Engineering 138 (2012) 98–104. https://doi.org/10.1061/(ASCE)TE.1943-5436.0000305.

[59] F.B. Pereira da Costa, L.M. Haselbach, L.C.P. da Silva Filho, Pervious concrete for desired porosity: Influence of w/c ratio and a rheology-modifying admixture, Construction and Building Materials 268 (2021) 121084. https://doi.org/10.1016/j.conbuildmat.2020.121084.

[60] P. Chindaprasirt, S. Hatanaka, T. Chareerat, N. Mishima, Y. Yuasa, Cement paste characteristics and porous concrete properties, Construction and Building Materials 22 (2008) 894–901. https://doi.org/10.1016/j.conbuildmat.2006.12.007.

[61] A. Ibrahim, E. Mahmoud, M. Yamin, V.C. Patibandla, Experimental study on Portland cement pervious concrete mechanical and hydrological properties, Construction and Building Materials 50 (2014) 524–529. https://doi.org/10.1016/j.conbuildmat.2013.09.022.

[62] Y. Qin, J. Liang, H. Yang, Z. Deng, Gas permeability of pervious concrete and its implications on the application of pervious pavements, Measurement 78 (2016) 104–110. https://doi.org/10.1016/j.measurement.2015.09.055.

[63] S.M. Hassanizadeh, W.G. Gray, High Velocity Flow in Porous Media, Transp Porous Med 2 (1987) 521–531. https://doi.org/10.1007/BF00192152.

[64] HE Rose, On the Resistance Coefficient–Reynolds Number Relationship for Fluid Flow through a Bed of Granular Material, Proceedings of the Institution of Mechanical Engineers 153 (1945) 154–161.

[65] E. Yaghmour, J. Fox, C. Romero, S. Neti, Pressure drop and heat transfer properties for normal weight and lightweight pervious concrete, Construction and Building Materials 425 (2024). https://doi.org/doi.org/10.1016/j.conbuildmat.2024.135947.

[66] S. Ergun, Fluid Flow Through Packed Columns, Chemical Engineering Progress 48 (1952) 89–94.

[67] E. Ozahi, M.Y. Gundogdu, M.Ö. Carpinlioglu, A Modification on Ergun's Correlation for Use in Cylindrical Packed Beds With Non-spherical Particles, Advanced Powder Technology 19 (2008) 369–381. https://doi.org/10.1163/156855208X314985.

[68] I.F. Macdonald, M.S. El-Sayed, K. Mow, F.A.L. Dullien, Flow through Porous Media-the Ergun Equation Revisited, Ind. Eng. Chem. Fund. 18 (1979) 199–208. https://doi.org/10.1021/i160071a001.

[69] Y. Zhao, W. Jin, A. Ikbarieh, J.L. Klinger, N. Saha, D.C. Dayton, S. Dai, SPH Modeling of Biomass Granular Flow: Engineering Application in Hoppers and

Augers, ACS Sustainable Chem. Eng. 12 (2024) 4213–4223. https://doi.org/10.1021/acssuschemeng.3c08090.

[70] A. Bonicelli, F. Giustozzi, M. Crispino, Experimental study on the effects of fine sand addition on differentially compacted pervious concrete, Construction and Building Materials 91 (2015) 102–110. https://doi.org/10.1016/j.conbuildmat.2015.05.012.

[71] A. Beeldens, D. Van Gemert, C. Caestecker, Porous Concrete: Laboratory Versus Field Experience, in: Istanbul, Turkey, 2003.

[72] J. Olek, W.J. Weiss, N. Neithalath, A. Marolf, E. Sell, W.D. Thornton, DEVELOPMENT OF QUIET AND DURABLE POROUS PORTLAND CEMENT CONCRETE PAVING MATERIALS, (2003). https://trid.trb.org/view/698009 (accessed April 26, 2023).

[73] A. Beeldens, D. Van Gemert, A.S. Poupeleer, B. Cornelis, Behavior of porous PCC under freeze-thaw cycling, in: Tenth International Congress on Polymers in Concrete, Honolulu, 2001.

[74] W. Goede, L. Haselbach, Investigation into the Structural Performance of Pervious Concrete, Journal of Transportation Engineering 138 (2012) 98–104. https://doi.org/10.1061/(ASCE)TE.1943-5436.0000305.

[75] A. Bonicelli, F. Giustozzi, M. Crispino, Experimental study on the effects of fine sand addition on differentially compacted pervious concrete, Construction and Building Materials 91 (2015) 102–110. https://doi.org/10.1016/j.conbuildmat.2015.05.012.

[76] G. Bumanis, D. Bajare, A. Korjakins, Mechanical and Thermal Properties of Lightweight Concrete Made from Expanded Glass, Journal of Sustainable

Architecture and Civil Engineering 2 (2013) 19–25. https://doi.org/10.5755/j01.sace.2.3.2790.

[77] S. Ghourchian, M. Wyrzykowski, P. Lura, M. Shekarchi, B. Ahmadi, An investigation on the use of zeolite aggregates for internal curing of concrete, Construction and Building Materials 40 (2013) 135–144. https://doi.org/10.1016/j.conbuildmat.2012.10.009.

[78] E. Mohseni, W. Tang, S. Wang, Development of thermal energy storage lightweight structural cementitious composites by means of macro-encapsulated PCM, Construction and Building Materials 225 (2019) 182–195. https://doi.org/10.1016/j.conbuildmat.2019.07.136.

[79] M.S. Rahman, S. MacPherson, M. Lefsrud, Experimental investigation of a novel evaporative cooling pad made of cement-free porous concrete, Building and Environment 228 (2023) 109867. https://doi.org/10.1016/j.buildenv.2022.109867.

[80] A. Timmer, Building Integrated Evaporative Cooling Utilizing Pervious Concrete, Technology|Architecture + Design 5 (2021) 73–81. https://doi.org/10.1080/24751448.2021.1863675.

[81] L. Yan, E. Yaghmour, D. Scott, M.I. Abu Qamar, J. Fox, C. Naito, S. Neti, C.E. Romero, N. Sarunac, M. Suleiman, Experimental investigation of the thermal performance of pervious concrete integrated with phase change material for dry cooling applications, Applied Thermal Engineering 236 (2024) 121749. https://doi.org/10.1016/j.applthermaleng.2023.121749.

[82] G. Kaplan, A. Gulcan, B. Cagdas, O.Y. Bayraktar, The impact of recycled coarse aggregates obtained from waste concretes on lightweight pervious concrete

properties, Environ Sci Pollut Res 28 (2021) 17369–17394. https://doi.org/10.1007/s11356-020-11881-y.

[83] E. Khankhaje, M.R. Salim, J. Mirza, M.W. Hussin, M. Rafieizonooz, Properties of sustainable lightweight pervious concrete containing oil palm kernel shell as coarse aggregate, Construction and Building Materials 126 (2016) 1054–1065. https://doi.org/10.1016/j.conbuildmat.2016.09.010.

[84] T. Xiaoge, W. Xiaofei, Y. Huitong, Standard of Crushing Value of Coarse Aggregates for Permeable Asphalt Mixture Based on Contact Stress between Aggregates, Journal of Engineering 2020 (2020) 1–7. https://doi.org/10.1155/2020/1261368.

[85] M. Reyna, V.M. Garcia, J. Garibay, I. Abdallah, S. Nazarian, Evaluation of Aggregate Crushing Tests and Their Correlation with Superpave Mix Design Properties, Journal of Materials in Civil Engineering 32 (2020) 04020141. https://doi.org/10.1061/(ASCE)MT.1943-5533.0003175.

[86] ISO 20290-3, Determination of aggregate crushing value (ACV), (2019).

[87] M. Reyna, V.M. Garcia, J. Garibay, I. Abdallah, S. Nazarian, Evaluation of Aggregate Crushing Tests and Their Correlation with Superpave Mix Design Properties, Journal of Materials in Civil Engineering 32 (2020) 04020141. https://doi.org/10.1061/(ASCE)MT.1943-5533.0003175.

[88] ASTM C230/C230M, Specification for Flow Table for Use in Tests of Hydraulic Cement, (2021). https://doi.org/10.1520/C0230_C0230M-21.

[89] NRMCA (National Ready Mixed Concrete Association), NRMCA Pervious Concrete Mix Design, 2004. https://www.perviouspavement.org/materials.html.

[90] Akers et al., 213R-03 Guide for Structural Lightweight-Aggregate Concrete, (2003) 38.

[91] V.R. Schaefer et al., Mix Design Development for Pervious Concrete In Cold Weather Climates, (2006) 85.

[92] S. Park, S. Ju, H.-K. Kim, Y.-S. Seo, S. Pyo, Effect of the rheological properties of fresh binder on the compressive strength of pervious concrete, Journal of Materials Research and Technology 17 (2022) 636–648. https://doi.org/10.1016/j.jmrt.2022.01.045.

[93] ASTM Standard C1754-12, Standard Test Method for Density and Void Content of Hardened Pervious Concrete (Withdrawn 2021), ASTM International, West Conshohocken, PA, 2012. https://www.astm.org/Standards/C1754 (accessed November 1, 2021).

[94] ASTM D5084-03, Test Methods for Measurement of Hydraulic Conductivity of Saturated Porous Materials Using a Flexible Wall Permeameter, (2003). https://doi.org/10.1520/D5084-03.

[95] ASTM C39/C39M, Test Method for Compressive Strength of Cylindrical Concrete Specimens, (2021). https://doi.org/10.1520/C0039_C0039M-21.

[96] ASTM C496/C496M, Test Method for Splitting Tensile Strength of Cylindrical Concrete Specimens, (2017). https://doi.org/10.1520/C0496_C0496M-17.

[97] ASTM C 469 - 02, Standard Test Method for Static Modulus of Elasticity and Poisson's Ratio of Concrete in Compression, (2002). https://doi.org/10.1520/C0469-02.

[98] T. Joshi, Evaluation of Strength, Permeability and Void Ratio of Pervious Concrete with Changing w/c Ratio and Aggregate Size, International Journal of Civil Engineering and Technology 7 (2016) 276–284.

[99] A.K.H. Kwan, W.W.S. Fung, Packing density measurement and modelling of fine aggregate and mortar, Cement and Concrete Composites 31 (2009) 349–357. https://doi.org/10.1016/j.cemconcomp.2009.03.006.

[100] T.Y. Lo, W.C. Tang, H.Z. Cui, The effects of aggregate properties on lightweight concrete, Building and Environment 42 (2007) 3025–3029. https://doi.org/10.1016/j.buildenv.2005.06.031.

[101] L.G. Li, J.-J. Feng, J. Zhu, S.-H. Chu, A.K.H. Kwan, Pervious concrete: effects of porosity on permeability and strength, Magazine of Concrete Research 73 (2021) 69–79. https://doi.org/10.1680/jmacr.19.00194.

[102] X. Cui, J. Zhang, D. Huang, Z. Liu, F. Hou, S. Cui, L. Zhang, Z. Wang, Experimental Study on the Relationship between Permeability and Strength of Pervious Concrete, J. Mater. Civ. Eng. 29 (2017) 04017217. https://doi.org/10.1061/(ASCE)MT.1943-5533.0002058.

[103] A. Ibrahim, E. Mahmoud, M. Yamin, V.C. Patibandla, Experimental study on Portland cement pervious concrete mechanical and hydrological properties, Construction and Building Materials 50 (2014) 524–529. https://doi.org/10.1016/j.conbuildmat.2013.09.022.

[104] J. Li, Y. Zhang, G. Liu, X. Peng, Preparation and performance evaluation of an innovative pervious concrete pavement, Construction and Building Materials 138 (2017) 479–485. https://doi.org/10.1016/j.conbuildmat.2017.01.137.

[105] H. Amer, K. Sheng, R. Okuno, A. Al-Gawfi, P. Nakutnyy, A systematic comparison of solvents and their concentrations in bitumen gravity drainage under controlled thermodynamic conditions, Fuel 357 (2024) 129723. https://doi.org/10.1016/j.fuel.2023.129723.

[106] N. Neithalath, M.S. Sumanasooriya, O. Deo, Characterizing pore volume, sizes, and connectivity in pervious concretes for permeability prediction, Materials Characterization 61 (2010) 802–813. https://doi.org/10.1016/j.matchar.2010.05.004.

[107] B. Debnath, P.P. Sarkar, Permeability prediction and pore structure feature of pervious concrete using brick as aggregate, Construction and Building Materials 213 (2019) 643–651. https://doi.org/10.1016/j.conbuildmat.2019.04.099.

[108] G.P. Ong, A. Jagadeesh, Y.-M. Su, Effect of pore network characteristics on non-Darcy permeability of pervious concrete mixture, Construction and Building Materials 259 (2020) 119859. https://doi.org/10.1016/j.conbuildmat.2020.119859.

[109] A. Akkaya, İ.H. Çağatay, Investigation of the density, porosity, and permeability properties of pervious concrete with different methods, Construction and Building Materials 294 (2021) 123539. https://doi.org/10.1016/j.conbuildmat.2021.123539.

[110] A. Timmer, Building Integrated Evaporative Cooling Utilizing Pervious Concrete, Technology|Architecture + Design 5 (2021) 73–81. https://doi.org/10.1080/24751448.2021.1863675.

[111] M.S. Rahman, S. MacPherson, M. Lefsrud, Experimental investigation of a novel evaporative cooling pad made of cement-free porous concrete, Building and Environment 228 (2023) 109867. https://doi.org/10.1016/j.buildenv.2022.109867.

[112] K. Tan, Y. Qin, T. Du, L. Li, L. Zhang, J. Wang, Biochar from waste biomass as hygroscopic filler for pervious concrete to improve evaporative cooling performance, Construction and Building Materials 287 (2021) 123078. https://doi.org/10.1016/j.conbuildmat.2021.123078.

[113] J.H. Park, Y.U. Kim, J. Jeon, S. Wi, S.J. Chang, S. Kim, Effect of eco-friendly pervious concrete with amorphous metallic fiber on evaporative cooling performance, Journal of Environmental Management 297 (2021) 113269. https://doi.org/10.1016/j.jenvman.2021.113269.

[114] J. Wang, Q. Meng, L. Zhang, Y. Zhang, B.-J. He, S. Zheng, M. Santamouris, Impacts of the water absorption capability on the evaporative cooling effect of pervious paving materials, Building and Environment 151 (2019) 187–197. https://doi.org/10.1016/j.buildenv.2019.01.033.

[115] S. He, Z. Guan, H. Gurgenci, K. Hooman, A.M. Alkhedhair, Experimental Study of Heat Transfer Coefficient and Pressure Drop of Cellulose Corrugated Media, (n.d.).

[116] K. Seifeddine, S. Amziane, E. Toussaint, Thermal Behavior of Pervious Concrete in Dry Conditions, Construction and Building Materials 345 (2022) 128300. https://doi.org/10.1016/j.conbuildmat.2022.128300.

[117] C. Ngohpok, V. Sata, T. Satiennam, P. Klungboonkrong, P. Chindaprasirt, Mechanical Properties, Thermal Conductivity, and Sound Absorption of Pervious Concrete Containing Recycled Concrete and Bottom Ash Aggregates, KSCE J Civ Eng 22 (2018) 1369–1376. https://doi.org/10.1007/s12205-017-0144-6.

[118] P. Chindaprasirt, P. Nuaklong, Y. Zaetang, P. Sujumnongtokul, V. Sata, Mechanical and Thermal Properties of Recycling Lightweight Pervious Concrete, Arab J Sci Eng 40 (2015) 443–450. https://doi.org/10.1007/s13369-014-1563-z.

[119] P. Yu, F.E. Richart, Stress Ratio Effects on Shear Modulus of Dry Sands, (n.d.) 15.

[120] H. Alqrinawi, H. Lin, S. Chen, Calibrations of the Innovative S $_3$ F Sensor for Normal Stress Measurements in Soil, in: Geo-Congress 2023, American Society of Civil Engineers, Los Angeles, California, 2023: pp. 185–193. https://doi.org/10.1061/9780784484685.019.

[121] H. Alqrinawi, H. Lin, S. Chen, Calibrations of the Innovative S $_3$ F Sensor for Shear Stress Measurements in Soil, in: Tran-SET 2022, American Society of Civil Engineers, San Antonio, Texas, 2022: pp. 166–172. https://doi.org/10.1061/9780784484609.018.

[122] S. He, Z. Guan, H. Gurgenci, K. Hooman, Y. Lu, A. M. Alkhedhair, Experimental study of the application of two trickle media for inlet air pre-cooling of natural draft dry cooling towers, Energy Conversion and Management 89 (2015) 644–654. https://doi.org/10.1016/j.enconman.2014.10.031.

[123] S.E. Gustafsson, Transient plane source techniques for thermal conductivity and thermal diffusivity measurements of solid materials, Review of Scientific Instruments 62 (1991) 797–804. https://doi.org/10.1063/1.1142087.

[124] T. Log, S.E. Gustafsson, Transient plane source (TPS) technique for measuring thermal transport properties of building materials, Fire Mater. 19 (1995) 43–49. https://doi.org/10.1002/fam.810190107.

[125] B. Adl-Zarrabi, L. Boström, U. Wickström, Using the TPS method for determining the thermal properties of concrete and wood at elevated temperature, Fire and Materials 30 (2006) 359–369. https://doi.org/10.1002/fam.915.

[126] A.L. Avila-Marin, M. Alvarez-Lara, J. Fernandez-Reche, A Regenerative Heat Storage System for Central Receiver Technology Working with Atmospheric Air, Energy Procedia 49 (2014) 705–714. https://doi.org/10.1016/j.egypro.2014.03.076.

[127] K. Tanimizu, K. Hooman, Natural draft dry cooling tower modelling, Heat Mass Transfer 49 (2013) 155–161. https://doi.org/10.1007/s00231-012-1071-1.

[128] C. Zhao, M. Wang, Q. Gao, S. Cheng, Z. Liu, Z. Geng, S. Zhang, S. He, J. Qi, K. Han, M. Gao, Y. Shi, Comparison on the cooling performance of mechanical draft dry cooling towers pre-cooled with nozzle spray and wet medium, International Journal of Refrigeration 156 (2023) 298–314. https://doi.org/10.1016/j.ijrefrig.2023.09.027.

[129] ASTM Standard C39-21, Standard Test Method for Compressive Strength of Cylindrical Concrete Specimens, ASTM International, West Conshohocken, PA, 2021. https://doi.org/10.1520/C0039_C0039M-21.

[130] ASTM Standard D5084-16, Standard Test Methods for Measurement of Hydraulic Conductivity of Saturated Porous Materials Using a Flexible Wall Permeameter, ASTM International, West Conshohocken, PA, 2016. https://www.astm.org/d5084-16a.html (accessed April 13, 2023).

[131] 318-19 Building Code Requirements for Structural Concrete and Commentary, American Concrete Institute, 2019. https://doi.org/10.14359/51716937.

8 VITA

Emad Yaghmour was born on August 19, 1995, in New York, to Khalid Yaghmour and Nadia Shawish. In 2021, he enrolled in the Ph.D. Program in Structural Engineering at the Department of Civil and Environmental Engineering at Lehigh University. Prior to this, Emad earned his Master of Science degree in structural engineering from Jordan University of Science and Technology (Irbid, Jordan) in 2019. He also holds a bachelor's degree in civil engineering from Jordan University of Science and Technology, awarded in 2017.

During his graduate studies at Lehigh University, Emad was under the advice of Dr. Clay Naito. Together, they focused on advancing the understanding of concrete as an energy storage system. Their research delved into innovations in dry cooling methods, specifically employing PCM pervious concrete as a precooling panel. Emad successfully completed his Ph.D. in Structural Engineering in May 2024, marking the culmination of one chapter in his academic journey, with more exciting endeavors on the horizon. (To be continued)